Dissertation

Submitted to the

Combined Faculty of Natural Sciences and Math

of the Ruperto Carola University Heidelberg, Germany

for the degree of

Doctor of Natural Sciences

Presented by

Parul Gupta, BS-MS

Born in Rewa, India

Oral Examination: 24 November 2025

Zeb1 is a key regulator of cardiomyocyte structure and function

Thesis Committee Members:
Prof. Georg Stoecklin
Prof. Mirko Völkers
Dr. Chi-Chung Wu
Dr. Maarten van den Hoogenhof

Abstract

Cardiomyocytes depend on tightly regulated gene networks for development, maturation, and function. Disruption of these networks can cause cardiomyopathies, such as hypertrophic or dilated forms, often leading to heart failure. RNA-binding protein Cpeb4 was previously identified as a dynamic regulator in cardiac hypertrophy and found Zinc Finger E-Box Binding Homeobox 1 (Zeb1) acting downstream. While Zeb1 is known for roles in cancer metastasis and epithelial-to-mesenchymal transition, its function in heart muscle remained unclear. Given its importance in skeletal muscle regeneration, it was hypothesized that Zeb1 supports cardiomyocyte development, structural stability, and contractile performance.

To test this, I used AAV9-Zeb1 to overexpress Zeb1 in 8-week-old mice. Elevated Zeb1 promoted maladaptive hypertrophy and impaired cardiac function, indicating that excessive Zeb1 is harmful. Complementary loss-of-function studies employed a cardiomyocyte-specific Zeb1 conditional knockout (Zeb1 cKO) via αMHC-Cre. By 12 weeks, cKO mice showed early systolic dysfunction, which worsened with age. At 25 weeks, histology and electron microscopy revealed sarcomeric disorganization and abnormal mitochondria. Female cKO mice were more severely affected than males, suggesting sex-specific dependence on Zeb1.

A tamoxifen-inducible knockout (Zeb1 icKO) model, deleting Zeb1 after full maturation, showed that only females experienced a significant decline in ejection fraction, reinforcing Zeb1's role in long-term cardiac maintenance, particularly in females. RNA-seq from Zeb1 KO hearts revealed epithelial-like gene expression patterns, implying cytoskeletal and structural changes.

In summary, Zeb1 is essential for cardiomyocyte integrity and contractility. Its loss disrupts sarcomeres and accelerates heart failure, especially in females, likely through transcriptional reprogramming. Conversely, Zeb1 overexpression drives pathological hypertrophy, underscoring the need for precise regulation in cardiac homeostasis and disease.

Zusammenfassung

Kardiomyozyten sind auf streng regulierte Gen-Netzwerke angewiesen, um Entwicklung, Reifung und Funktion zu gewährleisten. Störungen dieser Netzwerke können zu Kardiomyopathien wie hypertropher oder dilatativer Form führen, die häufig in Herzinsuffizienz münden. In früheren Arbeiten identifizierten wir das RNA-bindende Protein Cpeb4 als dynamischen Regulator bei kardialer Hypertrophie und fanden, dass Zinc Finger E-Box Binding Homeobox 1 (Zeb1) nachgeschaltet wirkt. Während Zeb1 für seine Rolle bei Krebsmetastasen und der epithelial-mesenchymalen Transition bekannt ist, ist seine Funktion im Herzmuskel weitgehend unerforscht. Aufgrund seiner Bedeutung in der Skelettmuskelregeneration vermuteten wir, dass Zeb1 die Entwicklung, strukturelle Stabilität und Kontraktilität von Kardiomyozyten unterstützt.

Zur Prüfung dieser Hypothese überexprimierten wir Zeb1 mithilfe von AAV9-Zeb1 in 8 Wochen alten Mäusen. Erhöhtes Zeb1 förderte maladaptive Hypertrophie und verschlechterte die Herzfunktion, was auf schädliche Effekte einer Überaktivität hinweist. Ergänzende Knockout-Studien nutzten ein kardiomyozytenspezifisches Zeb1-cKO-Modell (αMHC-Cre). Bereits nach 12 Wochen zeigte sich eine systolische Dysfunktion, die mit dem Alter zunahm. Nach 25 Wochen wiesen Histologie und Elektronenmikroskopie eine Desorganisation der Sarkomere und abnorme Mitochondrien nach. Weibliche cKO-Mäuse waren stärker betroffen, was auf geschlechtsspezifische Unterschiede hindeutet.

In einem Tamoxifen-induzierbaren Knockout (Zeb1 icKO) nach vollständiger Reifung sank die Ejektionsfraktion signifikant nur bei Weibchen, was die Bedeutung von Zeb1 für die langfristige Herzfunktion unterstreicht. RNA-Seq-Analysen von Zeb1-KO-Herzen zeigten epithelähnliche Genexpressionsmuster, was auf strukturelle Veränderungen hinweist.

Zusammenfassend ist Zeb1 entscheidend für die Integrität und Kontraktilität von Kardiomyozyten. Ein Verlust führt zu Sarkomerdefekten und beschleunigter Herzinsuffizienz, insbesondere bei Weibchen. Umgekehrt treibt eine Überexpression pathologische Hypertrophie an, was die Notwendigkeit einer präzisen Regulierung verdeutlicht.

Contents

List of Figures

List of Tables

Abbreviation

Abbreviation	Full Form
A260	Absorbance at 260 nm
ACE INHIBITORS	Angiotensin-Converting Enzyme Inhibitors
AAV9	Adeno-Associated Virus serotype 9
AKT	Protein Kinase B
A-MHC	Alpha-Myosin Heavy Chain
A-MHC-CRE	Alpha-Myosin Heavy Chain Cre Recombinase
AMCM	Adult Mouse Cardiomyocyte
AMPK	AMP-Activated Protein Kinase
ARBS	Angiotensin II Receptor Blockers
ATP	Adenosine Triphosphate
B2M	Beta-2 Microglobulin
BP	Base Pairs
BPM	Beats Per Minute
BSA	Bovine Serum Albumin
BTUB	Beta Tubulin
CDH1	Cadherin-1 (E-cadherin)
CDS	Coding DNA Sequence
CDK	Cyclin-Dependent Kinase

$CDCL_2$	Cadmium Chloride
CNS	Central Nervous System
CMV	Cytomegalovirus (promoter)
CKO	Conditional Knockout
CSC	Cancer Stem Cell
CSRP3	Cysteine and Glycine-Rich Protein 3
CT	Cycle Threshold
D1000	DNA ScreenTape for 100–1000 bp fragments
DAPI	4′,6-Diamidino-2-Phenylindole
DDH_2O	Double-distilled Water
DCM	Dilated Cardiomyopathy
DEGS	Differentially Expressed Genes
DESEQ2	Differential Expression Sequencing 2
DNA	Deoxyribonucleic Acid
E. COLI	Escherichia coli
ECM	Extracellular Matrix
ECC	Excitation–Contraction Coupling
EF	Ejection Fraction
ECL	Enhanced Chemiluminescence
EMCF	Electron Microscopy Core Facility

EMT	Epithelial-to-Mesenchymal Transition
ENOS	Endothelial Nitric Oxide Synthase
ERK	Extracellular Signal-Regulated Kinase
ERK/MAPK	ERK / MAPK signaling pathway
ETOH	Ethanol
FASTQC	Fast Quality Control (software tool)
FBS	Fetal Bovine Serum
FFPE	Formalin-Fixed, Paraffin-Embedded
FIJI	Fiji Is Just ImageJ (Image Analysis Software)
FITC	Fluorescein Isothiocyanate
FLAG	FLAG Epitope Tag
FOXP3	Forkhead Box P3
FCS	Fetal Calf Serum
GATA4	GATA Binding Protein 4
GRCM38/MM10	Genome Reference Consortium Mouse Build 38 / Mouse genome version 10
GO	Gene Ontology
HA	Hemagglutinin Epitope Tag
HBSS	Hank's Balanced Salt Solution
HCL	Hydrochloric Acid
HCM	Hypertrophic Cardiomyopathy

HDAC1	Histone Deacetylase 1
HDAC2	Histone Deacetylase 2
HERG	Human Ether-à-go-go-Related Gene (KCNH2)
HF	Heart Failure
HFPEF	Heart Failure with preserved Ejection Fraction
HFREF	Heart Failure with reduced Ejection Fraction
HIPERFECT	HiPerfect Transfection Reagent
H&E	Hematoxylin and Eosin
HOMER	Hypergeometric Optimization of Motif EnRichment
HPRT	Hypoxanthine Phosphoribosyltransferase
HW/BW	Heart Weight-to-Body Weight Ratio
IB4	Isolectin B4
ICKO	Inducible Conditional Knockout
IGG	Immunoglobulin G
IHD	Ischemic Heart Disease
IMAGEJ	NIH-developed Image Processing Software
IPSC	Induced Pluripotent Stem Cell
IPF	Idiopathic Pulmonary Fibrosis
JNK	c-Jun N-terminal Kinase
KCNQ1	Potassium Voltage-Gated Channel Subfamily Q Member 1

KO	Knockout
KRT8	Keratin 8
LB	Lysogeny Broth
LR	Ligation Reaction (Gateway Cloning)
LNCRNA	Long Non-Coding RNA
LV	Left Ventricle
LVAD	Left Ventricular Assist Device
MAPK	Mitogen-Activated Protein Kinase
MEF2	Myocyte Enhancer Factor 2
MER-CRE-MER	Tamoxifen-inducible Cre recombinase system under α-MHC promoter control
MIR / MIRNA	microRNA
MRNA	Messenger RNA / Messenger Ribonucleic Acid
MTOR	Mechanistic Target of Rapamycin
MYBPC3	Myosin Binding Protein C, Cardiac Type 3
MYH6	Myosin Heavy Chain 6
NANODROP	Spectrophotometer used for quantifying nucleic acids
NPPA	Natriuretic Peptide A (Atrial Natriuretic Factor)
NPPB	Natriuretic Peptide B (Brain Natriuretic Peptide)
NEB	New England Biolabs
NEBNEXT	New England Biolabs Next (library prep kit series)

NKX2-5	NK2 Homeobox 5
NRCM	Neonatal Rat Cardiomyocyte
NRF1	Nuclear Respiratory Factor 1
NRG1	Neuregulin-1
OE	Overexpression
P2FA	Paraformaldehyde
PCSK9	Proprotein Convertase Subtilisin/Kexin Type 9
PE	Phenylephrine
PEI	Polyethylenimine (transfection reagent)
PFA	Paraformaldehyde
PGC-1A	Peroxisome Proliferator-Activated Receptor Gamma Coactivator 1-alpha
PHEN	PIPES, HEPES, EGTA, and $MgCl_2$
PI3K	Phosphoinositide 3-Kinase
PI3K/AKT	PI3K / Protein Kinase B signaling pathway
PBS	Phosphate-Buffered Saline / Phosphate Buffered Saline
PDAC	Pancreatic Ductal Adenocarcinoma
PD-L1	Programmed Death-Ligand 1
PPARA	Peroxisome Proliferator-Activated Receptor Alpha
PROTEINASE K	Broad-spectrum serine protease
PVDF	Polyvinylidene Fluoride / Polyvinylidene Difluoride

QPCR	Quantitative Polymerase Chain Reaction
QRT-PCR	Quantitative Real-Time / Reverse Transcription PCR
RBM20	RNA Binding Motif Protein 20
RBP	RNA-Binding Protein
RIN	RNA Integrity Number
RNA	Ribonucleic Acid
RNASE A	Ribonuclease A
RPM	Revolutions Per Minute
RYR2	Ryanodine Receptor 2
SCN5A	Sodium Channel, Voltage-Gated, Type V Alpha Subunit
SDS	Sodium Dodecyl Sulfate
SDHA	Succinate Dehydrogenase Complex Subunit A
SERCA2A	Sarcoplasmic/Endoplasmic Reticulum Ca^{2+}-ATPase 2a
SIRNA	Small Interfering RNA
SISCR	Scrambled Small Interfering RNA (control)
SISMIM4	Small Interfering RNA targeting SMIM4
SGLT2	Sodium-Glucose Cotransporter 2
SP8	Leica SP8 Confocal Fluorescence Microscope / Leica SP8 Lightning Confocal Microscope
STAR	Spliced Transcripts Alignment to a Reference
TAC	Transverse Aortic Constriction

TAPESTATION	Agilent instrument for DNA/RNA quality control
TBST	Tris-Buffered Saline with Tween 20
TAE	Tris-Acetate-EDTA
TEM	Transmission Electron Microscopy
TGF-B	Transforming Growth Factor Beta
TNB	Tris-NaCl Blocking Buffer
TN BUFFER	Tris-NaCl Buffer
TOP10	A strain of chemically competent E. coli for cloning
TRIZOL	Reagent for RNA extraction
TREG	Regulatory T cell
TRITON X-100	Nonionic surfactant used for permeabilization
UC7	Leica Ultramicrotome model UC7
UHF	Ultra-High Frequency
VEVO	Visual Sonics Vevo (ultrasound imaging platform)
VEVOLAB	Visual Sonics Vevo Lab (image analysis software)
V5	V5 Epitope Tag
WGA	Wheat Germ Agglutinin
WHO	World Health Organization
WNT	Wingless-related Integration Site
WT	Wild Type / Wild-Type

YAP	Yes-Associated Protein
Z-DISC	Z-line or Z-disc (sarcomeric structure)
ZEB1	Zinc finger E-box binding homeobox 1
ZEB2	Zinc Finger E-box Binding Homeobox 2

1. Introduction

Cardiomyocytes are essential for generating the contractile force needed to circulate blood throughout the body (1). These cells arise from mesodermal progenitors and undergo tightly orchestrated processes of differentiation and maturation, eventually forming a highly specialized architecture (2). Mature cardiomyocytes are characterized by organized sarcomeres for contraction, abundant mitochondria to meet high energy demands, and well-formed intercalated discs that ensure synchronized electrical and mechanical activity (2–5). The interplay of these structural and functional components enables the heart to maintain an efficient and rhythmic output across a lifetime (6,7). Disruption of these features is central to the development of various cardiomyopathies, including Hypertrophic Cardiomyopathy (HCM) and Dilated Cardiomyopathy (DCM), which are major contributors to heart failure and remain among the leading causes of global cardiovascular mortality (8–11).

1.1 Global Burden and Disparities in Cardiovascular Disease: A Persistent Public Health Challenge

Cardiovascular Diseases (CVDs) are not merely abstract statistics in global health reports—they represent tangible human suffering, altered lives, and strained healthcare systems. As the leading cause of death worldwide, CVDs are responsible for over 20.5 million deaths annually, accounting for nearly one-third of all global fatalities (12–14)WHO,2023) (Fig. 1). Despite the rapid advancements in medical science, the burden of CVDs remains profound, especially in low- and middle-income countries where diagnostic and therapeutic resources are often limited (13).

The landscape of cardiovascular disease encompasses a broad range of conditions, including coronary artery disease, heart failure, arrhythmias, valvular pathologies, and cardiomyopathies. The global burden of disease study estimates that ischemic heart disease (IHD) alone contributes to more than 9 million deaths annually, while heart failure (HF) affects over 64 million individuals worldwide (13).

Notably, Heart Failure with preserved Ejection Fraction (HFpEF), once considered rare, has emerged as a prevalent and therapeutically challenging condition (15,16).

Figure 1. Current global scenario of cardiovascular diseases according to the World Health Organization (WHO).

In high-income countries, improvements in awareness, early detection, and treatment have led to declining mortality rates from CVDs. However, these gains are not equitably distributed. Low- and middle-income countries are experiencing

a surge in CVD-related mortality due to rapid urbanization, lifestyle changes, and inadequate healthcare infrastructure (12,13,17,18).

1.2 Clinical Overview and Classification of Heart Failure

Heart failure is a clinical syndrome characterized by the heart's inability to pump blood to meet the body's metabolic demands effectively. It is commonly classified by reduced Ejection Fraction (EF): where EF is less than 40%, and is typically associated with systolic dysfunction, patients with heart failure often have fatigue, dyspnea, and fluid retention, all of which significantly compromise their quality of life (8,19).

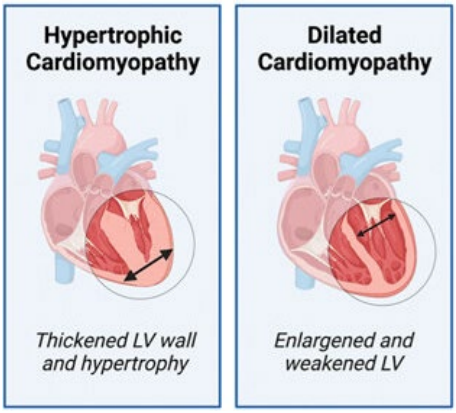

Figure 2. Changes in the left ventricle (LV) wall thickness during hypertrophic and dilated cardiomyopathies.

Cardiomyopathies refer to structural and functional abnormalities of the myocardium (20), which can be genetic or acquired. HCM, by contrast, is characterized by thickened ventricular walls (Fig. 2), often resulting in diastolic dysfunction and arrhythmic risk. DCM is marked by ventricular enlargement and reduced contractility (Fig. 2) (21).

HCM and DCM are two major forms of genetic cardiomyopathies, while both rooted in inherited defects of the myocardium, differ significantly in their genetic basis, pathophysiology, and clinical expression. HCM is most inherited in an autosomal dominant manner, with age-related penetrance and variable expressivity. Most pathogenic variants involve sarcomere protein genes, most notably *MYH7* (β-myosin heavy chain) and *MYBPC3* (myosin-binding protein C) (22). These mutations disrupt normal sarcomere function and lead to enhanced contractility, myocyte hypertrophy, and disarray, which underlie the characteristic phenotype of asymmetric left ventricular hypertrophy (22). Clinical outcomes often vary depending on the specific gene involved; for example, *MYBPC3* variants are frequently associated with later-onset disease (23).

In contrast, DCM represents a more genetically heterogeneous disorder, typically inherited in an autosomal dominant fashion but also occurring through autosomal

recessive, X-linked, or mitochondrial patterns (24). The most frequently implicated gene is *Ttn* (Titin), with truncating variants accounting for up to a quarter of familial cases (25). Increasing attention has also been given to *Rbm20* (RNA Binding Motif protein 20), which encodes an RNA-binding protein essential for the regulation of alternative splicing in cardiac muscle (26). Pathogenic variants or knockout (Rbm20 KO) models lead to widespread splicing defects in several critical cardiac genes, most notably *Ttn*, resulting in aberrant isoform expression that impairs sarcomere structure and calcium handling. Experimental Rbm20 KO models recapitulate human DCM phenotypes, demonstrating progressive ventricular dilation, systolic dysfunction, and arrhythmogenic remodeling (9). These findings highlight RBM20 as a central regulator of the cardiac transcriptome and underscore the importance of post-transcriptional regulation in the pathogenesis of DCM. Overall, the diverse genetic origins of DCM reflect disruptions across the sarcomere, cytoskeleton, nuclear envelope, ion channels, and RNA splicing machinery, which together converge on impaired contractile function and maladaptive ventricular remodeling.

Taken together, the genetic underpinnings of HCM and DCM highlight both shared and divergent mechanisms of inherited myocardial disease. HCM is largely a disease of the sarcomere, manifesting as hypertrophy with preserved or increased contractility, whereas DCM is genetically more diverse and characterized by ventricular dilation with impaired contractile function. Understanding these distinct genetic landscapes not only informs clinical diagnosis and family screening but also provides critical insight into disease-specific mechanisms and therapeutic strategies.

1.3 Various Available Therapeutics for CVDs

Cardiovascular disorders (CVDs) remain the leading cause of mortality worldwide, necessitating continuous innovation in therapeutic approaches. The current landscape includes well-established pharmacologic treatments alongside novel therapies emerging from advances in molecular biology, gene editing (27), and RNA-based technologies (28,29).

Medications form the foundation of CVD management, addressing blood pressure, clot prevention, cholesterol control, angina, and heart failure. Statins remain the

mainstay of lipid-lowering therapy, but PCSK9 (Proprotein Convertase Subtilisin/Kexin type 9) inhibitors and Inclisiran have expanded options for low-density lipoprotein (LDL) reduction (30–33). Beyond traditional drugs, newer classes have reshaped care: SGLT2 (sodium-glucose cotransporter 2) inhibitors reduce heart failure hospitalizations and mortality, while ARNi (sacubitril/valsartan) improves outcomes in reduced ejection fraction (32,33). RNA-based therapies and antisense oligonucleotides are emerging to target genetic risk factors such as lipoprotein(a) and apolipoprotein B (29).

In rare conditions like transthyretin amyloid cardiomyopathy (ATTR-CM), tafamidis and acoramidis stabilize transthyretin, while RNA interference therapies reduce its synthesis. Anti-inflammatory strategies, such as IL-6 (Interleukin-6) inhibition with ziltivekimab, and novel anticoagulants like factor XI inhibitors (abelacimab), further broaden the therapeutic landscape (34).

Altogether, CVD treatment has progressed from broad pharmacologic management to precision therapies targeting specific molecular pathways, underscoring the need for personalized, equitable approaches to reduce the global burden of cardiovascular disease.

1.4 Cardiomyocytes: The Structural and Functional Units of Myocardium

The rhythmic pumping action of the heart is sustained by the ability of cardiomyocytes to translate electrical signals into coordinated mechanical force, a process termed Excitation–Contraction Coupling (ECC) (Fig. 3) (35). This highly regulated mechanism ensures that each action potential evokes a well-timed contraction and subsequent relaxation, thereby maintaining effective cardiac output (35).

Cardiomyocyte contraction is initiated by the depolarization of the sarcolemma, which propagates along the transverse (T)-tubule system and activates voltage-gated L-type Ca^{2+} channels (dihydropyridine receptors). The small influx of extracellular Ca^{2+} through these channels serves as a critical trigger for the opening of RyR2 (Ryanodine Receptor type-2) channels on the Sarcoplasmic Reticulum (SR), resulting in Calcium-Induced Calcium Release (CICR). The transient rise in cytosolic Ca^{2+} concentration permits Ca^{2+} binding to troponin C, thereby activating the contractile machinery. Subsequent relaxation requires efficient Ca^{2+} clearance, mediated predominantly by SERCA2a (Sarcoplasmic/Endoplasmic Reticulum Ca^{2+}-ATPase) reuptake, Na^{+}/Ca^{2+} exchanger activity, and, to a lesser extent, plasma membrane Ca^{2+}-ATPase and mitochondrial sequestration. The precise temporal control of these Ca^{2+} fluxes ensure synchronized contraction and relaxation cycles, and their dysregulation is a hallmark of cardiac pathology (36–38).

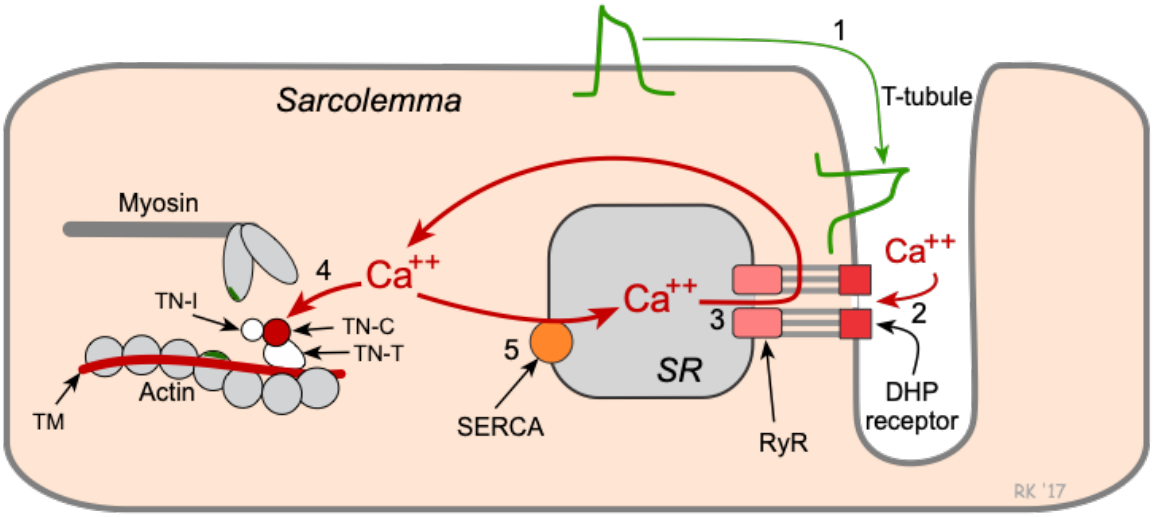

Figure 3. Excitation–Contraction Coupling (ECC) (39)

The mechanical force underlying contraction is generated by the cardiomyocyte contractile apparatus, a highly ordered sarcomeric system optimized for rhythmic activity. Each sarcomere, delineated by Z-discs, consists of thin filaments—composed of actin, tropomyosin, and the troponin regulatory complex, interdigitating with thick filaments formed by myosin heavy and light chains. Upon Ca^{2+} binding to troponin C, conformational changes in the troponin–tropomyosin complex expose actin's myosin-binding sites, enabling cross-bridge cycling. This

cyclical interaction of myosin heads with actin, powered by ATP hydrolysis, produces sarcomere shortening and myocardial contraction (40,41).

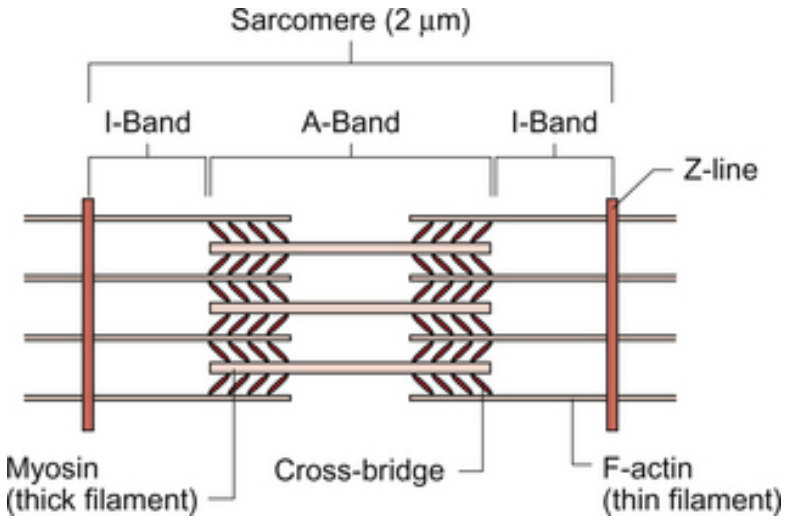

Figure 4. Structural organization of myofibrils in the Contractile unit of Heart.

Sarcomeric architecture is further reinforced by large structural proteins that ensure stability and elasticity. Titin spans half the sarcomere from Z-disc to M-line, acting as a molecular spring that contributes to passive stiffness and elastic recoil during diastole (Fig. 4). Additional scaffold proteins, including α-actinin, myomesin, and nebulin, maintain filament alignment and structural integrity (42,43). Importantly, contractile performance is dynamically modulated by post-translational modifications, such as phosphorylation of myofilament proteins by PKA (Protein Kinase A), PKC (Protein Kinase C), and CaMKII (Ca^{2+}/Calmodulin-Dependent Kinase II). These modifications alter Ca^{2+} sensitivity and cross-bridge kinetics, thereby adjusting contractility to meet acute physiological demands such as exercise or stress (44–46).

Perturbations in either the excitation–contraction coupling process or the structural integrity of the contractile apparatus have profound consequences for cardiac function. Mutations in sarcomeric proteins, including β-myosin heavy chain, cardiac troponin T, and titin are causally linked to inherited cardiomyopathies, while acquired alterations in Ca^{2+} handling and myofilament regulation contribute to heart failure progression (47–49). Thus, a comprehensive understanding of both the molecular mechanisms of ECC and the structural–functional organization of the

contractile apparatus is essential for elucidating the pathophysiology of cardiac disease.

1.5 Cardiomyocyte Homeostasis

Cardiomyocytes must maintain precise structural and functional equilibrium to meet the continuous demands of cardiac output. Disruptions in this finely balanced homeostasis often initiate or exacerbate cardiovascular diseases. Elucidating the molecular mechanisms that underpin cardiomyocyte integrity is therefore essential for advancing preventive and therapeutic strategies.

Mitochondrial health is cornerstone of cardiomyocyte homeostasis. Due to their immense energy requirements, cardiomyocytes rely heavily on mitochondrial oxidative phosphorylation (50). Regulators such as PGC-1α (Peroxisome proliferator-activated receptor-gamma coactivator 1-alpha) and AMPK (AMP-activated protein kinase) mediate mitochondrial biogenesis and energy adaptation (51). Impairments in these processes lead to diminished ATP production and increased oxidative stress, which collectively contribute to myocardial dysfunction and remodeling (50,52).

Cardiomyocyte function and survival depend on a finely tuned balance of cellular processes that respond to physiological demands and stress. Among these, proteostasis - the regulation of protein synthesis, folding, and degradation - is fundamental (53). Cellular balance is maintained by autophagy, which recycles cellular components, and the ubiquitin-proteasome system, which degrades misfolded proteins, both tightly regulated by nutrient-sensing pathways such as mTOR (mechanical Target of Rapamycin) and factors like Beclin-1 (54,55). When proteostasis is compromised, as seen in aging hearts and cardiomyopathies, toxic protein aggregates accumulate, disrupting cellular homeostasis and contributing to disease progression (56,57).

Gene expression in cardiomyocytes is governed by a complex interplay of transcriptional and epigenetic mechanisms (58). Key cardiac transcription factors -GATA4 (GATA-binding protein 4), MEF2 (Myocyte Enhancer Factor-2), and NKX2-5 (NK2 homeobox 5), drive the expression of genes critical for contractile function and stress adaptation (59,60). In parallel, epigenetic modifications, including

histone acetylation and DNA methylation, shape chromatin accessibility, and gene activity, influencing whether the heart adapts or maladapts under stress (61).

At the signaling level, intracellular pathways such as PI3K/Akt (Phosphatidylinositol 3-Kinase/Protein Kinase B) and MAPK (Mitogen-Activated Protein Kinase)–ERK (Extracellular Signal-Regulated Kinase), JNK (c-Jun N-terminal Kinase), and p38- translate extracellular cues into functional responses. These pathways support growth and survival in healthy conditions, but when persistently activated, especially through chronic β-adrenergic stimulation, they can trigger pathological hypertrophy, apoptosis, and ultimately heart failure (61).

In recent years, non-coding RNAs, particularly microRNAs (miRNAs) and long non-coding RNAs (lncRNAs), have emerged as pivotal regulators of cardiac gene expression. miR-1 and miR-133, for example, influence electrical conduction and hypertrophic signaling, and their dysregulation is linked to arrhythmias and structural heart disease (62,63). These molecules not only serve as potential biomarkers but also offer promising therapeutic avenues.

Adding a further layer of post-transcriptional regulation are RNA-binding proteins (RBPs), which control RNA splicing, translation, stability, and degradation. RBPs enable dynamic and coordinated gene expression in response to stress and developmental cues. When dysregulated, they contribute to diverse cardiac pathologies, including cardiomyopathies, arrhythmias, and heart failure (64–66).

Together, these interconnected molecular and cellular pathways form the foundation of cardiomyocyte health. Their precise coordination ensures effective cardiac function, while their disruption contributes to the onset and progression of cardiovascular disease. Understanding these multifaceted molecular mechanisms of cardiomyocyte homeostasis not only enriches our fundamental knowledge of cardiac biology but also paves the way for novel, targeted therapies in the management of cardiovascular disease.

1.6 Cardiomyocyte Proliferation and Maturation.

Cardiomyocyte proliferation and maturation are two tightly orchestrated processes that determine how the heart grows, adapts, and responds to injury. In the early stages of development, cardiomyocytes proliferate rapidly to build the heart’s

structure (67,68). However, this proliferative capacity is sharply curtailed soon after birth, a shift that has long challenged regenerative efforts in adult cardiac tissue (68).

During fetal development, cardiomyocytes arise from mesodermal progenitors and expand under the influence of key signaling pathways (69). Wnt/β-catenin signaling promotes early progenitor proliferation, while growth factors like FGF (Fibroblast Growth Factor) and IGF (Insulin-like Growth Factor) activate intracellular cascades (PI3K/Akt, ERK/MAPK) that further drive cell cycle progression. NRG1 (Neuregulin-1), acting through ErbB (Erythroblastic Leukemia Viral Oncogene) receptors, is also vital for supporting proliferation, particularly in the development of ventricular trabeculation (69,70). At the molecular level, these cells express a host of cyclins and cyclin-dependent kinases (CDKs) that push them through the cell cycle. But shortly after birth, particularly in rodents by postnatal day 7, cardiomyocytes exit the cell cycle, and the expression of CDK inhibitors like p21 and p27 increases, effectively halting further division (71).

Adding to this proliferative shutdown, postnatal cardiomyocytes often undergo a process called endoreduplication, where they replicate their DNA without dividing, leading to binucleation or polyploidy. This structural change makes it even harder for these cells to re-enter the cell cycle later in life (72). Though a small amount of cardiomyocyte turnover continues into adulthood (estimated at around 1% per year), it is insufficient to repair significant damage, such as that from a myocardial infarction (73).

Meanwhile, as proliferation slows, maturation accelerates (68). Cardiomyocytes undergo dramatic structural and functional changes to support the increasing mechanical demands of the postnatal heart. Sarcomeres, the contractile units of the cell, become more organized and densely packed, enabling efficient force generation. T-tubules, absent in fetal cells, develop to facilitate synchronized calcium signaling through tight coupling between L-type calcium channels and ryanodine receptors. Intercalated discs mature to ensure strong mechanical and electrical connections between neighboring cells, driven by proteins such as connexin-43 and N-cadherin (74).

Electrophysiological maturation is also key. The expression of potassium channels such as KCNQ1 (potassium voltage-gated Channel subfamily Q member 1) and HERG (Human Ether-à-go-go-related Gene) increases, refining the heart's repolarization capability. Sodium channels like SCN5A (Sodium voltage-gated Channel alpha subunit 5) become more prominent, improving conduction velocity. The resting membrane potential becomes more negative, which is critical for maintaining the heart's rhythm and contractility (75,76).

In parallel, epigenetic regulation, through histone modifications, DNA methylation, and chromatin remodeling, contributes to the silencing of fetal gene programs and the activation of adult-specific expression profiles. This ensures that cardiomyocytes are not only structurally and functionally mature but also transcriptionally stable (77).

Despite these barriers, researchers are finding ways to coax adult cardiomyocytes back into the cell cycle. Manipulating genes involved in cell cycle regulation (e.g., overexpressing cyclin D2 or YAP-Yes-Associated Protein), exposing cells to hypoxic environments, or delivering specific microRNAs like miR-199a and miR-590 can promote limited proliferation and improve cardiac function after injury (78,79).

Interestingly, not all species lose regenerative ability. Zebrafish and neonatal mice can regenerate heart tissue through cardiomyocyte proliferation, offering valuable models for understanding and reactivating these programs in adult humans (80). Similarly, efforts to mature cardiomyocytes derived from induced pluripotent stem cells (iPSCs) are ongoing, with a focus on mimicking the physiological cues, electrical stimulation, mechanical stretch, biochemical signals, that drive natural maturation (75).

In sum, cardiomyocyte proliferation and maturation are two sides of a finely tuned developmental process. Proliferation builds the heart, while maturation perfects it. Understanding how these processes are regulated, and how they might be modulated, could increase our knowledge in the field of cardiac regeneration (81).

1.7 Post-Transcriptional Control of Cardiac Stress: Cpeb4-Mediated Regulation of Zeb1 in Hypertrophy

Recent studies have underscored the role of RNA-binding proteins (RBPs) in modulating cardiac stress responses through translational control of key regulatory genes (66,82,83). One such RBP, Cytoplasmic Polyadenylation Element Binding Protein 4 (Cpeb4), has been implicated in cardiac hypertrophy and remodeling by regulating mRNA translation in response to pathological stimuli (84). Notably, Zeb1 (Zinc finger E-box binding homeobox 1) was identified as a downstream effector of Cpeb4 in hypertrophic conditions, highlighting a post-transcriptional mechanism of Zeb1 regulation during cardiac stress (84) (Fig. 5). This connection provides a compelling rationale to further investigate Zeb1's role in cardiomyocyte biology.

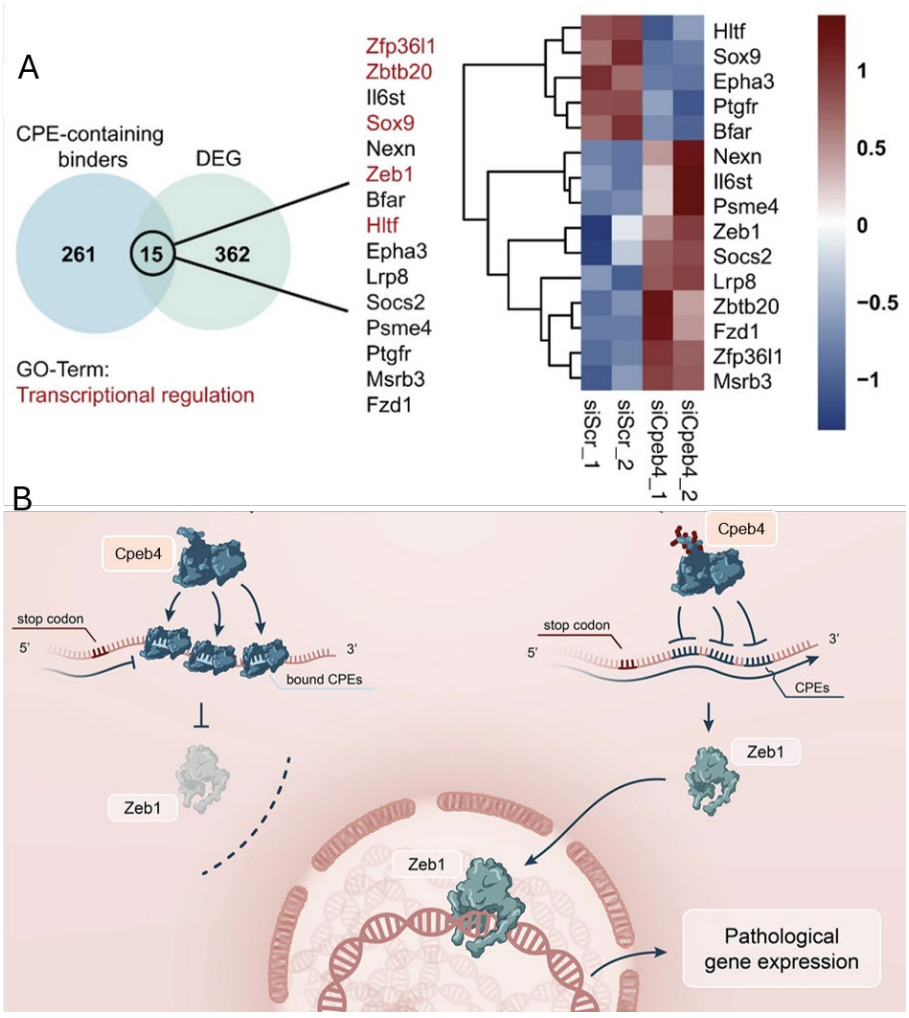

Figure 5. Previous data identifying Zeb1 as a downstream target of RNA binding protein CPEB4 (84)**.**

(a) Left: Venn diagram comparing Cpeb4 target mRNAs containing a CPE element (RIP-seq) and differentially expressed genes (DEGs) after Cpeb4 KD (Ribo-seq) with a list of 15 overlapping genes. Right: heatmap of

the 15 DEGs from the Ribo-seq data of biological replicates. (b) Schematic representation of Cpeb4's effect on Zeb1.

I hypothesize that Zeb1 functions as a master regulator of cardiomyocyte identity, not unlike its well-established roles in other mesenchymal and epithelial systems. Given its known function in suppressing epithelial gene programs and maintaining mesenchymal identity, we propose that Zeb1 helps sustain sarcomeric integrity, mitochondrial homeostasis, and transcriptional networks essential for cardiomyocyte structure and contractility. Such a role would be consistent with the cellular demands placed on cardiac tissue, particularly under conditions of stress and injury.

1.8 ZEB as a Central Regulator of Cardiac Remodeling

ZEB proteins, primarily ZEB1 and ZEB2 (Zinc Finger E-Box Binding Homeobox 2) are central transcriptional regulator with widespread roles across multiple organ systems (85–91). In non-cardiac contexts, they orchestrate key developmental processes (92–94), maintains immune and neural homeostasis (86,87), and drives disease mechanisms such as cancer metastasis and organ fibrosis (85,95–98). Its ability to interact with non-coding RNAs (93,99–101), chromatin remodelers (102), and signaling pathways (85,103,104) enables it to act as a context-specific modulator of cell fate and function (103,105,106).

Given its role in diverse pathologies, ZEB1 is increasingly viewed as a therapeutic target. Strategies to modulate ZEB1 activity - whether through microRNA mimics (e.g., miR-200 family) (100,101), small molecules (107), or epigenetic modulators (96) - are under active investigation. As we gain a deeper understanding of how ZEB1 integrates cellular signaling with gene expression, new opportunities will emerge to exploit its biology for diagnostic and therapeutic purposes across multiple disciplines.

Although Zeb1 has not been extensively investigated in the context of cardiomyopathies, studies have examined the role of its closest homolog, Zeb2, in cardiac dysfunction (91). Zeb2 shares similar zinc finger and homeodomain structures with Zeb1 and has overlapping functions in other biological contexts, including epithelial-to-mesenchymal transition (EMT) and neural development.

In the heart, ZEB2 plays a multifaceted role, affecting both cardiomyocytes and supporting stromal cells in distinct ways. In cardiomyocytes, ZEB2 expression rises rapidly in response to low oxygen levels or injury, driven by activation through HIF1α (Hypoxia-Inducible Factor 1 Alpha) signaling. This increase appears to promote cardiac adaptation and repair. Functionally, ZEB2 enhances contractility by improving calcium handling, specifically by increasing phosphorylation of phospholamban, which activates SERCA2A and accelerates calcium reuptake into the sarcoplasmic reticulum. More efficient calcium cycling results in stronger, more coordinated contractions. In addition, ZEB2 suppresses the calcineurin–NFAT (Nuclear Factor of Activated T-cells) signaling pathway, a major driver of pathological hypertrophy, thereby limiting maladaptive remodeling. ZEB2 also promotes angiogenesis after injury, improving perfusion of damaged tissue. Experimental gene therapy studies delivering ZEB2 to the heart have demonstrated improved recovery following myocardial infarction (91).

In cardiac fibroblasts, ZEB2 exerts a markedly different influence. It drives the transition to a myofibroblast phenotype, characterized by elevated expression of α-SMA (alpha-Smooth Muscle Actin), Smemb (Embryonic Form of Smooth Muscle Myosin Heavy Chain), and ED-A fibronectin (Extra domain type III A fibronectin). These cells exhibit reduced motility but increased contractile force, properties beneficial for wound stabilization yet potentially harmful if excessive, as they contribute to fibrosis. Mechanistically, this fibroblast activation appears to involve TGF-β–dependent signaling and repression of antifibrotic genes such as Meox2 (Mesenchyme Homeobox 2), pointing to the ZEB2–Ski–Meox2 axis as a potential target for modulating cardiac scarring (108).

Thus, ZEB2 functions as both a protector of cardiomyocyte performance and a driver of fibroblast-mediated fibrosis, underscoring its complex, context-dependent role in cardiac health and disease.

Understanding the pathways governing cardiac remodeling is critical because maladaptive remodeling underpins the progression from compensated hypertrophy to overt heart failure. This remodeling involves cardiomyocyte hypertrophy, fibrosis, altered extracellular matrix composition, and changes in cellular metabolism, all of which compromise myocardial function (18,109). Central transcriptional regulators

like ZEB1 and ZEB2 likely coordinate these processes by modulating gene expression networks that control cardiomyocyte phenotype and intercellular interactions. Consequently, dissecting their roles could illuminate novel therapeutic targets.

Taken together, these findings suggest ZEB1 and ZEB2 as a potential regulator of cardiomyocyte identity and structural integrity. It is dynamically regulated in response to cardiac stress, capable of driving maladaptive remodeling, and essential for preserving function under physiological conditions. Since ZEB1 is still poorly understood as comparison to ZEB2, understanding the molecular programs governed by ZEB1 in the heart may open the door to novel therapeutic strategies for heart failure.

1.9 ZEB1 as a Context-Dependent Transcriptional Repressor

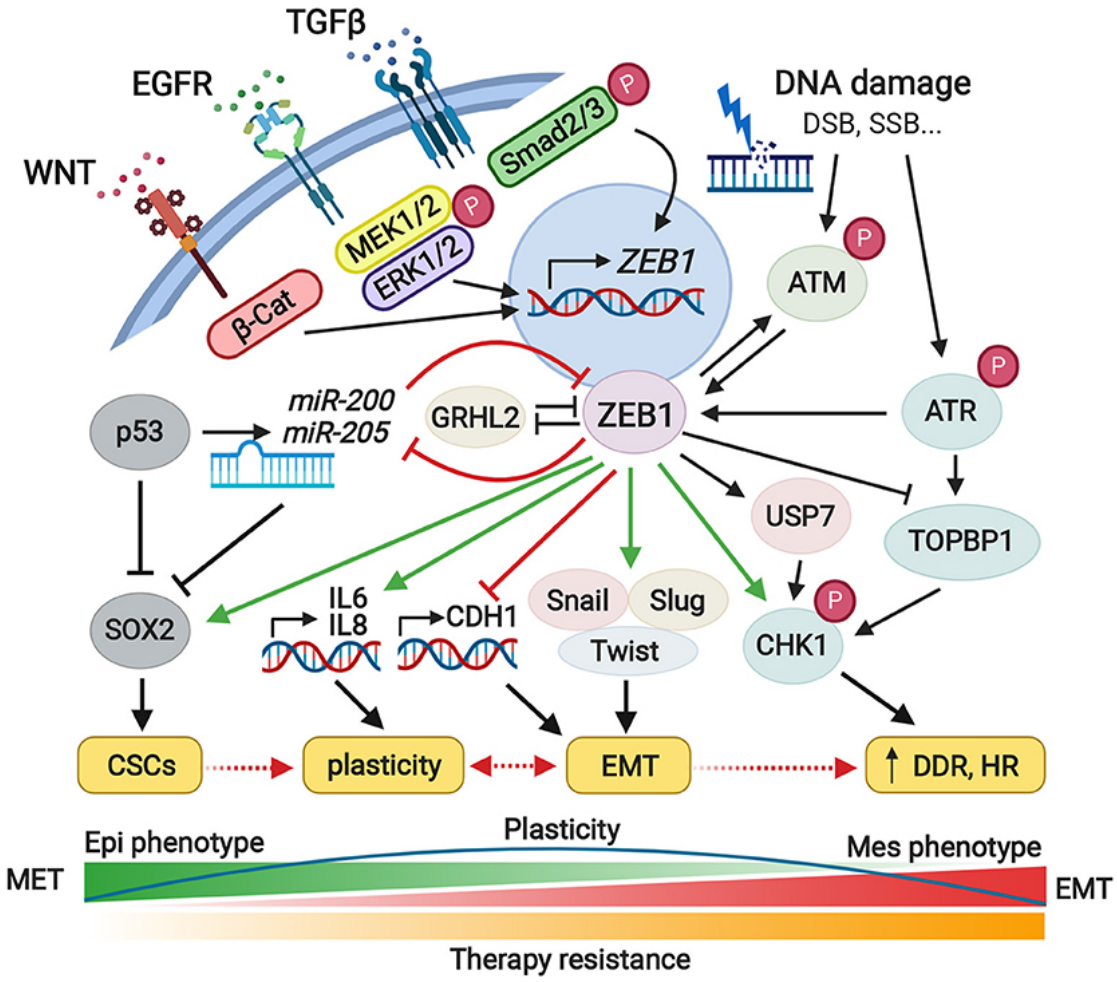

Figure 6. Zeb1 at the center of various signaling pathways (106).

Zeb1 integrates biomechanical, metabolic, and stress-related signals to maintain mesenchymal cellular identity. Upstream regulators include TGF-β, Wnt/β-catenin, and stress-responsive kinases, while downstream

Zeb1 activity suppresses epithelial gene programs, stabilizes mesenchymal genes, and induces cellular plasticity.

ZEB1 is a transcription factor best known for its role in EMT, a process crucial for embryogenesis, tissue repair, and cancer metastasis (102,110,111) (Fig. 6). ZEB1 functions primarily as a transcriptional repressor, suppressing epithelial genes such as *Cdh1* (E-cadherin) (112) while promoting mesenchymal traits, enabling increased cellular motility and plasticity (90,113,114) (Fig. 6). Beyond its established role in cancer biology, where it promotes tumor progression, metastasis, and treatment resistance, ZEB1 is also critical in tissue regeneration, fibrosis, and stem cell maintenance (87,89,97,101) (Fig. 7). For instance, in skeletal muscle, ZEB1 maintains the mesenchymal phenotype of satellite cells to facilitate effective repair (109). Through its interactions with chromatin remodelers, histone deacetylases, microRNAs, and signaling molecules, ZEB1 regulates transcriptional programs vital for tissue remodeling, stem cell maintenance, immune responses, and organ fibrosis (86,87,89,101,105,107). Despite these broad biological functions, ZEB1's role in the heart has remained largely unexplored until recently.

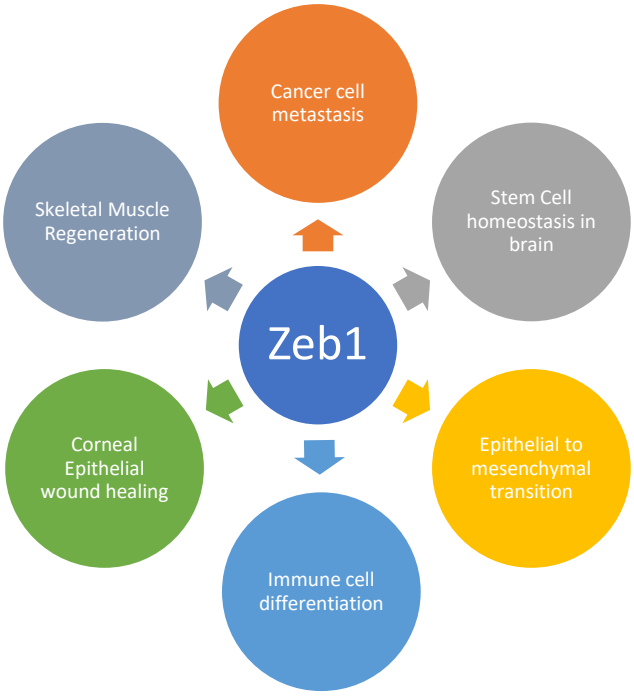

Figure 7. Zeb1 as a master regulator of different cellular processes.

1.9.1 Embryonic Development and Lineage Specification

ZEB1 is dynamically expressed during embryogenesis, particularly in regions undergoing EMT such as the neural crest, mesoderm, and somites. By repressing epithelial adhesion molecules like E-cadherin (CDH1) and promoting mesenchymal gene expression (e.g., vimentin, fibronectin), ZEB1 facilitates cell migration, differentiation, and organogenesis (92,94,104) (Fig. 8).

ZEB1's established reputation as a developmental regulator stems from its ability to control multiple cellular processes simultaneously. It influences collagen production and suppresses epithelial characteristics - functions that are particularly relevant during heart development, where cells must precisely coordinate their fate decisions and tissue organization (115).

1.9.2 ZEB1 in Cancer Progression and EMT

ZEB1 is perhaps best known for its role in promoting tumor progression and metastasis through EMT. By directly repressing genes like *CDH1*, *claudin*, and *occludin*, and upregulating mesenchymal markers, ZEB1 enables epithelial cells to acquire migratory and invasive capabilities (111) (Fig. 8). Its activation is frequently observed in aggressive tumors, including those of the breast, pancreas, prostate, and colon (97,98,116–118).

In breast cancer, ZEB1 expression correlates strongly with triple-negative and basal-like subtypes, where it promotes both metastasis and resistance to chemotherapy (100). It also drives cancer cell plasticity, allowing transitions between epithelial, mesenchymal, and cancer stem cell (CSC) states. Notably, ZEB1 interacts with the miR-200 family in a double-negative feedback loop: while ZEB1 represses miR-200 expression, miR-200 targets ZEB1 mRNA for degradation. This loop controls epithelial and mesenchymal phenotypes and regulates CSC characteristics and drug resistance (119) (Fig. 6).

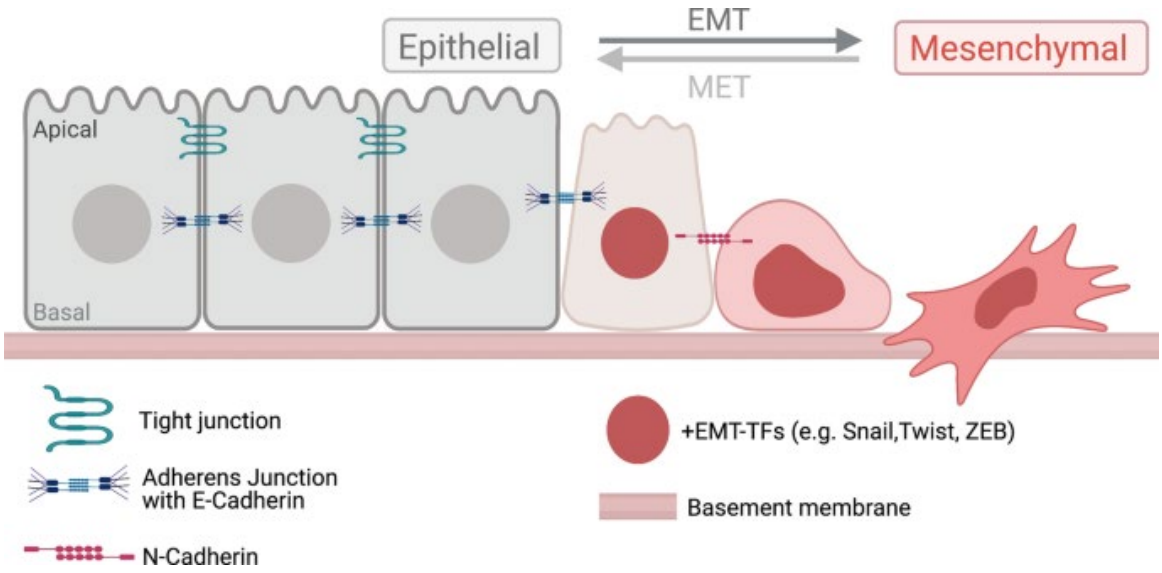

Figure 8. Epithelial to mesenchymal transition.

Schematic representing the morphological and cellular changes during Epithelial to mesenchymal transition leading to cellular plasticity and cancer cell metastasis (103).

In pancreatic ductal adenocarcinoma (PDAC), high ZEB1 expression is associated with poor prognosis, EMT induction, and immune evasion through PD-L1 (Programmed death-ligand 1) upregulation (120). ZEB1 also modulates the tumor microenvironment by promoting the secretion of immunosuppressive cytokines and altering fibroblast phenotypes.

1.9.3 Roles of Zeb1 in Different Biological Systems

In the central nervous system (CNS), ZEB1 regulates the balance between neural progenitor proliferation and differentiation. Loss of ZEB1 in murine models disrupts neural tube closure and neuroepithelial integrity, underscoring its developmental importance (86,121).

ZEB1 is critical in regulating neurogenesis, glial differentiation, and neural plasticity. It maintains neural stem cell self-renewal and influences radial glial progenitor differentiation. In adult neurogenesis, ZEB1 expression persists in the hippocampus and subventricular zone, where it modulates neural progenitor proliferation in response to injury or aging (121). Moreover, recent studies have implicated ZEB1 in neuroinflammatory responses and reactive gliosis following CNS injury (86), although these roles are still under investigation.

Zeb1 plays a critical role in corneal homeostasis, and its dysregulation has been implicated in corneal dystrophies, particularly posterior polymorphous corneal dystrophy (PPCD). Mutations or reduced expression of ZEB1 disrupt endothelial cell identity and function, leading to abnormal cell proliferation and fibrosis, which contribute to progressive vision impairment in affected individuals (122,123).

In macrophages, ZEB1 modulates polarization states, enhancing M2-type anti-inflammatory responses under certain conditions, suggesting it plays a role in both acute and chronic inflammation (124,125).

ZEB1 also contributes to immune escape mechanisms in cancer by inducing PD-L1 expression on tumor cells, leading to T cell anergy and immune tolerance (99). These findings position ZEB1 as a potential immunomodulatory target in both autoimmunity and oncology.

Recent research suggests ZEB1 may also participate in the regulation of glucose metabolism, insulin sensitivity, and adipose tissue inflammation. In models of type 2 diabetes, ZEB1 is found to modulate hepatic gluconeogenesis and may interact with Peroxisome Proliferator-Activated Receptor (PPAR) signaling pathways (126,127). In adipose tissue, ZEB1 expression is altered in obesity and may influence macrophage infiltration and cytokine production, linking it to metabolic syndrome and systemic inflammation (128,129).

Fibrotic disorders are characterized by chronic activation of mesenchymal programs and extracellular matrix deposition (130). ZEB1 is upregulated in fibroblasts during tissue injury and fibrosis, where it promotes myofibroblast activation and collagen synthesis (95). In Idiopathic Pulmonary Fibrosis (IPF), ZEB1 expression is elevated in lung epithelial cells and fibroblasts, facilitating EMT and contributing to matrix stiffening and impaired gas exchange (85). Similar roles have been identified in hepatic fibrosis and renal tubulointerstitial fibrosis, where TGF-β induces ZEB1 and acts downstream to propagate fibrotic gene expression (131).

While transient ZEB1 activation may aid in tissue repair, sustained expression often results in pathological scarring, organ dysfunction, and progression to failure.

1.9.4 Zeb1 in Cardiomyocyte Identity and Function

Given that cardiomyocytes are derived from mesoderm and retain mesenchymal characteristics, it is plausible that Zeb1 serves an analogous function in maintaining their differentiated state. Unlike in epithelial tissues, where Zeb1 promotes a mesenchymal shift (131), in cardiomyocytes, it may preserve mesenchymal traits by actively repressing epithelial gene expression and safeguarding organelle architecture critical for contractile function. However, the role of Zeb1 in the myocardium has remained largely unexplored.

During cardiac development, ZEB1 contributes to several essential morphogenetic events, including mesoderm formation, early cardiac progenitor specification, and chamber morphogenesis. Its expression is dynamically regulated in the embryonic heart, where it influences the balance between cellular proliferation, differentiation, and migration. ZEB1 also modulates key signaling pathways such as TGF-β, Wnt/β-catenin, and Notch, each crucial for heart formation and maturation. Additionally, its interaction with microRNAs and epigenetic regulators allows ZEB1 to fine-tune gene expression networks involved in cardiac cell lineage decisions and structural organization (132).

The heart's formation requires carefully choreographed transitions where cells change their identity and behavior, processes reminiscent of EMT. ZEB1's expertise in suppressing epithelial markers while promoting mesenchymal characteristics positions it as a potential conductor of these cardiac developmental transitions (114,133,134). During heart tube formation and valve development, such cellular flexibility is essential for proper organ construction (135).

During early cardiac development, cardiomyocyte proliferation is essential to build myocardial mass (84). Although ZEB1 is traditionally associated with cell cycle repression in many tissues, its role in cardiomyocyte proliferation appears nuanced (71).

Studies have shown that ZEB1 is dynamically regulated in the developing heart. In early stages, ZEB1 may contribute to proliferative expansion by repressing epithelial differentiation genes and maintaining a more progenitor-like, mesenchymal phenotype (136). In support of this, ZEB1 has been linked to

repression of cell cycle inhibitors and may allow transit through G1/S by modulating key cell cycle checkpoints under certain conditions (71).

One of the most compelling discoveries about ZEB1's cardiac role comes from studies of embryonic stem cells - the cellular starting point for all tissues in the developing embryo. Researchers have uncovered an intricate molecular partnership between ZEB1, HDAC2 (Histone Deacetylase 2), and eNOS (endothelial nitric oxide synthase) that appears crucial for steering stem cells toward becoming cardiovascular tissues (107). The ZEB1-HDAC2-eNOS circuit seems to be the molecular machinery that enables this mechanism (107). The production of nitric oxide during these early developmental stages is not just coincidental - it triggers a cascade of cellular conversations that push cells toward mesendoderm formation, the tissue layer that gives rise to the heart and blood vessels (107). This represents a previously unrecognized way that ZEB1 contributes to cardiovascular development, extending beyond its well-known role in cell type transitions.

1.10 Preliminary Data and Project Aims

Preliminary studies suggest that ZEB1 expression is dynamically regulated in the myocardium, particularly under pathological stress. In a mouse model of pressure overload using transverse aortic constriction (TAC), ZEB1 protein expression increased markedly as early as two days post-surgery and remained elevated for several weeks, despite stable mRNA levels, indicating a likely post-transcriptional regulatory mechanism. RNA-binding protein such as CPEB4 has been implicated in this regulation, stabilizing Zeb1 mRNA translation under stress conditions. In genetically driven cardiomyopathies, divergent Zeb1 expression patterns have been observed: it is upregulated in hypertrophic models such as Mybpc3 KO mice (137) but downregulated in dilated models like Rbm20 KO mice (9,138). These findings point to Zeb1 as a context-sensitive modulator of cardiac remodeling, whose regulation may be critical to the balance between adaptive and maladaptive responses.

Based on these initial observations and literature survey we formulated the following hypothesis:

Zeb1 is essential for maintaining cardiomyocyte structure and function.

We propose that its overexpression contributes to maladaptive cardiac hypertrophy, loss of Zeb1 leads to cardiac dysfunction as well.

To address this hypothesis, we have the following aims:

Aim 1: Checking the Zeb1 overexpression phenotype *in vitro* and *in vivo*.

To test whether ZEB1 is not only associated with but also causally involved in cardiac remodeling, we aim to conduct gain-of-function experiments. Zeb1 will be overexpressed in neonatal rat cardiomyocytes (NRCMs), and the cell size and gene expression of hypertrophic markers, such as *Nppa* and *Nppb,* will be measured. In addition to that, we are also planning *in vivo*, adeno-associated virus (AAV9)-mediated cardiac-specific overexpression of Zeb1 in adult mice. Left ventricular hypertrophy would be checked by echocardiography, histopathology, and molecular markers to confirm that elevated ZEB1 is sufficient to induce maladaptive remodeling.

Aim 2: Checking the structure and function of cardiomyocytes in a conditional Zeb1 KO model.

We bred a cardiomyocyte-specific Zeb1 knockout by crossing mice carrying a floxed Zeb1 allele with a Myh6-Cre driver line, enabling targeted deletion of Zeb1 in heart muscle cells (citation). This model would be used to assess the impact of Zeb1 loss-of-function on cardiac health. Left ventricular performance would be evaluated using echocardiography, complemented by histological examinations and molecular analyses. Based on these findings, we would further characterize ultrastructural alterations in cardiomyocytes employing techniques such as transmission electron microscopy (TEM) and contractility measurements using IonOptix.

Aim 3: Checking the structure and function of cardiomyocytes in an inducible conditional Zeb1 KO model.

To understand the role of Zeb1 in adult cardiomyocytes after complete maturation we generated an inducible conditional knockout (icKO) mouse line to delete Zeb1 specifically in adult cardiomyocytes, allowing us to bypass developmental effects of gene loss. This was achieved by crossing mice harboring a floxed Zeb1 allele with a Myh6-MerCreMer (α-myosin heavy chain promoter–driven, tamoxifen-

inducible Cre recombinase) transgenic line. This results in precise, temporally controlled excision of Zeb1 specifically in cardiomyocytes of adult mice. The echocardiography and histological analysis would be done to investigate whether Zeb1 plays an important role in the maintenance of cardiomyocyte homeostasis after maturation.

Aim 4: Identifying the differentially regulated genes involved and the Zeb1 target genes responsible for cardiomyocyte structural and functional defects.

To uncover the molecular consequences of ZEB1 loss, we would be performing bulk RNA-sequencing on left ventricular tissue from Zeb1 cKO and wild-type mice. We would look for the differentially regulated genes involved in different biological processes involved in the maintenance of cardiomyocyte structure and function. To identify the Zeb1 target genes we would also perform Chromatin immunoprecipitation sequencing.

2. Materials

2.1 Chemicals and reagents

Table 1. List of chemicals and reagents

Chemical or reagent	Vendor	Catalog number
2-deoxy-D-glucose	Sigma-Aldrich	D8375-5G
2-mercaptoethanol	Sigma-Aldrich	M6250-250ML
4-(2-hydroxyethyl)-1-piperazineethanesulfonic acid (HEPES)	Thermo Fisher Scientific	15630056
6bK (IDE inhibitor)	Tocris / Bio-Techne	5402/500U
Acetic acid	Honeywell	64-19-7
Agarose	Carl Roth	2267.4
Ampicillin	Sigma-Aldrich	A9518-25G
Azidohomoalanine (AHA)	AnaSpec	AS-63669
BDM	Sigma-Aldrich, Singapore	B0753
Bouin's solution	Sigma-Aldrich	HT10132
Bovine Serum Albumin	Sigma-Aldrich, Singapore	A1470
Butanedione monoxime	Sigma-Aldrich	B0753-100G
Cadmium chloride (CdCl2)	Honeywell	20899
Calcium chloride (CaCl2)	Carl Roth	A119.1
Chemically defined lipid concentrate	Thermo Scientific, Singapore	11905-031
Chloroform	Merck	32211
Citric acid, anhydrous	Sigma-Aldrich	C3674-500G
Collagenase 2	Worthington, USA	LS004176
cOmplete Protease Inhibitor Cocktail	Sigma-Aldrich	11873580001
Cycloheximide (CHX)	Sigma-Aldrich	C1988
DAPI	Thermo Fisher Scientific	D21490
Di-sodium hydrogen phosphate (Na2HPO4)	Carl Roth	P030.2
Dialyzed fetal bovine serum	Thermo Fisher Scientific	A3382001
Dithiothreitol (DTT)	Sigma-Aldrich	43819
DMEM (high glucose, with pyruvate)	Thermo Fisher Scientific	21969035
DMEM (no glucose, no glutamine, no phenol red)	Thermo Fisher Scientific	A1443001
DMEM for SILAC	Thermo Fisher Scientific	88364
DMEM/F12 Medium	Thermo Scientific, Singapore	11320-033

Dynabeads Sheep Anti-Rabbit IgG	Thermo Fisher Scientific	11203D
Dynabeads Sheep Anti-Rat IgG	Thermo Fisher Scientific	11035
Endothelial Cell Growth Medium 2	PromoCell	C-22111
Endothelial Cell Growth Supplement /Heparin	PromoCell	C-30120
Ethanol (EtOH)	Sigma-Aldrich	51976
Ethidium bromide	Sigma-Aldrich	E1510
Ethylenediaminetetraacetic acid (EDTA)	Sigma-Aldrich	E5134
Eukitt quick-hardening mounting medium	Sigma-Aldrich	03989-100ML
Fetal bovine serum (FBS)	Thermo Fisher Scientific	10270
Fibronectin	Sigma-Aldrich	F1141
Formaldehyde	Carl Roth	4980.4
Gelatine	Sigma-Aldrich	G9391-100G
Gene Ruler 1 kb DNA ladder	Thermo Fisher Scientific	SM0313
Glucose	Sigma-Aldrich, Singapore	G8270
Glutaraldehyde solution	Sigma-Aldrich	G6257-100ML
GlycoBlue coprecipitant	Thermo Fisher Scientific	AM9516
HBSS (without Ca, Mg)	Thermo Fisher Scientific	14175053
Heparin	Ratiopharm	N68542.04
HEPES	1st Base, Singapore	BIO-1825
HiPerFect Transfection Reagent	Qiagen	301704
Hydrochloric acid	Honeywell	30721
Hydrogen peroxide (H2O2)	Merck-Millipore	107209
Isoflurane	Baxter	HDG9623
Isolectin IB4, Alexa Fluor 594 conjugate	Thermo Fisher Scientific	I21413
Isopropanol	Sigma-Aldrich	I9516
iTaq Universal SYBR Green Supermix	Bio-Rad Laboratories	1725124
ITS supplement	Sigma-Aldrich, Singapore	I3146
KCl	Sigma-Aldrich, Singapore	P9541
L-arginine (13C6,15N4)	Cambridge Isotope Laboratories	CNLM-539-H-PK
L-arginine (13C6)	Cambridge Isotope Laboratories	CLM-2265-H-PK
L-Glutamine	Thermo Fisher Scientific	25030081

L-lysine (13C6,15N2)	Cambridge Isotope Laboratories	CNLM-291-H-PK
L-lysine (4,4,5,5-D4)	Cambridge Isotope Laboratories	DLM-2640-PK
Laemmli Sample Buffer	Bio-Rad Laboratories	161-0747
Laminin (murine)	Thermo Scientific, Singapore	23017-15
LB-Agar	Carl Roth	6671
M199 Medium	Sigma-Aldrich, Singapore	M4530
Magnesium chloride (MgCl2)	Sigma-Aldrich	P9333-1KG
Magnesium sulfate (MgSO4)	Sigma-Aldrich	M2643-500G
Mammalian Polysome Buffer	Illumina	ASBHMR1212
Matrigel Growth Factor Reduced Basement Membrane Matrix	Corning	356231
MEM Amino Acids Solution	Thermo Fisher Scientific	11130036
MEM Non-Essential Amino Acids Solution	Thermo Fisher Scientific	11140035
Methanol	VWR Chemicals	20847.307
MgCl2	Sigma-Aldrich, Singapore	M8266
NaH2PO4	Sigma-Aldrich, Singapore	S8282
Nonidet P-40 Substitute (NP-40)	Sigma-Aldrich	74385-1L
Paraffin Paraplast	Leica	39601006
Paraformaldehyde	Electron Microscopy Sciences	15713-S
Penicillin-Streptomycin	Thermo Fisher Scientific	15140122
Penicillin-Streptomycin-Glutamine	Thermo Fisher Scientific	10378016
Percoll	GE Healthcare	17-0891-02
Phenol Red	Sigma-Aldrich	P3532-25G
Phenylephrine hydrochloride (PE-HCl)	Sigma-Aldrich	P6126-10G
Phosphate buffered saline	Lonza, USA	17-512F
Phosphate buffered saline (PBS)	Sigma-Aldrich	D8537-500ML
PhosSTOP phosphatase inhibitors	Sigma-Aldrich	4906837001
Polyethylenimine hydrochloride (PEI)	Polysciences	24765-2
Ponceau S	Sigma-Aldrich	P3504
Potassium chloride (KCl)	Carl Roth	6781.1
Potassium hydrogen carbonate (KHCO3)	Carl Roth	P748.2

Powdered milk	Carl Roth	T145.2
primaAMP 2× PCR Master Mix Red	Steinbrenner	SL-9612
Primocin	Invivogen	ant-pm-2
Protease XIV	Sigma-Aldrich, Singapore	P5147
Puromycin	Sigma-Aldrich	540411
QIAzol Lysis Reagent	Qiagen	79306
RPMI 1640 medium without amino acids	US-Biological	R8999-04A
Sodium chloride (NaCl)	Carl Roth	9265.2
Sodium deoxycholate	Sigma-Aldrich	D6750-100G
Sodium dodecyl sulfate (SDS)	Serva	20765.03
Sodium hydrogen carbonate (NaHCO3)	Carl Roth	6885.5
Sodium hydroxide (NaOH)	Sigma-Aldrich	30620
SUPERase In RNase Inhibitor	Thermo Fisher Scientific	AM2696
SYBR Safe DNA Gel Stain	Thermo Fisher Scientific	S33102
Taurine	Sigma-Aldrich	T8691-100G
Thiazolyl Blue Tetrazolium Bromide (MTT)	Sigma-Aldrich	M5655-500MG
Tris	Carl Roth	4855.1
Tris hydrochloride (Tris-HCl)	Carl Roth	9090.2
Triton X-100	Sigma-Aldrich	X100-500ML
Trypsin	Thermo Fisher Scientific	15090046
Trypsin-EDTA	Thermo Fisher Scientific	25200056
TSA Blocking Reagent	PerkinElmer	FP1012
Tween 20	Carl Roth	25300-120
Vectashield Antifade Mounting Medium	Vector Laboratories	H-1000
Water, nuclease-free	Thermo Fisher Scientific	AM9937
Weigert's iron hematoxylin solution	Sigma-Aldrich	HT1079-1SET
WesternBright ECL	Advansta	541005
Wheat Germ Agglutinin (WGA), FITC conjugate	Sigma-Aldrich	L4895-2MG
XT MES Running Buffer	Bio-Rad Laboratories	1610789
XT MOPS Running Buffer	Bio-Rad Laboratories	1610788
Xylene	Carl Roth	9713.5

2.2 Kits

Table 2. List of kits

Chemical or Reagent	Vendor	Catalog number
DC-Protein Assay	Bio-Rad Laboratories	5000112
First Strand cDNA Synthesis Kit	Thermo Fisher Scientific	K1612
Hematoxylin & Eosin fast staining kit	Carl Roth	9194.1
High Sensitivity DNA Kit	Agilent Technologies	5067-4626
HiSpeed Plasmid Midi Kit	Qiagen	12643
iScript cDNA Synthesis Kit	Bio-Rad	1708891
iTaq Universal SYBR Green Supermix	Bio-Rad	1725124
peqGOLD Plasmid Miniprep Kit I	VWR Chemicals	13-6943-02
Pierce Silver Stain Kit	Thermo Fisher Scientific	24612
Qubit dsDNA High Sensitivity Assay Kit	Thermo Fisher Scientific	Q32855
Quick-RNA MiniPrep Kit	Zymo Research	R1055
Quant-Seq	Lexogen	15.24
RNA Clean & Concentrator	Zymo Research	R1013
TMT10plex Isobaric Label Reagent Set	Thermo Fisher Scientific	90110
Trichrome Stain (Masson) Kit	Sigma-Aldrich/Merck	HT15-1KT
TruSeq Ribo Profile (Mammalian) Library Prep Kit	Illumina	ASLPA1212

2.3 Enzymes

Table 3. List of enzymes

Enyzme	Vendor	Catalog number
Collagenase type 2	Worthington Biochemical	LS0004176
Deoxyribonuclease I	Worthington Biochemical	LS002006
DNase I (grade II)	Sigma-Aldrich	10104159001
Gateway LR Clonase II Enzyme mix	Thermo Fisher Scientific	11791020

Liberase DH	Sigma-Aldrich	5401054001
PacI	New England Biolabs	R0547L
Protease		
RNase I	Invitrogen	AM2295
SacII	New England Biolabs	R0157L
T4 Polynucleotide Kinase	New England Biolabs	M0201S
TURBO DNase	Invitrogen	AM2239

2.4 Antibodies

Table 4. List of antibodies

Target	Species	Dilution	Supplier	Catalog number
Western Blot				
Zeb1	Rabbit	1:1000	Thermo Scientific	703354
B-Tubulin	Rabbit	1:1000	Abcam	Ab6046
Actin	Mouse	1:1000	Santa Cruz Biotechnology	sc-8432
Troponin T	Rabbit	1:2000	Abcam	ab209813
E Cadherin	Rabbit	1:1000	Proteintech	20874-1-AP
Cytokeratin 8	Rabbit	1:1000	Proteintech	27105-1-AP
Peroxidase-AffiniPure Anti-Mouse	donkey		Jackson Immuno Research	715035151
Peroxidase-AffiniPure Anti-Rabbit	Goat		Jackson Immuno Research	111035144
Immunohistochemistry				
Zeb1	Rabbit	1:100	Thermo Scientific	703354
Sarcomeric Actinin	Mouse	1:1000	Santa Cruz Biotechnology	sc-8432
CSRP3	Rabbit	1:1000	Proteintech	10721-1-AP
Wheat Germ Agglutinin, FITC conjugate		1:50	Sigma-Aldrich	L4895-2MG

Anti-rabbit IgG-FITC	Donkey	1:100	Jackson Immuno Research	711-095-152
Anti-rabbit IgG-Cy3	Donkey	1:100	Jackson Immuno Research	711-165-152
Anti-Mouse IgG-FITC	Donkey	1:100	Jackson Immuno Research	715-095-151
Anti-Mouse IgG-Cy3	Donkey	1:100	Jackson Immuno Research	715-165-151

Immunoprecipitation			
Zeb1	Rabbit	Thermo Scientific	703354
(DA1E) mAb IgG XP®	Rabbit	Cell Signalling Technology	D2A11
Dynabeads Anti-Rabbit IgG	Sheep	Thermo Fisher Scientific	11203D

2.5 Primers

Table 5. List of primers

Antibody	FOR	REV
Mouse and Rat 18s	CGA GCC GCC TGG ATA CC	CAT GGC CTC AGT TCC GAA AA
Mouse *Hprt*	GGGGCTGTACTGCTTAAC CAG	TCAGTCAACGGGGGACATAA A
Rat *Nppa*	GGAGCAAATCCTGTGTAC AGTG	ACCTCATCTTCTACCGGCAT
Rat *Nppb*	GCAGCATGGATCTCCAGA AGG	CTGCAGCCAGGAGGTCTTCC
Mouse *Nppa*	TTG TGG TGT GTC ACG CAG CT	TGT TCA CCA CGC CAC AGT G
Mouse *Nppb*	TCC TAG CCA GTC TCC AGA GCA A	GGT CCT TCA AGA GCT CTG TCT G
Mouse *Zeb1*	ATT CAG CTA CTG TCA GCC CTG C	CAT TCT GGT CCT CCA CAG TGG A
Mouse *Zeb2*	GAG CAG GTA ACC GCA AGT TC	AAG CGT TTC TTG CAG TTT GG
Rat *Myh6*	TAA CCG GAG TTT AAG AGT GAC AGG	TAG GCG CTC CTT CTC TGA CT
Mouse *Myh6*	GCA AAG GAG GCA AGA AGA AAG G	TGA GGG TGG GTG GTC TTC AG
Mouse *Col1a1*	GCT CCT CTT AGG GGC CAC T	CCA CGT CTC ACC ATT GGG G

2.6 Buffers and Solutions

2.6.1 Buffers for genotyping

Table 6. List of buffers for genotyping

Buffer	Composition
Buffer A	25 mM NaOH, 200 µM EDTA
Buffer B	40 mM Tris-HCl
TAE (50×)	2 M Tris, 1 M acetic acid, 50 mM EDTA

2.6.2 Buffers for cell and tissue lysate preparation

Table 7. List of buffers for cell and tissue lysate preperation

Buffer	Composition
Mammalian Lysis Buffer	1× Mammalian Polysome Buffer (Illumina), 1 % (v/v) Triton X-100, 1 mM DTT, 0.01 U/µL TURBO DNase, 0.1 mg/mLcycloheximide
RIPA buffer	150 mM NaCl, 25 mM Tris-HCl (pH=7.4), 1 % (v/v) NP-40, 0.5 % (w/v) sodium deoxycholate, 1 % (w/v) SDS, cOmplete Protease Inhibitor Cocktail, PhosSTOP phosphatase inhibitors

2.6.3 Buffers for immunoprecipitation of Zeb1 from mouse heart lysates

Table 8. List of buffers for immunoprecipitation

Buffer	Composition
Lysis buffer	150 mM NaCl, 25 mM Tris-HCl (pH=7.4), 1 % (v/v) NP-40, 0.5 % (w/v) sodium deoxycholate, 0.1 % (w/v) SDS, cOmplete Protease Inhibitor Cocktail
Wash buffer	lysis buffer with 500 mM NaCl

2.6.4 Buffers for immunohistochemistry and immunofluorescence

Table 9. List of buffers for immunohistochemistry and immunoflorescence

Buffer	Composition
Citrate buffer	10 mM citric acid (anhydrous), pH=6.0
PBS	137 mM NaCl, 2.7 mM KCl, 10 mM Na2HPO4, 1.8 mM KH2PO4, pH=7.4
TN buffer	0.1 M Tris, 0.15 M NaCl, pH=7.5-8.0
TNB blocking solution	0.5 TSA blocking reagent in TN buffer

2.6.5 Buffers for western blotting

Table 10. List of buffers for western blotting

Buffer	Composition
Ponceau S solution	0.1 % (w/v) Ponceau S, 5 % (v/v) acetic acid
TBST	150 mM NaCl, 20 mM Tris, 0.1 % (v/v) Tween 20, pH=7.4
Transfer buffer	190 mM glycine, 25 mM Tris, 20 % (v/v) methanol

2.6.6 Cell culture solutions and media for neonatal rat cardiomyocytes

Table 11. List of cell culture solutions and media for neonatal rat cardiomyocytes

Solution	Composition
Digestion Solution (in HBSS)	0.25 % (v/v) trypsin, 300 U/mL DNase I (grade II), 0.4 M HEPES, 0.0016 M NaOH, 2% (v/v) Penicillin-Streptomycin
Stop Solution (in HBSS)	4 % (v/v) FBS, 300 U/mL DNase I (grade II), 2% (v/v) Penicillin-Streptomycin
ADS (10×)	1.16 M NaCl, 180 mM HEPES, 8.45 mM Na2HPO4, 55.5 mM glucose, 53.7 mM KCl, 8.31 mM MgSO4, pH=7.35±0.5
NRCM Culture Medium	DMEM/F-12, 10% (v/v) FBS, 1% (v/v) Penicillin-Streptomycin-Glutamine
NRCM Treatment Medium	DMEM/F-12, 0.5% (v/v) FBS, 1% (v/v) Penicillin-Streptomycin-Glutamine

2.6.7 Buffers and cell culture media for adult mouse cardiomyocytes

Table 12. List of buffers and cell culture media for adult mouse cardiomyocytes

Solution	Composition
EDTA buffer	130 mmol/l NaCl, 5 mmol/l KCl, 0.5 mmol/l NaH2PO4, 10 mmol/l HEPES, 10 mmol/l Glucose, 10 mmol BDM, 10 mmol/l Taurine, and 5 mmol/l EDTA. Make in 1 litre ultrapure 18.2 MΩ.cm H2O. Adjust to pH 7.8 using NaOH. Sterile filter.
Perfusion buffer	130 mmol/l NaCl, 5 mmol/l KCl, 0.5 mmol/l NaH2PO4, 10 mmol/l HEPES, 10 mmol/l Glucose, 10 mmol BDM, 10 mmol/l Taurine, and 1 mmol/l MgCl2. Make in 1 litre ultrapure 18.2 MΩ.cm H2O. Adjust to pH 7.8 using NaOH. Sterile filter.
Collagenase buffer	Prepare Collagenase buffer by diluting 2.5 mg/ml Collagenase Type 2 in Perfusion buffer. Make fresh immediately before isolation.
Stop buffer	Stop buffer is made with Perfusion buffer containing 5% sterile FBS. Make fresh on day of isolation.

Media constituents	Note 1: 100x BDM stocks (= 1 mol/l) are prepared by dissolving 1.01 g BDM in 10 ml ultrapure 18.2 MΩ.cm H2O, filter-sterilised, and stored in aliquots at -20°C. Note 2: 50x bovine serum albumin (BSA) stocks (= 5% w/v) are prepared by dissolving 1 g BSA in 20 ml PBS, filter-sterilized, and stored at 4°C. Keep sterile. Note 3: M199 and DMEM/F12 media used here are supplied with l-glutamine already included. Ensure l-glutamine addition if using different suppliers. Note 4: Penicillin/Streptomycin (P/S) antibiotic addition is optional.
Plating media (for 100ml)	93ml M199, 5% FBS, 10 mmol/l BDM, and 1ml P/S. Sterile filter, and keep sterile.
Culture media (for 100ml)	94 ml M199, 0.1% BSA, 1ml ITS (Insulin, transferrin, selenium.), 10 mmol/l BDM, 1ml CD lipid (chemically defined lipid concentrate), and 1ml P/S. Sterile filter, and keep sterile. Protect from light.
Calcium reintroduction buffers	For total volume of 20 ml per calcium reintroduction buffer. Make fresh on day of isolation. Buffer 1: 15 ml Perfusion Buffer and 5 ml Culture Media Buffer 2: 10 ml Perfusion Buffer and 10 ml Culture Media Buffer 3: 5 ml Perfusion Buffer and 15 ml Culture Media

2.7 Plasmids

Table 13. List of plasmids

Name	Supplier	Details
pExp_ZEB1 (NM_011546.3)	V. Kamuf-Schenk	Mus musculus zinc finger E-box binding homeobox 1 (Zeb1), transcript variant 1, mRNA
pAD_ZEB1 (NM_011546.3)	V. Kamuf-Schenk	Viral Expression (Adenoviral)
pSSV9_hTNT_Zeb1	V. Kamuf-Schenk	Viral Expression (Adeno assozierte Viren) smaler promotor and no viral enhancer, cardiac myocyte promotor (limit <5000bp)
CO pSSV9_hTNTV	V. Kamuf-Schenk	Viral Expression (Adeno assozierte Viren) smaler promotor and no viral enhancer, cardiac myocyte promotor (limit <5000bp)

2.8 Consumables

Table 14. List of consumables

Item	Supplier	Catalog number
96 well lates, 0.2ml	Greiner	655180
Amersham Hybond-N+ membrane	GE Healthcare	RPN203B
Aspiration Pipettes, sterile 2 ml	Greiner bio-one	710183
Bis-Tris Protein Gel: 4-12% Criterion™ XT, 18 well	Bio-Rad	3450124
Bis-Tris Protein Gel: 4-12% Criterion™ XT, 26 well	Bio-Rad	3450113
Cell Scraper	Greiner bio-one	341070
CL-XPosure™ Film, 20 x 25 cm	Thermo Fisher	34091
Conical Centrifuge Tubes 15 ml	Greiner bio-one	188271
Conical Centrifuge Tubes 50 ml	Greiner bio-one	352070
Cover slips (24 x 60 mm)	Marienfeld GmbH	101242
E-Plate Cardio 48	ACEA Biosciences	300600940
Filter Tip1 10 µl	Neptune Scientific	976-010
Filter Tip1 1000 µl	Neptune Scientific	976-1250
Filter Tip1 20 µl	Neptune Scientific	976-020
Filter Tip1 200 µl	Neptune Scientific	976-200
Gel loading Tips: Gel-Saver	Kisker, Steinfurt	GSII054R
MicroAmp™ Fast Optical 96 well, 0.1 ml	Applied Biosystems™	4346907
Nunclon R Cell Culture, 15 cm	Merck	Z755923-150EA
Nunc™ Cell Culture/Petri Dishes	Thermo Scientific	168381
Nunc™ Lab-Tek™ Chamber Slide	Thermo Fisher	177429PK
Parafilm	Sigma-Aldrich/Merck	P7793
PCR plate, 96-well	Steinbrenner	SL-PP96-3L
Pipette Tips 10 µl	StarLab	S1111-3700
Pipette Tips 1000 µl	StarLab	S1111-6810-C
Pipette Tips 20 µl	StarLab	S1111-070
Pipette Tips 200 µl	StarLab	S1111-0706

Primer bundle for qPCR	Steinbrenner Laborsystemes	SL-PP-PB3LB
PVDF-Membrane Immobilion-P	Millipore/Merck	IPVH00010
Scalpel	Feather	02.001.30.010
Serological Pipette, 10 ml	Sarstedt	356551
Serological Pipette, 25 ml	Sarstedt	861.685.001
Serological Pipette, 5 ml	Sarstedt	356543
Tissue culture flasks T25	Sarstedt	833.910.002
Tissue culture flasks T75	Sarstedt	833.911
Well Plates 12-wells	Greiner bio-one	665180
Well Plates 6-wells	Greiner bio-one	657160
White opaque 96 well Microplate, Optiplate	PerkinElmer	6005290
Zymo-Spin IC Columns	Zymo research	C1004-250
Zymo-Spin IIICG columns	Zymo research	C1006-250-G

2.9 Lab equipments

Table 15. List of lab equipments

Devices	**Supplier**
Agilent 2100 Bioanalyzer	Agilent
Axio Observer Z1 fluorescence microscope	Zeiss
Bioruptor® Plus sonication device	Diagenode
Cell Incubator: Hera Cell® 240i	Thermo Fisher Scientific
Criterion Cell System	Bio-Rad
Enspire Multimode Plate Reader	Perkin Elmer
Gel Imaging System, UV Transilluminator	Biostep
Harvard volume-cycled rodent ventilator	Harvard Apparatus
HistoCore PEARL	Leica
Horizontal electrophoresis system	Bio-Rad
Hypoxia cell incubator	Binder
IonOptix Cytocypher	Ionoptix
Laminar Flow Hood: Herasafe 2030i	Thermo Fisher Scientific
Laser Scanning Microscope: Cell Observer SD	Zeiss
Leica Confocal Microscope: SP8	Leica
LI-COR odyssey XF	Licorbio
Multi Shaker, Plattform 409 x 297 mm	NeoLab
Magnetic stirrer: neo Mag® 1500 UpM	NeoLab

Microtome	Leica
Mini Trans-Blot Cell	Bio-Rad
Nanodrop™ spectrometer	Thermo Fisher Scientific
Power Pac™ HC	Bio-Rad
Real-time PCR system: Viia 7	Thermo Fisher Scientific
Thermal Cycler: C1000 Touch™	Bio-Rad
Tissue homogenizer, Bullet Blender	Next Advance
Visual Sonics Vevo F2 Imaging System	Visual sonics

2.10 Softwares

Table 16. List of softwares used

Software	Publisher
Biorender	Biorender
Blast	NCBI
ChatGPT	ChatGPT
IGV Viewer	IGV
Image J (Fiji)	SciJava
Microsoft Office	Microsoft
Primer-Blast	NCBI
Prism	Graphpad
R Studio	RStudio, Inc
Illustrator	Adobe
VevoLab 5.9.0	Visualsonics

3. Methods

3.1 Animal models

Animal procedures for this project were approved by the regional council of Baden-Württemberg and executed in accordance with the Animal Welfare Regulation Governing Experimental Animals (Approval number is G190/21). Zeb1 cKO mice were generated using the C57BL/6J mouse strain in the laboratory of Prof. Dr. Thomas Brabletz at the Clinical Molecular Biology Research Center (KMFZ), Friedrich-Alexander University Erlangen-Nuremberg (139). Zeb1 cKO mice were crossed with the MerCreMer line to generate a tamoxifen-inducible Zeb1 cKO model. Animals were kept and bred in the central animal facility of the University of Heidelberg, in a temperature- and humidity-controlled environment with a 12:12-hour light-dark cycle and with ad libitum access to standard chow.

3.1.1 Genotyping Zeb1 KO mouse

To isolate genomic DNA, ear clips from Zeb1 KO mice were boiled in 50 µL Buffer A for 35 min at 95◦C. 50 µL Buffer B was then added, and samples were thoroughly mixed. Compositions of these buffers are given in section 2.6.1. PCR amplification was performed using primaAMP 2× PCR Master Mix Red, 800 nM Zeb1 genotyping forward primer, 800 nM Zeb1 genotyping reverse primer, and 4 µL of ear clip extract. Cycling conditions were as follows: 2 min at 94◦C, followed by 35 cycles of 10 sec at 96◦C, 15 sec at 60◦C, 45 sec at 72◦C, and a final 10 min extension at 72◦C. PCR products were loaded on a 1.5 % agarose gel with ethidium bromide, run in 1× TAE buffer, and visualized under a UV light. Expected amplicons are shown in Fig.9.

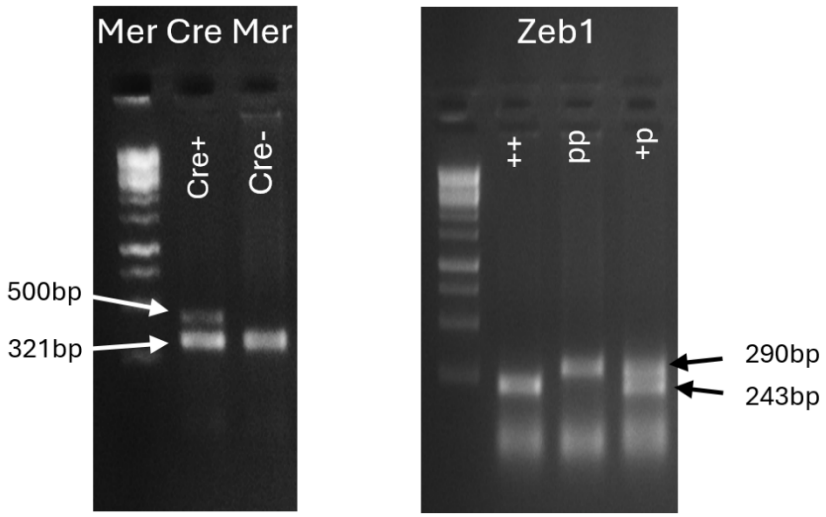

Figure 9. Agarose gel picture for Zeb1cKO/Zeb1icKO genotyping.

3.1.2 Echocardiography

For the echocardiography, the Visual Sonics Vevo F2 Imaging System was utilized. The UHF46x b transducer was used to capture images from the parasternal long and short heart axes to describe the thickness and function of the anterior and posterior walls. Images were first captured in B-mode, and then a time-dependent cross-section was captured in M-mode. Before measurements, animals were shaved to improve image quality and reduce background. The animals were placed horizontally on the 37°C heated plate with 1.5 vol% isoflurane anesthesia. Electrode gel was utilized to transmit heart and breathing rates. To enable picture comparison and prevent bias in heart function measures, images were taken with a heart rate ranging from 350 to 500 beats per minute. The evaluation was accomplished using the VevoLab 5.9.0 software.

3.1.3 Preparation of mouse heart lysates

Mice were sacrificed by cervical dislocation, the chest was opened, and the heart was carefully removed. Following a brief washing step in cold PBS, hearts were weighed and frozen in liquid nitrogen. Frozen heart tissue was then homogenized in 700 µL RIPA buffer, in screw-cap tubes with ceramic beads, using a Precellys tissue homogenizer (Bertin Technologies). To ensure complete lysis, tissue homogenates were passed several times through a syringe with a 25-gauge needle (Braun, 10162148) and incubated on ice for 5 min before centrifugation at 20,000 ×g for 15 min at 4 ◦C. Only the clear supernatant was retained for further analyses.

3.1.4 Mouse heart fixation for histology

Mice were sacrificed by cervical dislocation, and the chest was promptly opened to expose the beating heart. 1 mL of 100 mM CdCl2 was carefully injected into the left ventricle to stop beating in diastole. A small incision was made in the right atrium to enable drainage, and 5 mL of heparin (diluted in PBS to 100 U/mL) was slowly perfused through the right ventricle into the left ventricle to remove excess blood. 10 mL of 10% formaldehyde (in PBS) was then perfused the same way to fix the heart tissue. Finally, the heart was excised, cleaned, and kept in 4% formaldehyde (in PBS) for 24 hours at 4◦C, before being transferred to fresh PBS for short-term storage or immediately embedded in paraffin.

3.2 Histological methods

3.2.1 Mouse heart embedding and sectioning

After fixation, mouse hearts were dehydrated and infiltrated with paraffin using the HistoCore PEARL tissue processor (Leica). Next, hearts were embedded in paraffin blocks using the Histo-Core Arcadia H embedding station (Leica). Solid paraffin blocks were kept at -20◦C overnight before being cut at room temperature into 6 µm histological sections using a microtome (RM2145, Leica). Heart sections were transferred onto glass slides and left to dry overnight on a flattening table (HI1220, Leica) preheated to 37◦C. Tissue slides were then kept at room temperature until further use. Before histological staining was performed, heart sections were deparaffinized in xylene (3× 5 min) and rehydrated in a descending ethanol series (2× absolute EtOH, 1× 95 % EtOH, 1× 70 % EtOH, 5 min each) before 3 final washes in ddH2O (3 min each).

3.2.2 Hematoxylin and eosin staining

The staining was performed using the Hematoxylin & Eosin fast staining kit as per the manufacturer's instructions. Briefly, tissue slides were stained for 6 min in Hematoxylin, washed for 10 sec in tap water, and differentiated for 10 sec in 0.1% HCl. Next, slides were rinsed for 6 min in running tap water before they were stained for 30 sec in Eosin and finally washed for 30 sec in running tap water. Slides were then dehydrated (3 min in 95 % EtOH, 2× 3 min in absolute EtOH, and 3× 5 min in xylene), mounted with Eukitt quick-hardening mounting medium, and covered with a coverslip. Images of sections were taken on an Axio Vert.A1 microscope (Zeiss), and quantification of hematoxylin-positive regions was done in ImageJ.

3.2.3 Masson Trichrome staining

The staining was performed using Masson Trichrome Stain Kit as per the manufacturer's instructions. Briefly, tissue slides were incubated in preheated Bouin's Solution at 60◦C for 15 min, then washed with running tap water for 5 min and stained in Weigert's Iron Hematoxylin Solution for 5 min. Following another washing step in running tap water, slides were quickly rinsed with ddH2O and incubated in Bieberich Scarlet-Acid Fuchsin solution for 5 min. After another rinse

with ddH2O, slides were placed in working Phosphotungstic/Phosphomolybdic Acid Solution for 5 min and then directly transferred to Aniline Blue Solution for 5 min. Slides were incubated in 1% acetic acid for 2 min and rinsed with ddH2O. After dehydration series (3 min in 95% EtOH, 2× 3 min in absolute EtOH, and 3× 5 min in xylene), heart sections were mounted with Eukitt quick-hardening mounting medium and covered with a coverslip. Images of sections were taken on an Axio Vert.A1 microscope (Zeiss), and quantification of collagen deposits displaying purple-blue coloration was done in ImageJ.

3.2.4 Immunohistochemistry

After deparaffinization and rehydration of the tissue samples, antigen retrieval was performed by boiling heart tissue slides in citrate buffer in the microwave (700 W for 3 min, followed by 450 W for 12 min). Slides were cooled at 4 ◦C for 20 - 30 min, washed with ddH2O (2 × 3 min), and equilibrated in TN buffer (2 × 3 min). Blocking was achieved with TNB blocking solution for 60 min at room temperature. The antibodies and reagents were diluted in TNB blocking solution and used for staining. They were pipetted onto heart sections and incubated in a humid chamber overnight at 4◦C. The next day, slides were washed with TN buffer (3× 3 min) and if required, incubated with a secondary antibody (diluted in TNB blocking solution) for 2 hours at room temperature. The used antibodies and their dilutions are listed in section 2.4. After washing with TN buffer (3× 3 min), sections were mounted with Vectashield Antifade Mounting Medium containing 5 µg/mL DAPI. Specimens were imaged on a Leica SP8 confocal fluorescence microscope, and image analyses were carried out using ImageJ.

3.2.5 WGA staining and quantification

Formalin-fixed, paraffin-embedded (FFPE) left ventricle sections (6 µm) were deparaffinized, rehydrated, and stained overnight at 4 °C with Alexa Fluor 488-conjugated Wheat Germ Agglutinin (1:50 in PBS) to label cardiomyocyte membranes. After PBS washes, sections were counterstained with DAPI (1 µg/mL), mounted with Vectashield Antifade Mounting Medium, and imaged using a Leica SP8 confocal fluorescence microscope. The cardiomyocyte cross-sectional area was quantified in transverse sections using ImageJ by tracing membrane-bound borders and analyzing ≥100 cells per heart from multiple fields.

3.2.6 Electron microscopy

Heart tissue samples (outer wall, septum, apex) were fixed in 2.5% glutaraldehyde and 4% paraformaldehyde in 0.1 M PHEM buffer (pH 6.9) at room temperature, washed, cut into 1 mm^3 and post-fixed with 1% osmium tetroxide in PBS on ice for 1 hour. After washing, samples were stained overnight at 4°C with 1% uranyl acetate in water, dehydrated in a graded acetone series, and embedded in Spurr resin, polymerized at 60°C overnight. Ultrathin sections (70 nm) were cut with a Leica UC7 ultramicrotome, mounted on formvar-coated slot grids, and contrast-stained with 3% uranyl acetate in 70% methanol and 3% lead citrate. Imaging was performed on a JEOL JEM-1400 TEM at 80 kV using a 4K TemCam F416 CMOS camera, at magnifications of 8kX and 10kX (pixel sizes 1.36 and 1.09 nm, respectively).

*Larissa Eis *Charlotta Funaya *Réza Shahidi

*University of Heidelberg, Electron Microscopy Core Facility - EMCF, INF345, EG

3.3 Cell culture methods

3.3.1 Isolation of neonatal rat cardiomyocytes

Wistar rats (RjHan: WI, Janvier Labs). Following euthanasia by decapitation, hearts were excised and washed in cold HBSS. Atria and any remaining vessels were removed, and ventricles were minced into small pieces. These were then resuspended in Digestion Solution and incubated for 10 min at 37◦C with gentle agitation. The digest was stopped by the addition of Stop Solution, followed by gentle resuspension by pipetting to ensure proper tissue homogenization. Undigested material was allowed to settle, and supernatant containing isolated cells was collected and kept on ice. Digestion was repeated as described for 6 - 8 times with the remaining undigested tissue. Collected supernatants were pooled together and centrifuged at 500 ×g for 15 min at 4◦C. The cell pellet was resuspended in NRCM Culture Medium, and cells were counted using a hemocytometer. The cells were then pre-plated for one hour to remove noncardiomyocytes. After 1-hour, floating cells (cardiomyocytes) were collected by centrifugation and resuspended in DMEM F12 with 10% FCS and 1% PSG. After determining the cell count, NRCMs were plated in NRCM Culture Medium at a cell density of approximately 50,000 cells/cm2. Plastic culture plates were precoated

with 0.1% gelatin for one hour before plating. Isolated cultures were kept in a humidified incubator at 37◦C and 5 % CO2. The following day, cells were washed with PBS and cultured in NRCM Treatment Medium for subsequent experiments (Fig. 10) (140).

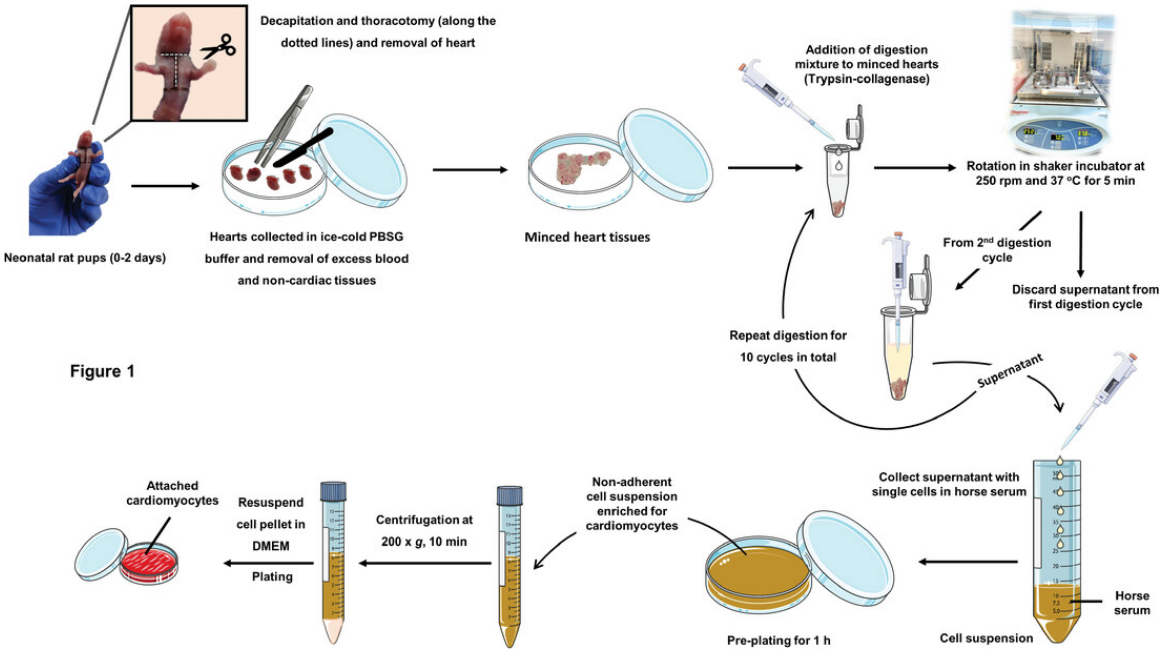

Figure 10. Workflow for the isolation of Neonatal Rat ventricular Cardiomyocytes (NRCMs) (140).

3.3.2 Transfection of NRCMs with small interfering RNA

24 hours after isolation and plating of NRCMs, cells were transfected with small interfering RNA (siRNA) to achieve a transient knockdown of Zeb1. For that purpose, control scrambled siRNA (siScr; Thermo Fisher Scientific, 4390843) or siRNA targeting Zeb1 transcript (siZeb1; Thermo Fisher Scientific, s130527) were delivered into NRCMs using HiPerfect transfection reagent according to the manufacturer's protocol. Briefly, 5 µL of HiPerfect transfection reagent was used per well of a 12-well plate to a total volume of 500 µL per well, and the final siRNA concentration was kept at 100 nM. NRCMs were incubated with transfection mixes overnight, then the medium was replaced with fresh NRCM Treatment Medium, and cells were cultured for another 48 hours to ensure efficient knockdown.

3.3.3 Treatment of NRCMs with phenylephrine

48 48 hours after transfection with siRNA, NRCMs were treated with alpha-1 adrenergic receptor agonist phenylephrine (PE), which simulates pathological hypertrophy by inducing NRCM growth. A fresh stock solution of PE (1 mg/mL in PBS) was prepared before each experiment and diluted in NRCM Treatment Medium to a final concentration of 50 µM. NRCMs were kept in PE-containing medium for 24 hours.

3.3.4 Adenovirus production and viral transduction

Entry clones were ordered from BioCat and cloned in pDONR221 backbone with the following coding DNA sequences (CDS): pEntr_ZEB1 (NM_011546.3, M. musculus CDS). These were subcloned into pAd/CMV/V5-DEST expression vector (Invitrogen, V49320) by performing the LR reaction using Gateway LR Clonase II Enzyme mix per manufacturer's instructions. The obtained construct was transformed into One Shot TOP10 Chemically Competent E. coli cells (Thermo Fisher Scientific, C404010) as indicated in the product information sheet, spread onto plates with LB-agar and ampicillin (100 µg/mL) and incubated at 37◦C overnight. The next day, colonies were picked and plasmids were isolated using the peqGOLD Plasmid Miniprep Kit I. The correct insert sequence was confirmed by Sanger sequencing (Mix2Seq Service, Eurofins). Glycerol stock of initial bacterial transformation was then used to prepare a liquid culture, and the expression plasmid was isolated using HiSpeed Plasmid Midi Kit. 6 µg of each expression plasmid was linearized with restriction enzyme PacI for 3 hours at 37◦C, before the enzyme was inactivated for 20 min at 65◦C. The linearized plasmid was transfected into HEK293A cells (10 cm plate) using PEI transfection reagent. Two days later, the cells were split into three 10 cm plates and cultured in antibiotic-free medium. Plates were inspected every day under a microscope and were harvested once 30 % of the cells detached. Following 3 freeze-thaw cycles, the lysate was used to reinfect HEK293A cells (T175 flask), which were harvested once 70% of the cells detached. After 3 freeze-thaw cycles, benzonase was added to the lysate, and tubes were incubated for 90 min in a heated water bath (37◦C). Finally, tubes were centrifuged at 3700 rpm for 40 min at 4◦C, the supernatant was collected and aliquoted for further use. To determine the number of adenoviral particles, a small

aliquot of each virus was diluted in 0.1% SDS, and absorbance at 260 nm was measured on a NanoDrop Lite spectrophotometer (Thermo Fisher Scientific). The number of viral particles per mL was calculated as follows: A260 × dilution factor × 1.1 × 1012 particles. Before viral transduction, the cell culture medium was removed and then replaced with fresh one. Adenoviruses were added directly into the medium, and plates were incubated for 24 hours to achieve overexpression. Control samples were transduced with a control adenovirus (empty vector adenovirus control), using the same number of viral particles.

3.3.5 Cell lysate preparation

Cultured cells were washed with PBS and then harvested in RIPA buffer with added protease and phosphatase inhibitors. Cell lysates were collected by carefully scraping cell culture dishes and subsequently centrifuged at 20,000 x g for 15 min at 4◦C. Only soluble fractions (supernatants) were retained for further use.

3.3.6 Immunoprecipitation

Dynabeads Sheep anti-Rabbit (Invitrogen, #11203D) were resuspended, transferred (50 µL per 10 cm dish), and washed twice with lysis buffer. Beads were incubated with anti-Zeb1 antibody (1 µg per 50 µL beads; Invitrogen, 0.5 mg/mL) for 1 h at room temperature with rotation, washed twice, and resuspended in 100 µL lysis buffer. Control beads were prepared similarly using Rabbit IgG (Cell Signaling, 2.5 mg/mL; 1.25 µg per 50 µL beads). Cells were washed with cold PBS, lysed on ice with 400 µL lysis buffer, scraped, and collected; an additional 200 µL was used to re-scrape. Lysates were sheared with a 25G needle (8×), incubated on ice for 5 min, and centrifuged (14,000 rpm, 15 min, 4 °C). Protein concentration was determined, and 850 µg total protein in 950 µL lysis buffer was incubated with 50 µL antibody-coupled beads overnight at 4 °C. After magnetic separation, beads were washed three times with 500 µL wash buffer (2 min each) and proteins were eluted with 50 µL SDS buffer, boiled at 95 °C for 5 min.

3.3.7 Isolation of adult mouse cardiomyocytes (AMCM)

Adult mouse cardiomyocytes were isolated using the Langendorff-free method (Ackers-Johnson et al.) (141). Briefly, 8-week-old Zeb1KO and WT mice were anesthetized, and the thoracic cavity was opened. After transecting the descending

aorta, 7 mL EDTA buffer was injected into the left ventricle (LV), followed by clamping the ascending aorta and transferring the heart to a dish with fresh EDTA buffer. An additional 10 mL EDTA buffer, 3 mL perfusion buffer, and 30–50 mL warm collagenase buffer (37 °C) was sequentially injected into the LV until the tissue appeared soft and translucent. The LV was dissected, minced, and gently dissociated by pipetting. Enzyme activity was stopped using 5 mL stop buffer (perfusion buffer + 5% FCS), and cells were filtered (100 µm cell strainer). Calcium was gradually reintroduced using three intermediate buffers as described in table 12. Cardiomyocytes were plated at ~50,000 cells/cm² in prewarmed plating medium, allowed to settle for 1–2 hours, and then switched to culture medium (Fig.11).

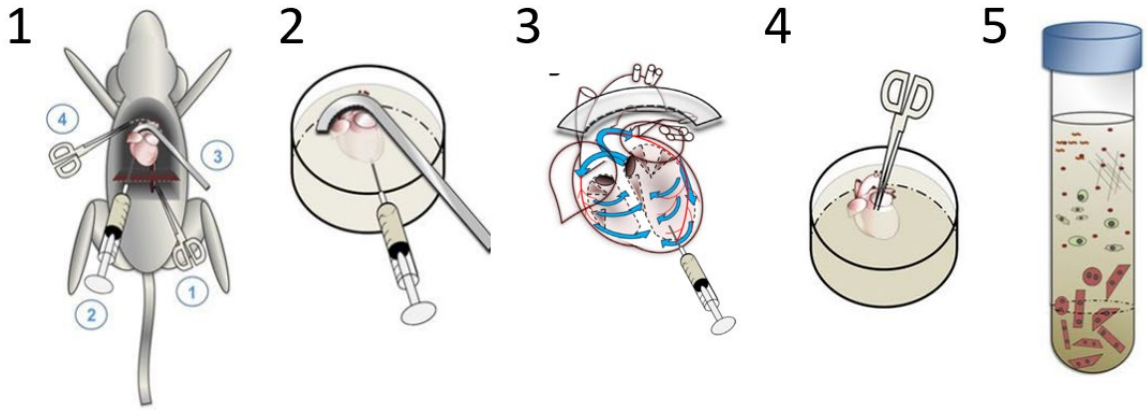

Figure 11. Workflow of Adult cardiomyocyte isolation.

1. EDTA injection, clamping the aorta and removal of heart. 2. EDTA buffer and digestion buffer perfusion. 3. Internal picture of heart undergoing perfusion. 4. Removal of Left ventricle and cutting them into smaller pieces. 5. Gravity sedimentation process to isolate the cardiomyocytes at the bottom of the tube.

3.4 Molecular and biochemical methods

3.4.1 Western blot

Protein concentration of lysates was measured in 96-well microplates using the DC Protein Assay according to the manufacturer's protocol. 15 - 30 µg of total protein per sample was mixed with Laemmli Sample Buffer (with added 10% (v/v) 2-mercaptoethanol) and boiled for 5 min at 95◦C. 10-15µg Denatured samples were then subjected to SDS-PAGE on 4-12% Bis-Tris polyacrylamide precast gels (Bio-Rad Laboratories, 3450124/3450125) using XT MOPS or XT MES running buffer and 150 V. Proteins were transferred onto PVDF membrane (Immobilon P with

pore size 0.45 µm, Merck-Millipore, IPVH00010) with a wet transfer (100 V, 35 min). Total protein staining was done after air drying the membrane for 30 min, where the membrane was first incubated with the total protein stain for 5 min with gentle shaking. Then, after removing the total protein stain, it was washed twice for 30 seconds each with wash buffer. Before imaging, the membranes were rinsed with ddH2O. Membranes were subsequently blocked with 5% milk solution (prepared in TBST) for 1 hour at room temperature and then incubated with primary antibodies in 5% milk solution (prepared in TBST) overnight at 4◦C. The following day, membranes were washed three times with TBST (10 min each wash) and incubated with the corresponding peroxidase-conjugated secondary antibodies in 5% milk for 1 hour at room temperature. Finally, membranes were washed three more times with TBST (10 min for each wash) before being visualized using WesternBright ECL and Fusion FX Imaging System (Vilber). Used antibodies and their dilutions are listed in section 2.4, and buffer compositions are given in section 2.6.5. Following chemiluminescent detection of proteins, membranes were stained with Ponceau S (if total protein staining was not done) for 10 min at room temperature with gentle shaking. After several washes with ddH2O to remove unwanted background, membranes were left to air-dry before scanning. Acquired images and scans were then used for semi-quantitative densitometry analysis in ImageJ. Densitometry values for proteins of interest were normalized to the values of the loading control (Total protein stain or Ponceau S-stained membranes, or a loading control like Actin or Tubulin).

3.4.2 RNA isolation

Cultured cells were harvested in RNA Lysis Buffer, and isolation of total RNA was performed by using the Quick-RNA MiniPrep Kit per the manufacturer's instructions (including on-column DNase I digest). RNA isolation from mouse heart tissue was done by first homogenizing the organs as described above in section 3.1.5. 100 µL of the heart lysate was then thoroughly mixed with 1 mL of QIAzol Lysis Reagent and 200 µL of chloroform and centrifuged at 12,000 ×g for 15 min at 4◦C. The upper aqueous phase was carefully collected and mixed with 1 volume of isopropanol, and isolation of total RNA was completed using the Quick-RNA MiniPrep Kit according to the manufacturer's protocol (including on-column DNase I digest).

RNA concentration and purity were measured on a NanoDrop Lite spectrophotometer (Thermo Fisher Scientific).

3.4.3 Reverse transcription and quantitative real-time PCR

500 – 1000 ng of total RNA was subjected to reverse transcription with the First Strand cDNA Synthesis Kit, and oligo-dT primers were used to specifically detect mature polyadenylated mRNAs and produce a more consistent qRT-PCR signal. The resulting cDNA samples were diluted ten- to twenty-fold with nuclease-free H2O and used for quantitative real-time PCR (qRT-PCR) analysis with iTaq universal SYBR Green Supermix. Each reaction consisted of 5 µL iTaq universal SYBR Green Supermix, 300 nM forward primer, 300 nM reverse primer, and 3 µL diluted cDNA. Samples were pipetted into 96- or 384-well microplates and analyzed with the QuantStudio5 real-time PCR System (Thermo Fisher Scientific). The sequences of primers used are given in section 2.5. Each primer pair was tested before use to ensure an amplification efficiency between 90% and 110%. Additionally, melting curves were carefully inspected, and agarose gel electrophoresis was performed to verify that a single gene-specific amplicon of the correct size was produced. Ct values of genes of interest were normalized to one or the mean of two reference genes (18S rRNA and Hprt). Relative abundances and changes in expression were calculated using the 2–ΔΔCt method.

3.4.4 Immunofluorescence

Cells were cultured in 12-well plates that contained glass coverslips. After the desired experimental treatments were performed, cells were washed with PBS and fixed with 4% paraformaldehyde for 10 min at room temperature. Following another washing step with PBS, cells were permeabilized with 0.3% Triton X-100 (in PBS) for 10 min at room temperature. Blocking was performed for 1 hour in 10% horse serum at room temperature. Coverslips were then incubated overnight at 4◦C with primary antibodies in 10% horse serum in PBS. The next day, coverslips were washed three times with PBS (5 min each wash) and incubated with secondary antibodies in 10% horse serum for 1 hour at room temperature in the dark. The used antibodies and their dilutions are listed in section 2.4. After 3 final washing steps with PBS (5 min each wash), coverslips were mounted on glass slides using Vectashield Antifade Mounting Medium containing 5 µg/mL DAPI. Specimens were

then imaged on a SP8 Lightning confocal microscope (Leica). Microscopy image analyses, such as cell size measurements, were carried out using ImageJ.

3.4.5 Cell size measurement

ImageJ/Fiji software (https://imagej.net/software/fiji/) was used to assess cell size. Cell size was determined manually. Using a blinded technique, in which the treatment allocation for each sample was not known. No identifying information was included in the imported photos, and each sample was given an anonymous label. An unbiased analysis was ensured by using randomized measurements to prevent biases and by compiling and analyzing the results without disclosing the treatment allocation. In each experiment, at least 100 cardiomyocytes were examined.

3.5 Sequencing Methods

3.5.1 Bulk RNA sequencing

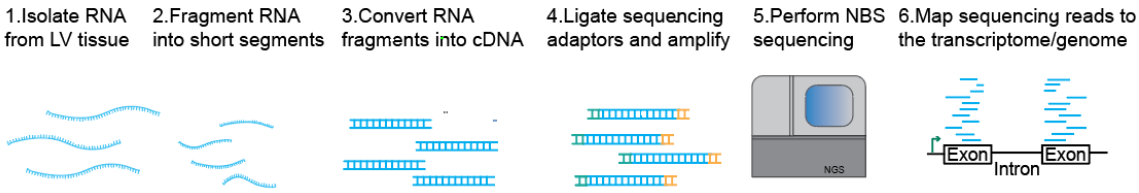

Figure 12. Bulk RNA sequencing workflow.

Total RNA from left ventricular tissue was extracted using TRIzol and RIPA homogenization. RNA quality was confirmed via NanoDrop and Bioanalyzer (RIN >7). mRNA libraries were prepared with NEBNext Ultra II and sequenced (150 bp paired-end) on Illumina NovaSeq (Fig. 12). Paired-end, rRNA-depleted sequencing data were analyzed following quality control. Low-quality regions and adapter sequences were removed using Flexbar (PMID 28541403), and residual rRNA reads were filtered with Bowtie2 (PMID 22388286) using an rRNA-specific index. Reads were aligned to the ENSEMBL mouse genome build 107 (mm39) using STAR (PMID 23104886), and gene-level counts were obtained with Rsubread (PMID 30783653). Quality metrics and mapping summaries were assessed via MultiQC (PMID 27312411). Differential expression was analyzed with edgeR

(PMID 39844453). GO analysis was performed with topGO, using genes with RPKM ≥ 1 across all samples as background. Heatmaps were generated using ComplexHeatmap (PMID 27207943). All downstream analyses were conducted in R. DESeq2 in R, and genes with an adjusted *p*-value < 0.05 and $|\log_2$ fold change| > 1 were considered significantly differentially expressed (Analysis performed by Prof. Tobias Jakobi, University of Arizona).

3.5.2 Chromatin immunoprecipitation sequencing

For chromatin immunoprecipitation (ChIP), cells were crosslinked with 1.0% formaldehyde in PBS for 10 minutes at 150 rpm, followed by quenching with 250 mM glycine for an additional 10 minutes. Cells were centrifuged (2000 rpm, 5 min), washed twice with PBS, and pelleted again. Pellets were resuspended in 1 mL of Lysis Buffer 1 and rocked at 4 °C for 10 minutes. After centrifugation (1000 rpm, 5 min, 4 °C), nuclei were resuspended in 1 mL of Buffer 2 and incubated for 10 minutes at room temperature with rocking. Following another centrifugation step, nuclei were resuspended in 300 µL of Buffer 3, transferred to polystyrene tubes (e.g., TPX), and sonicated using a Bioruptor (3 × 15 cycles, 30 s on/off, high power). Lysates were cleared by centrifugation (14,000 rpm, 10 min, 4 °C), and the supernatant was collected for ChIP (Fig. 13).

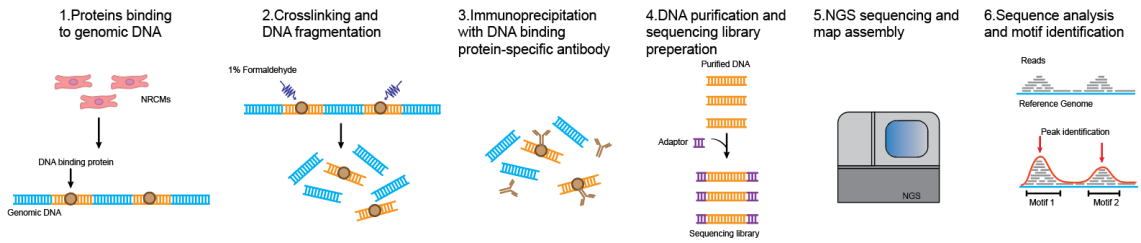

Figure 13. Chromatin immunoprecipitation sequencing (ChIP seq) workflow.

Post-immunoprecipitation, samples were treated with RNase A (1 µL/100 µL, 30 min, 37 °C), followed by Proteinase K (2.5 µL/100 µL) and 5 µL of 10% SDS overnight at 65 °C to reverse crosslinks. DNA was purified using phenol/chloroform/isoamyl alcohol in Phase-Lock tubes, followed by chloroform extraction. The aqueous phase was precipitated with 1 µL glycogen (20 mg/mL), 25 µL 3 M sodium acetate (pH 5.2), and 550 µL ethanol at –80 °C for 1 h. DNA was pelleted (15,000 g, 30 min, 4 °C), washed with 70% ethanol, air-dried, and

resuspended in 10 µL water. Library preparation was performed using the NEBNext Ultra II DNA Library Prep Kit for Illumina (E7645S) and Multiplex Oligos (E7335S). Fragment size distribution was assessed using a TapeStation with High Sensitivity D1000 ScreenTape, and libraries were submitted for sequencing (Analysis performed by Daniel Finke, Uniklinik Heidelberg).

3.6 Statistics

All statistical analyses were performed using GraphPad Prism 10 software. Data are presented as mean ± standard error of the mean (SEM), unless otherwise specified.

For comparisons between two experimental groups, unpaired two-tailed Student's *t*-test was used. When comparing more than two groups, one-way analysis of variance (ANOVA) was performed, followed by appropriate post hoc tests (such as Tukey's or Bonferroni's) to assess group-wise differences.

Prior to analysis, data were tested for normal distribution and homogeneity of variances to ensure the validity of parametric tests. In cases where assumptions were violated, appropriate data transformations or alternative statistical methods were considered.

A p-value less than 0.05 was considered statistically significant. Significance thresholds were reported as $p < 0.05$ (*), $p < 0.01$ (**), $p < 0.001$ (***), and $p < 0.0001$ (****).

All experiments included at least three independent biological replicates, and the number of replicates is indicated in the figure legends or corresponding text. Sample sizes were chosen based on previous studies and standard practices in the field to ensure adequate statistical power.

4. Results

4.1 ZEB1 Protein is Dynamically Regulated in Models of Cardiac Hypertrophy and Cardiomyopathy

Zeb1 is a transcription factor widely recognized for its pivotal role in EMT. While its functions have been extensively characterized in non-cardiac tissues, considerably less is known about its role within the heart, particularly in mature cardiomyocytes subjected to pathological stress.

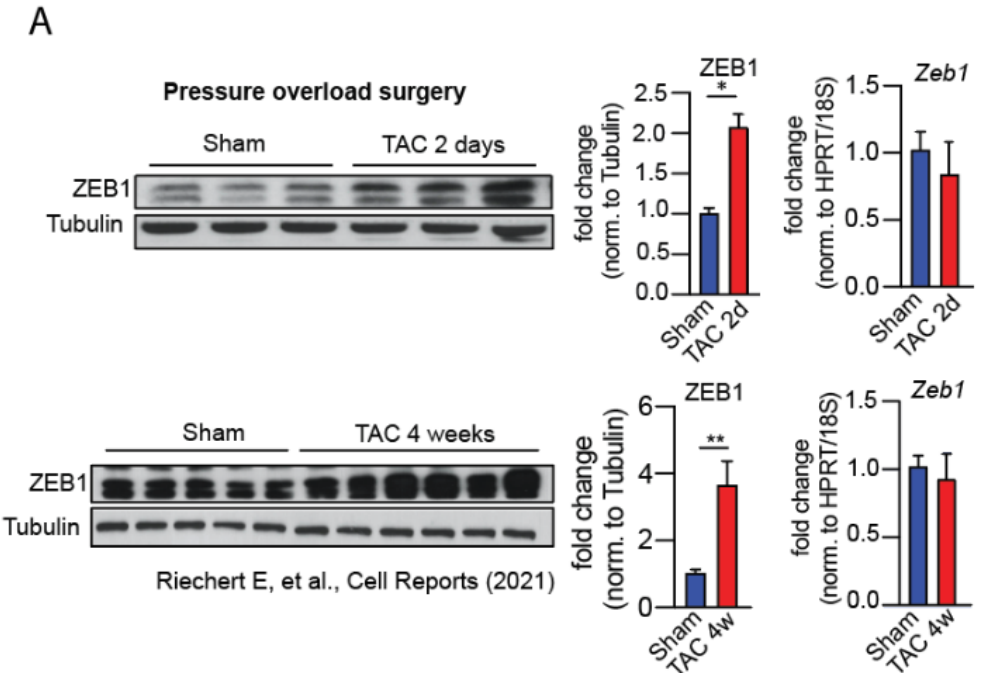

Figure 14. Regulation of Zeb1 protein expression in cardiomyopathy models.

(a) Western blot with significant increase in Zeb1 protein levels in the left ventricles of mice subjected to Transverse Aortic Constriction (TAC) at 2 days and at 4 weeks post-surgery, with no corresponding change in Zeb1 mRNA levels, indicating post-transcriptional regulation (Data shown as mean ± SEM; *=p<0.05, **=p<0.01, ***=p<0.001, ****=p<0.0001 by unpaired Student's t-test or one-way ANOVA as appropriate.) (84)

Our published data already indicated an alteration of Zeb1 expression in the heart during disease conditions. The well-established TAC model, which imposes pressure overload on the left ventricle, provoked a rapid hypertrophic response that closely resembled human cardiac pathology.

The analyses revealed a significant increase in ZEB1 protein levels in the left ventricles as early as two days post-TAC, with elevated expression sustained

through four weeks (Fig. 14a) (84). Notably, despite this pronounced rise in protein abundance, *Zeb1* mRNA levels remained unchanged at both time points (Fig. 14a).

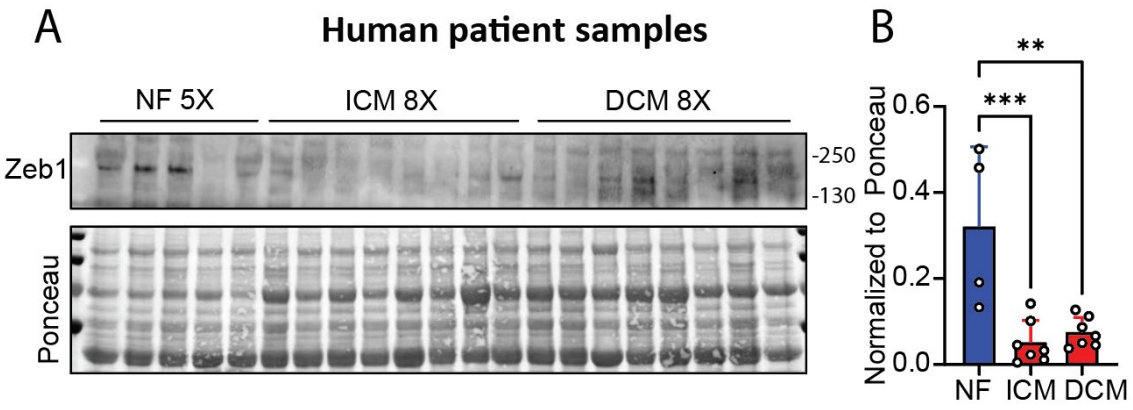

Figure 15. Zeb1 expression in human patient samples.

(a) Western blot of left ventricle tissue lysates from 5 Non failing hearts, 8 Ischemic cardiomyopathy hearts and 8 Dilated cardiomyopathy hearts. (b) Graph showing the quantification of Zeb1 bands from the western blot normalized to ponceau. (Data shown as mean ± SEM; *=p<0.05, **=p<0.01, ***=p<0.001, ****=p<0.0001 by unpaired Student's t-test or one-way ANOVA as appropriate.)

Hence, within my PhD project, Zeb1 expression pattern was also checked in human Ischemic Cardiomyopathy (ICM) hearts and Dilated Cardiomyopathy (DCM) patient samples. A significant decrease in ICM hearts and DCM hearts was found as compared to Non-Failing (NF) hearts (Fig. 15a, b). This corroborates with the underlying hypothesis of that project that during cardiomyopathy Zeb1 is differentially regulated.

To determine whether Zeb1 modulation is specific to pressure overload or represents a broader feature of pathological remodeling, I assessed its expression in two genetic mouse models of cardiomyopathy: Mybpc3 KO, which models HCM, and Rbm20 KO, which models DCM. These models reflect distinct remodeling phenotypes, Mybpc3 KO hearts display concentric hypertrophy and diastolic impairment, while Rbm20 KO hearts exhibit chamber dilation and systolic dysfunction.

ZEB1 protein was significantly elevated in Mybpc3 KO hearts whereas the *Zeb1* mRNA level was reduced (Fig. 16a). But it was markedly reduced in Rbm20 KO hearts with an increase in *Zeb1* mRNA level (Fig. 16b).

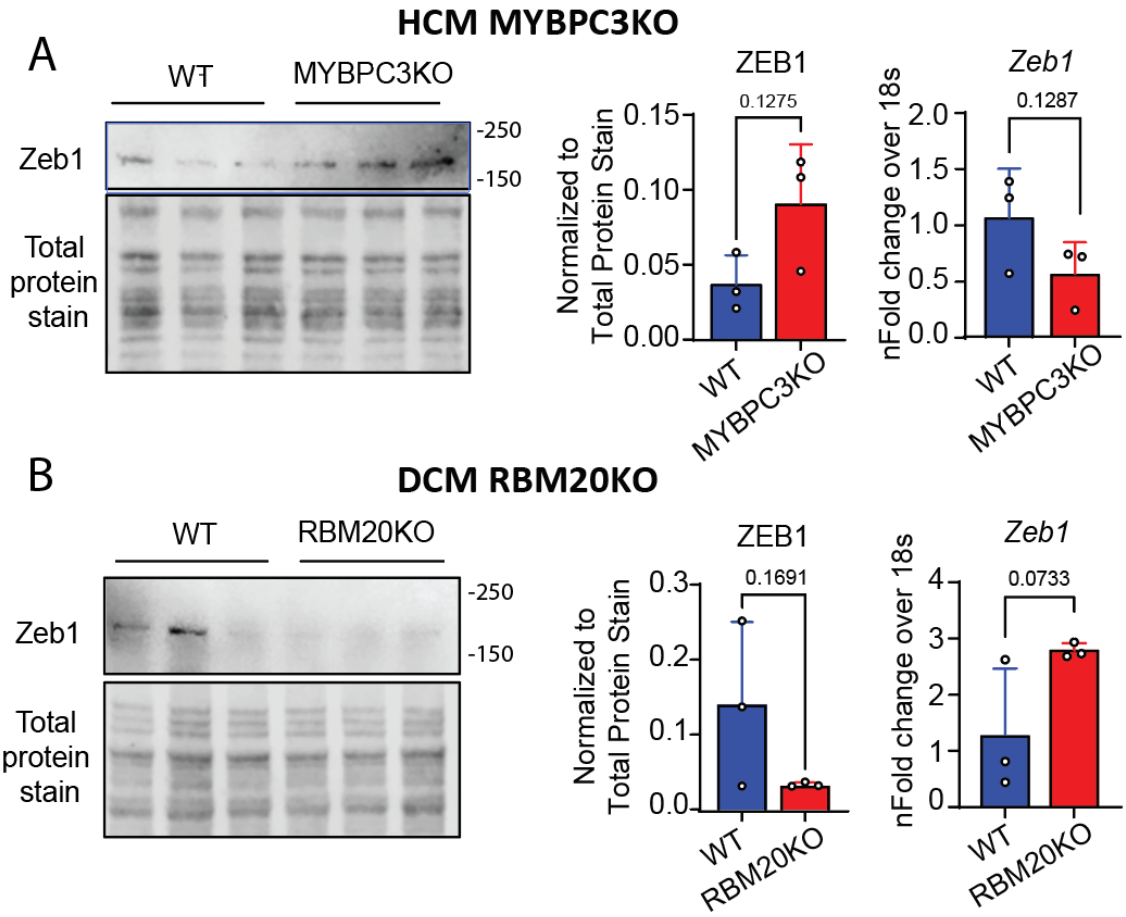

Figure 16. Zeb1 expression in different cardiomyopathy mice model.

(a) Increased ZEB1 protein expression in Mybpc3 KO mice, a model of HCM. (b) Reduced ZEB1 protein expression in left ventricular tissue from RBM20 KO mice exhibiting DCM. (Data shown as mean ± SEM; *=p<0.05, **=p<0.01, ***=p<0.001, ****=p<0.0001 by unpaired Student's t-test or one-way ANOVA as appropriate.)

Collectively, these findings demonstrate that Zeb1 protein levels are dynamically and differentially regulated in the heart in response to both mechanical and genetic stress.

4.2 Overexpression of Zeb1 in Cardiomyocytes Induces Hypertrophic Remodeling

To determine whether Zeb1 functions as a direct mediator of pathological cardiac hypertrophy and structural remodeling, I utilized both *in vitro* and *in vivo* models. These experiments aimed to test the role of Zeb1 in cardiac remodeling, moving beyond correlative associations toward a mechanistic understanding of its function in cardiomyocytes.

4.2.1 Effect of Zeb1 Overexpression in Neonatal Rat Cardiomyocytes

I first conducted *in vitro* studies using Neonatal Rat Cardiomyocytes (NRCMs), a widely accepted model system for investigating cardiomyocyte growth, gene expression, and hypertrophic signaling. NRCMs are particularly amenable to molecular manipulations and respond robustly to pro-hypertrophic stimuli, making them highly suitable for dissecting early transcriptional events during hypertrophy.

To overexpress Zeb1, I employed an adenoviral-mediated gene delivery approach, ensuring high transduction efficiency and robust expression of full-length ZEB1 protein specifically in cardiomyocytes. Western blot analysis of transduced NRCMs confirmed a substantial increase in ZEB1 protein levels compared to control cells, validating the effectiveness of our overexpression system. When NRCMs were treated with phenylephrine (PE), a potent α_1-adrenergic receptor agonist commonly used to mimic neurohormonal stress and stimulate hypertrophic signaling, I observed a marked elevation of endogenous ZEB1 protein levels (Fig. 17a, b). Morphological assessment by immunofluorescence staining for sarcomeric α-actinin, a cytoskeletal marker that delineates cell borders and sarcomere organization, revealed that NRCMs overexpressing Zeb1 exhibited a pronounced increase in cellular surface area (Fig. 17c, d).

RT-PCR analysis showed significant upregulation of the fetal gene markers *Nppa* (encoding atrial natriuretic peptide, ANP) and *Nppb* (encoding B-type natriuretic peptide, BNP) genes that are minimally expressed in healthy adult cardiomyocytes but are robustly reactivated in response to pathological stress. These peptides serve as molecular biomarkers for cardiovascular disorders. Additionally, I observed a significant downregulation of *Myh6*, the gene encoding α-myosin heavy chain, a key component of the mature sarcomeric contractile apparatus in healthy adult hearts. *Myh6* suppression is a hallmark of fetal gene reactivation, in parallel to *Myh7* upregulation and impaired contractile function, commonly seen in various models of heart failure. I also saw a marked increase in *Col1a1* (Collagen type1 alpha 1) suggesting increased fibrosis (Fig. 17e).

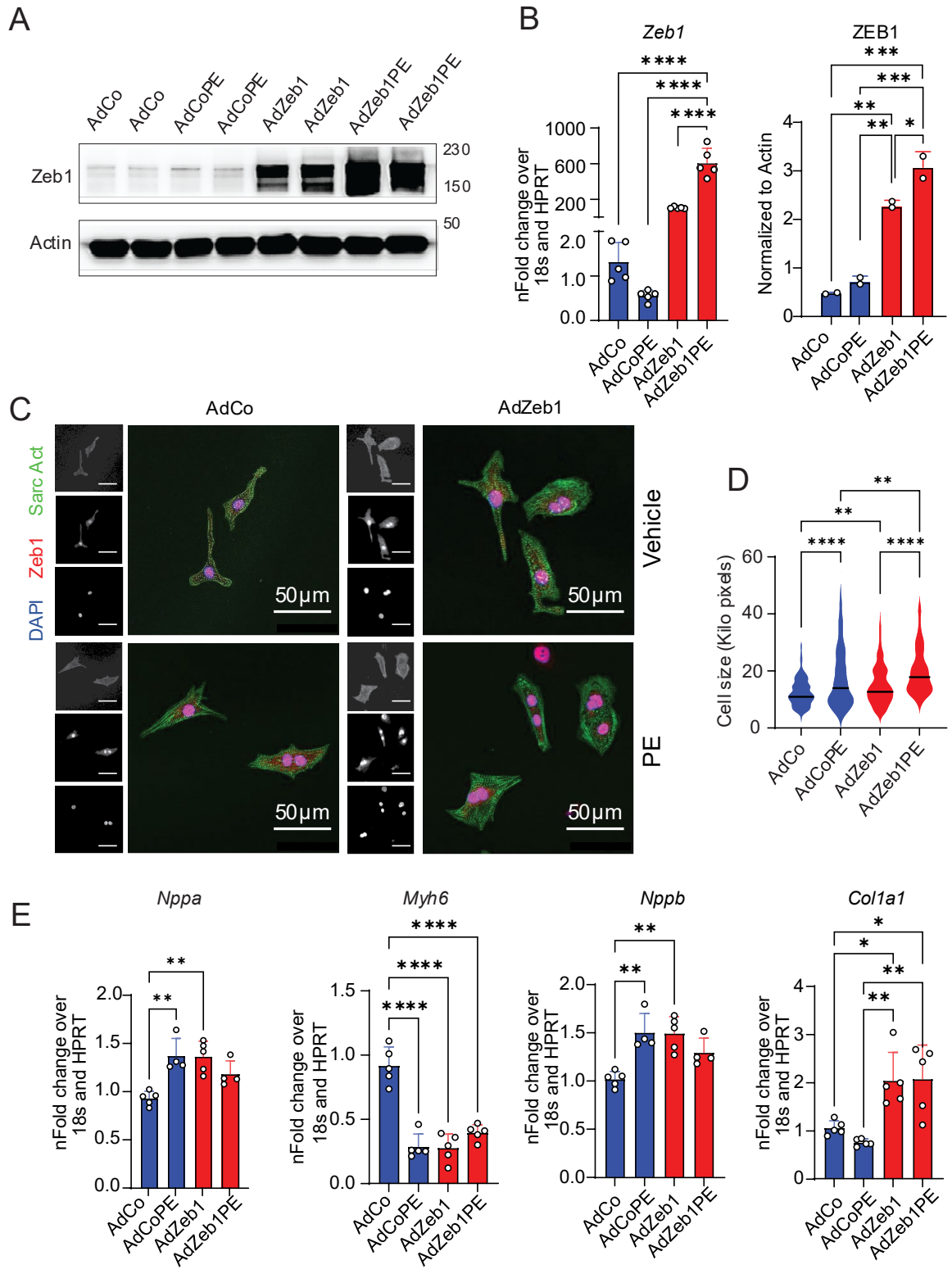

Figure 17. Zeb1 overexpression induces cardiomyocyte hypertrophy and cardiac dysfunction *in vitro*.

(a) Western blot analysis confirming increased Zeb1 protein expression in neonatal rat cardiomyocytes (NRCMs) following adenoviral-mediated Zeb1 overexpression (Zeb1 OE), and further enhancement upon PE treatment. (b) RT-PCR confirming increased Zeb1 mRNA expression in NRCMs and western blot protein quantification of Zeb1 normalized to actin. (c) Representative immunofluorescence images of NRCMs stained for sarcomeric α-actinin (green), Zeb1 (red), and DAPI (blue) showing increased cell size in Zeb1 OE cells. Scale bar = 50 µm. (d) Quantification of NRCM cell surface area upon Zeb1 overexpression, further augmented

by PE treatment (n = 200). (e) RT-PCR analysis showing elevated expression of cardiac pathology marker Nppa, Nppb, and Cola1a and decreased Myh6 levels in Zeb1 OE NRCMs, recapitulating the PE-induced hypertrophic gene expression pattern. (Data shown as mean ± SEM; *=p<0.05, **=p<0.01, ***=p<0.001, ****=p<0.0001 by unpaired Student's t-test or one-way ANOVA as appropriate.)

Together, these findings demonstrate successful ZEB1 overexpression in NRCMs, and document associated molecular and morphological changes under the experimental conditions described.

4.2.2 Zeb1 Overexpression Induces Maladaptive Cardiac Remodeling and Systolic Dysfunction in Adult Mice

To extend my *in vitro* observations into a more physiologically relevant setting and to investigate the *in vivo* consequences of Zeb1 upregulation in adult cardiomyocytes, I employed a gene delivery strategy using adeno-associated virus serotype 9 (AAV9). AAV9 vectors are known for their high tropism for cardiac tissue and have been widely used in preclinical and clinical studies targeting the heart due to their efficient transduction of post-mitotic cardiomyocytes with minimal off-target effects.

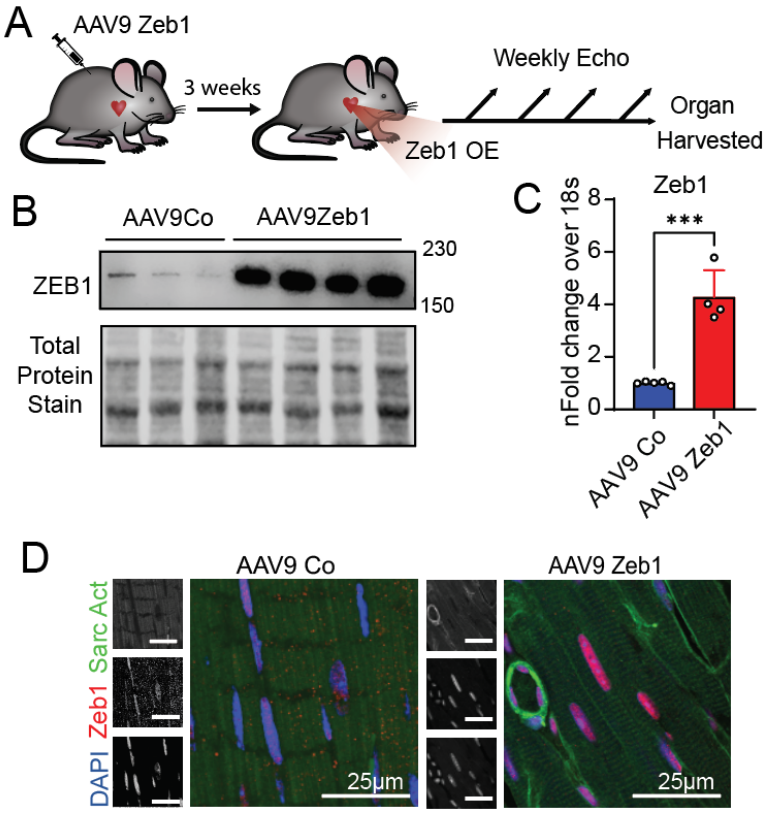

Figure 18. Zeb1 overexpression model *in vivo*.

(a) Schematic timeline of *in vivo* AAV9-mediated Zeb1 overexpression via tail vein injection in 8-week-old male mice and subsequent echocardiographic assessments. (b, c, d) Validation of Zeb1 overexpression in left

ventricular (LV) tissue by Western blot, RT-PCR, and immunostaining (n = 3 per group). (Data shown as mean ± SEM; *=p<0.05, **=p<0.01, ***=p<0.001, ****=p<0.0001 by unpaired Student's t-test or one-way ANOVA as appropriate.)

AAV9 vector encoding full-length Zeb1 under the control of a cardiomyocyte-specific promoter was generated by our lab technician Verena. To achieve targeted overexpression of Zeb1 in the myocardium I administered the AAV9 containing either no CDS (Co) or Zeb1 CDS, via systemic intravenous injection into 8-week-old adult wild-type mice, both male and female (Fig. 18a). At both mRNA and protein levels, I confirmed robust Zeb1 expression in the left ventricular (LV) tissue using quantitative western blotting (Fig. 18b), RT-PCR (Fig. 18c), and immunohistochemical analysis (Fig. 18d), validating the effectiveness of the AAV9-Zeb1 construct for *in vivo* manipulation of Zeb1 levels in the heart.

To assess the functional consequences of sustained Zeb1 overexpression, I conducted serial transthoracic echocardiography at defined intervals following AAV9 administration (Fig. 18a). Remarkably, as early as three weeks post-injection, Zeb1-overexpressing male mice began to show signs of systolic impairment, including a decrease in left ventricular ejection fraction (LVEF). This systolic dysfunction progressively deteriorated over time, and by seven weeks, mice exhibited a significant reduction in LVEF accompanied by an increase in left ventricular wall thickness, a characteristic feature of concentric hypertrophic remodeling (Fig. 19a). Whereas the female mice did not show any pathological phenotype assessed by echocardiography (Fig. 20a).

Interestingly, despite the functional and structural changes, the heart weight-to-body weight (HW/BW) ratio did not significantly differ from controls at this time point in both male and females (Fig. 19b, 20b).

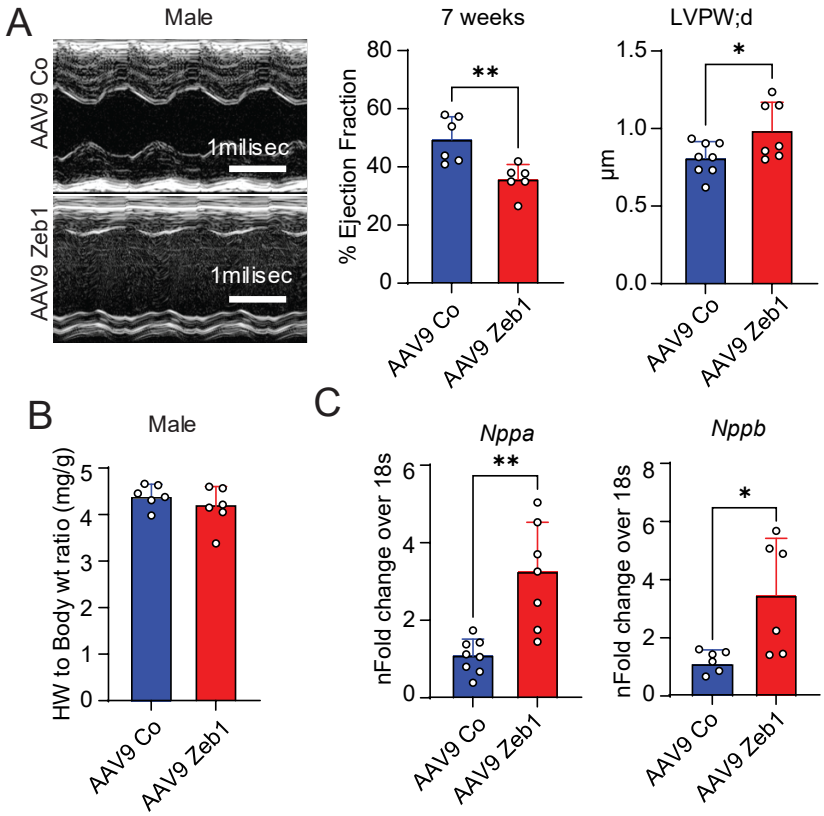

Figure 19. Zeb1 overexpression in male mice induces cardiomyocyte hypertrophy and cardiac dysfunction *in vivo*.

(a) Echocardiographic analysis of male mice showing a significant reduction in % ejection fraction and an increase in LV posterior wall thickness during diastole (LVPW;d) at 7 weeks post-injection in Zeb1 OE mice, indicating hypertrophic dysfunction (n = 6–8). (b) No significant change in heart weight-to-body weight ratio was observed. (c) qRT-PCR analysis of LV tissue showing upregulation of cardiac pathology markers Nppa and Nppb in Zeb1 OE mice, consistent with in vitro findings. (Data shown as mean ± SEM; *=p<0.05, **=p<0.01, ***=p<0.001, ****=p<0.0001 by unpaired Student's t-test or one-way ANOVA as appropriate.)

To determine whether these structural alterations were accompanied by a corresponding shift in gene expression, I performed RT-PCR analysis of classical cardiac pathological and dysfunction markers. Consistent with the *in vitro* data, hearts both male and female of mice overexpressing Zeb1 displayed a significant upregulation of fetal gene program components, including *Nppa* and *Nppb* (Fig. 19c, 20c). These data confirm that Zeb1 overexpression is sufficient to induce pathological remodeling, even in the absence of exogenous hemodynamic stress. While I could only observe the functional changes in the male mice, at the molecular level both male and female show hypertrophic remodeling of cardiomyocytes.

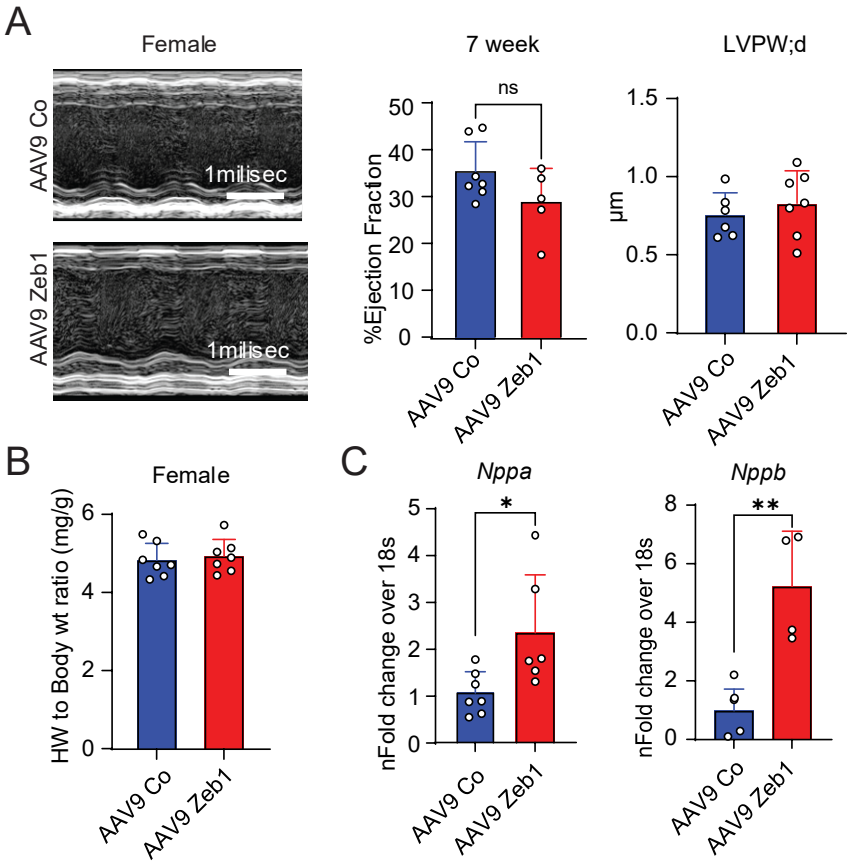

Figure 20. Zeb1 overexpression in female mice does not induce cardiomyocyte hypertrophy and cardiac dysfunction in vivo.

(a) Echocardiographic analysis of female mice showing no significant reduction in % ejection fraction and no change in LV posterior wall thickness during diastole (LVPW;d) at 7 weeks post-injection in Zeb1 OE mice (n = 6–8). (b) No significant change in heart weight-to-body weight ratio was observed. (c) qRT-PCR analysis of LV tissue showing upregulation of cardiac pathology markers Nppa and Nppb in Zeb1 OE mice, consistent with in vitro findings. (Data shown as mean ± SEM; *=p<0.05, **=p<0.01, ***=p<0.001, ****=p<0.0001 by unpaired Student's t-test or one-way ANOVA as appropriate.)

In summary, Zeb1 overexpression in adult mouse hearts was successfully achieved using AAV9 delivery, validated at both transcript and protein levels, and was sufficient to instigate functional, structural, and molecular alterations assessed through echocardiography and gene expression profiling.

4.3 Cardiomyocyte-specific Zeb1 Deletion Model

After demonstrating that sustained Zeb1 overexpression contributes to pathological cardiac remodeling and dysfunction, I next sought to explore the physiological requirement for Zeb1 in the heart by examining the effects of its genetic ablation in cardiomyocytes. To investigate this, a cardiomyocyte-specific Zeb1 conditional knockout (Zeb1 cKO) mouse model was generated by crossing Zeb1 flox/flox mice with transgenic mice expressing Cre recombinase under the

control of the α-myosin heavy chain (αMHC) promoter (Fig. 21a). This promoter becomes active in cardiomyocytes during the late embryonic to early postnatal period, thereby enabling Zeb1 deletion specifically in cardiac muscle cells while leaving its expression intact in other tissues and other cardiac cell types.

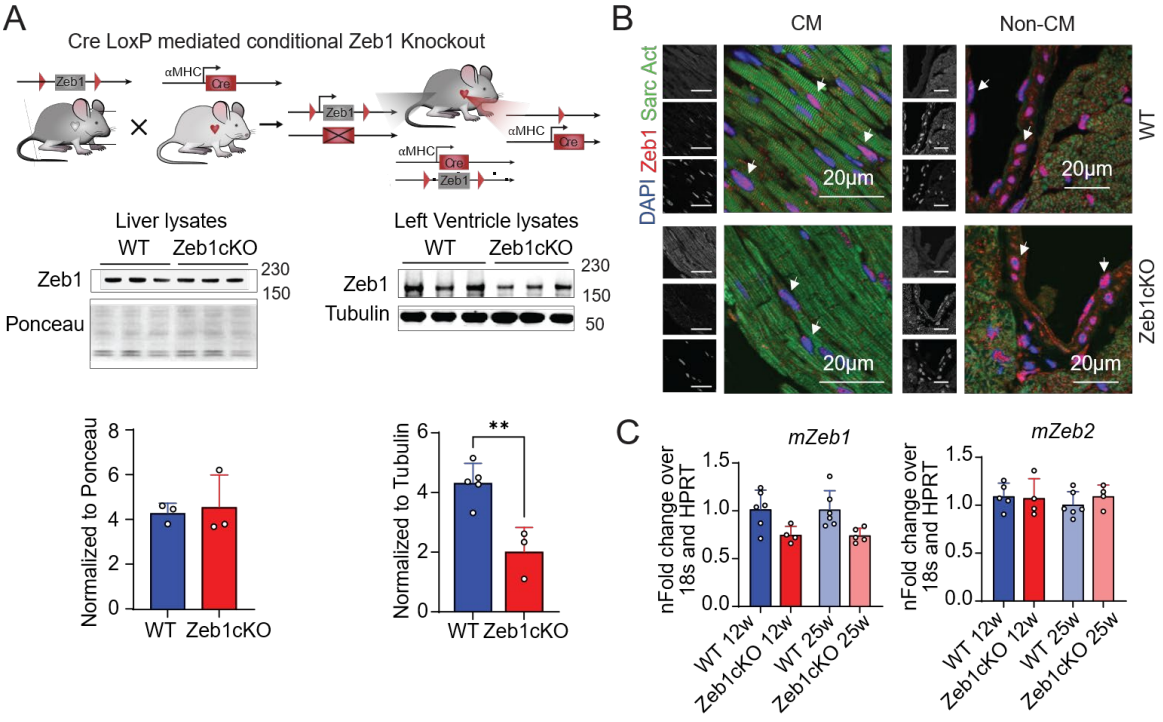

Figure 21. Cardiomyocyte-specific deletion of Zeb1 leads to progressive cardiac dysfunction and pathological remodeling.

(a) Schematic overview of the generation of a cardiomyocyte-specific Zeb1 conditional knockout (Zeb1 cKO) mouse using Cre recombinase driven by the myosin heavy chain alpha (MHC-α) promoter. Western blot validation of Zeb1 deletion in the left ventricle (LV) but not in liver tissue of adult Zeb1 cKO versus WT mice. (b) Immunostaining of LV sections confirm Zeb1 loss specifically in cardiomyocytes. Scale bar = 20 μm. (c) RT-PCR of Zeb1 and Zeb2 validating Zeb2 does not compensate for Zeb1 cKO. (Data are shown as mean ± SEM. Statistical analysis was performed using unpaired Student's t-test or one-way ANOVA, *=p<0.05, **=p<0.01, ***=p<0.001, ****=p<0.0001.)

Zeb1 deletion was confirmed by western blot analysis. A significant reduction in Zeb1 protein levels was observed in left ventricular lysates, whereas liver lysates showed no change, consistent with the cardiomyocyte-specific nature of the knockout, since cardiomyocytes represent only a fraction of total cardiac cells. Importantly, Zeb1 expression remained unaffected in non-cardiac tissues such as the liver (Fig. 21a). Cardiomyocyte-specific Zeb1 deletion was further validated by immunofluorescent staining of left ventricular tissue, which revealed decreased Zeb1 protein expression in cardiomyocytes of Zeb1 cKO mice but not in non-

cardiomyocyte populations, such as endothelial cells (Fig. 21b). Together, these findings confirm successful recombination and efficient, myocardium-specific deletion of Zeb1.

Notably, I found no evidence of compensatory upregulation of Zeb2, the closest homolog of Zeb1, in either young or aged Zeb1 cKO hearts, as assessed by RT-PCR analysis of left ventricular tissue (Fig. 21c). Despite sharing similar zinc finger and homeodomain structures and overlapping roles in other systems, such as during EMT and neural development, Zeb2 does not appear to compensate for the loss of Zeb1 in cardiomyocytes.

4.3.1 Functional Characterization of Zeb1 cKO mice

To evaluate the long-term physiological consequences of Zeb1 deficiency in cardiomyocytes, I assessed cardiac structure and function in male Zeb1 cKO mice from early adulthood (12 weeks) into middle age (25–30 weeks).

Signs of cardiac impairment became evident as early as 12 weeks of age, with echocardiographic analysis revealing a significant reduction in LVEF, dropping to approximately 40%, compared to ~60% in age-matched wild-type (WT) controls. Concomitant with the reduction in systolic performance, chamber dilation of the left ventricle was observed, as evidenced by increased end-diastolic volume and diameter (Fig. 22a). These findings are indicative of pathological cardiac remodeling, which typically precedes overt heart failure.

As the mice aged, these impairments became progressively more pronounced. By 25 weeks of age, male Zeb1 cKO mice exhibited severe systolic dysfunction, with ejection fractions falling below 20% (Fig. 22a). Structural imaging and gross pathological evaluation further confirmed a DCM phenotype, characterized by ventricular chamber enlargement and marked wall thinning (Fig. 22b, c), hallmarks of contractile decompensation and maladaptive remodeling.

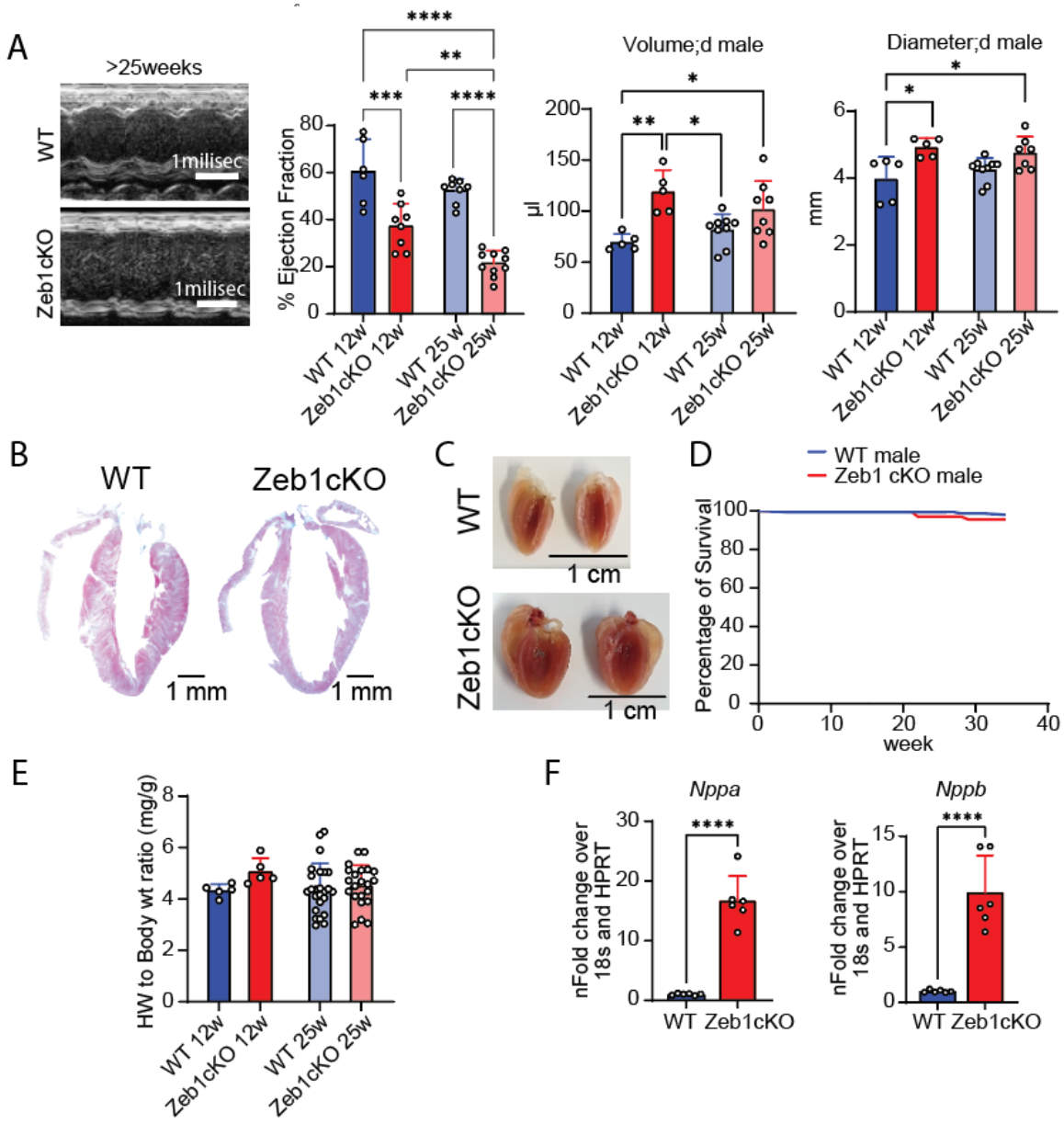

Figure 22. Cardiomyocyte-specific deletion of Zeb1 leads to progressive cardiac dysfunction and pathological remodeling.

(a) Echocardiographic analysis at 12 and ≥25 weeks of age shows significantly reduced ejection fraction in Zeb1 cKO mice, with an early decrease to ~40% at 12 weeks and further decline to ~20% by 25 weeks, compared to stable function in WT controls. LV diastolic volume and diameter were significantly increased in Zeb1 cKO mice (n = 5–10 per group). (b, c) Gross morphology and histological sections of adult hearts reveal ventricular dilation and wall thinning in Zeb1 cKO mice. (d) Survival curve shows only 5% male Zeb1 cKO die starting at 20 weeks of age. (e) Heart weight to body weight ratio was not significantly different between groups. (f) RT-qPCR analysis of cardiac pathology markers Nppa and Nppb shows increased expression in Zeb1 cKO LV lysates, indicating pathological remodeling. (Data are shown as mean ± SEM. Statistical analysis was performed using unpaired Student's t-test or one-way ANOVA, *=p<0.05, **=p<0.01, ***=p<0.001, ****=p<0.0001.)

In parallel, I investigated the longevity of Zeb1 cKO mice. The absence of Zeb1 in cardiomyocytes resulted in the mortality of 5% of the male mice after reaching 20

weeks of age (Fig. 22d). These findings suggest that the loss of Zeb1 has minimal impact on overall survival, despite significant cardiac dysfunction.

Interestingly, despite the severity of the morphological and functional alterations, there was no significant change in heart HW/BW ratio (Fig. 22e). At the molecular level, Zeb1-deficient hearts showed robust activation of fetal gene expression programs, a well-characterized signature of cardiac stress and failure. Expression levels of *Nppa* and *Nppb* were significantly elevated in Zeb1 cKO hearts relative to controls (Fig. 22f).

In conclusion, Zeb1 cKO male mice exhibited progressive structural, functional, and molecular alterations in the heart, as demonstrated by echocardiography, gross pathology, survival assessment, morphometric analysis, and gene expression profiling.

4.3.2 Female Mice are More Severely Affected by Zeb1 Deletion

Sex differences in cardiovascular disease are well documented, with males and females often exhibiting distinct pathophysiological responses, progression rates, and outcomes following cardiac injury or stress. To investigate whether cardiomyocyte-specific loss of Zeb1 induces sex-dependent phenotypic variations, I performed a comprehensive comparative analysis of male and female Zeb1 conditional knockout mice across their lifespan.

The results revealed pronounced sex-specific disparities in the severity and progression of cardiac dysfunction following Zeb1 deletion. Female Zeb1 cKO mice exhibited a significantly more severe cardiac phenotype compared to their male counterparts. Survival analysis showed that by 30 weeks of age, only approximately 80% of female Zeb1 cKO mice survived, whereas male Zeb1 cKO mice demonstrated a higher survival rate of about 95% (Fig. 23a). This survival difference underscores an increased vulnerability in females to the detrimental consequences of Zeb1 loss in cardiomyocytes.

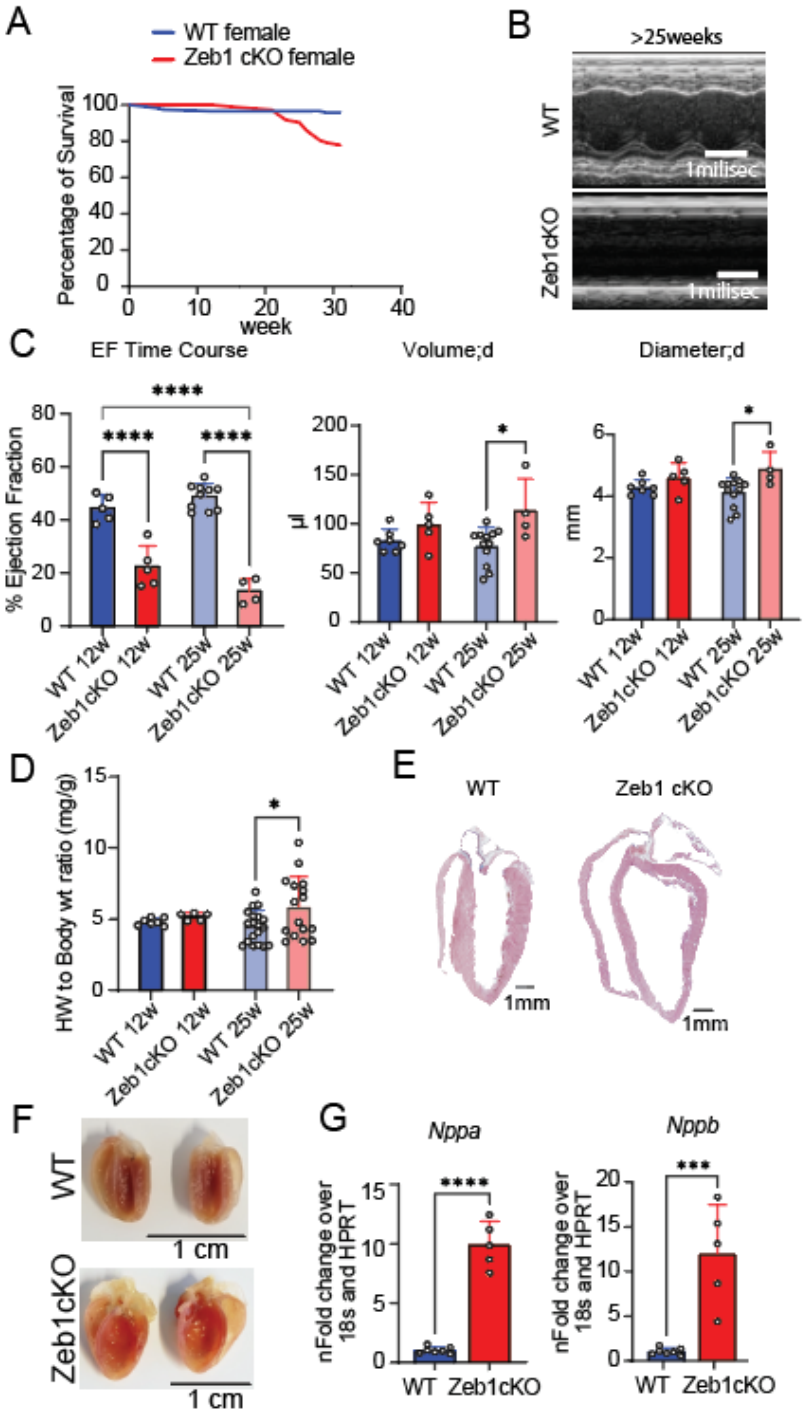

Figure 23. Female Zeb1 cKO mice develop a severe dilated cardiomyopathy phenotype, while adult-onset Zeb1 deletion causes cardiac dysfunction without structural remodeling.

(a) Survival analysis shows a progressive decline in female Zeb1 cKO survival beginning at 20 weeks of age, with only ~80% surviving to 30 weeks. (b) M-mode from echocardiography showing severe LV dilation and wall thinning. (c) Echocardiographic analysis of 25-week-old and older female Zeb1 cKO mice reveals a marked reduction in ejection fraction (EF) to 8–10%, accompanied by increased LV volume and diameter, indicative of end-stage dilated cardiomyopathy (n = 6–8 per group). (d) Heart weight-to-body weight (HW/BW) ratio is significantly increased in aged female Zeb1 cKO mice. (e) Masson's Trichrome Staining of LV tissue shows extensive dilation in female Zeb1 cKO hearts. Scale bar = 500 µm. (f) Gross images of female Zeb1 cKO hearts show severe ventricular dilation. (g) RT-qPCR analysis of LV tissue shows upregulation of Nppa and Nppb in female Zeb1 cKO mice, indicating pathological remodeling. (Data are shown as mean ± SEM. Statistical analysis was performed using unpaired Student's t-test or one-way ANOVA, *=p<0.05, **=p<0.01, ***=p<0.001, ****=p<0.0001.)

Functional cardiac assessments by transthoracic echocardiography demonstrated that female Zeb1 cKO mice developed profound systolic dysfunction, with left ventricular ejection fractions declining precipitously to around 8–10%, indicative of severe heart failure (Fig. 23b). This was accompanied by significant left ventricular chamber dilation, with markedly increased end-diastolic volumes and diameters, reflecting advanced adverse remodeling and ventricular dilatation characteristic of late-stage cardiomyopathy (Fig. 23b). In contrast, male Zeb1 cKO mice displayed comparatively milder functional impairment.

Additionally, female Zeb1 cKO mice exhibited a significant increase in the HW/BW ratio (Fig. 23c), suggesting the presence of pathological hypertrophy in the context of cardiac dilation, a phenotype often associated with maladaptive remodeling.

Histopathological examination revealed drastic reduction in left ventricular wall thickness (Fig. 23d). This was further corroborated by the gross images of the paraffin fixed heart underlining the severity of disease in female Zeb1 cKO hearts (Fig. 23e). Concurrently, molecular analyses showed marked upregulation of canonical cardiac stress-response genes, including *Nppa* and *Nppb*, further validating the activation of pathological gene expression programs consistent with heart failure progression (Fig. 23f).

Collectively, these data demonstrate that the absence of Zeb1 in cardiomyocytes precipitates a more aggressive and severe cardiomyopathic phenotype in females compared to males.

4.3.3 Zeb1 has a Pivotal Role in Cardiac Development by Influencing Cardiomyocyte Proliferation and Maturation

Zeb1 is a well-established transcription factor critically involved in driving EMT. Given that cardiomyocytes (CMs) originate from a mesenchymal lineage during embryogenesis, Zeb1 plays an essential role in their proper maturation and functional acquisition. Loss of Zeb1 function prior to CM maturation impairs their developmental trajectory, leading to defective differentiation and compromised cardiac function (107).

As previously mentioned, the cardiomyocyte-specific Zeb1 cKO model was generated using Cre recombinase under the control of the α-MHC promoter, which is known to be activated predominantly during the late embryonic to early postnatal period, with a sharp increase in activity perinatally (Fig. 24a). Consequently, Zeb1 deletion in the present model occurs primarily around this critical window of cardiac maturation. Gene expression profile of α-MHC and Zeb1 in mouse was generated from “Evo-devo mammalian organs” app from the Kaessmann lab (142) (Fig. 24b). It was found that Zeb1 expression goes down once the cardiomyocytes are matured. This was further confirmed by RT-PCR of *Zeb1* in isolated cardiomyocytes from postnatal day 2 hearts and 8-week-old mouse hearts (Fig. 24c).

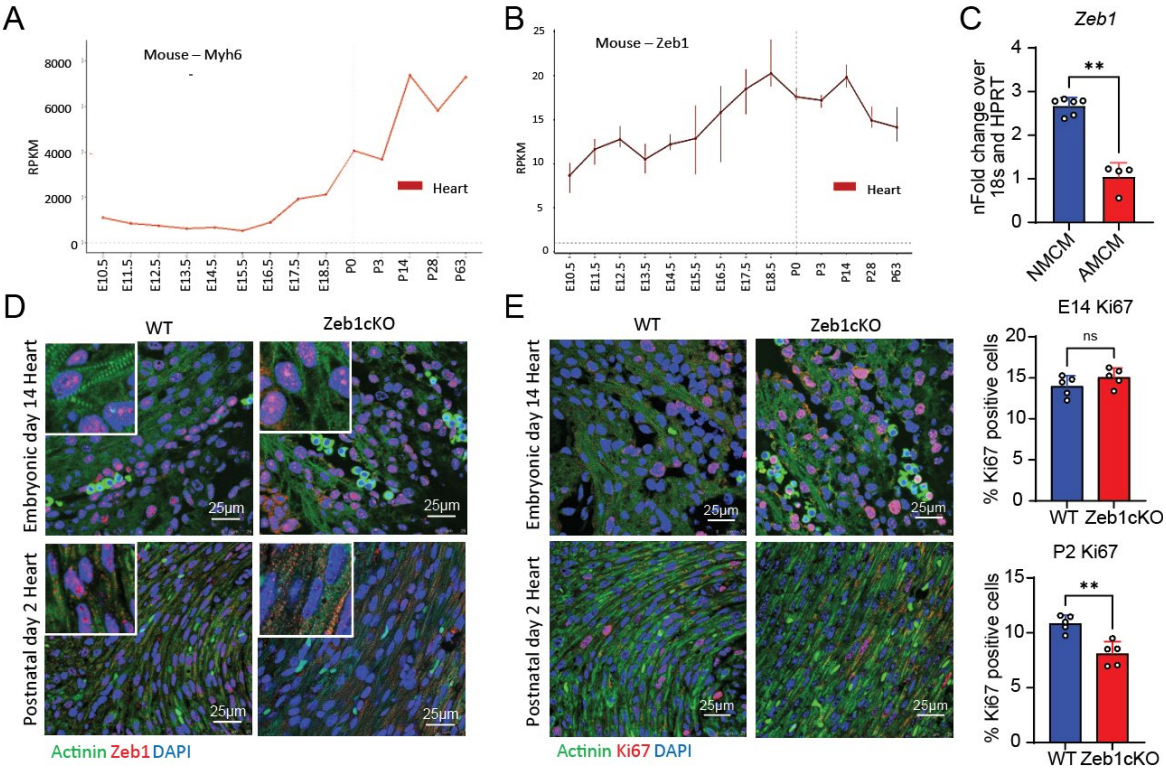

Figure 24. Perinatal Loss of Zeb1 Impairs Cardiomyocyte Proliferation and Maturation During Cardiac Development.

(a, b) Gene expression profile of Myh6 and Zeb1 in mouse generated from “Evo-devo mammalian organs” app from the Kaessmann lab (142). (c) RT-PCR of Zeb1 in isolated cardiomyocytes from postnatal day 2 hearts (NMCM) and 8-week-old mouse hearts (AMCM). (d) Immunofluorescence staining for ZEB1 in heart sections from control and Zeb1 conditional knockout (cKO) mice at embryonic day 14 (E14) and postnatal day 2 (P2), confirming efficient Zeb1 deletion by P2 but not at E14. Nuclei were counterstained with DAPI. (e) Representative immunofluorescence images showing Ki67 (a proliferation marker) staining in ventricular sections from E14 and P2 Zeb1 cKO hearts. Quantification of Ki67-positive cardiomyocytes reveals a significant decrease in the proportion of proliferating CMs at P2 in Zeb1 cKO hearts compared to E14 (n = 5/group). Scale bar: 25 µm. (Data are shown as mean ± SEM. Statistical analysis was performed using unpaired Student’s t-test or one-way ANOVA, *=p<0.05, **=p<0.01, ***=p<0.001, ****=p<0.0001.)

I experimentally confirmed the timing of Zeb1 deletion by comparing ZEB1 protein levels in hearts harvested at embryonic day 14 (E14) versus postnatal day 2 (P2). Immunostaining analyses showed that Zeb1 expression persisted at E14 in the cKO mice but was effectively abolished by P2 (Fig. 24d), validating that recombination and gene knockout occur perinatally, coinciding with key maturation events.

To further investigate the consequences of Zeb1 loss on CM proliferation, we performed immunostaining for Ki67 (antigen Kiel 67), a canonical marker of cell cycle activity and proliferation. Quantitative analysis revealed a significant reduction in the proportion of Ki67-positive cardiomyocytes in P2 hearts from Zeb1 cKO mice compared to E14 hearts (Fig. 24e).

In summary, Zeb1 deletion in cardiomyocytes was confirmed to occur perinatally, coinciding with the critical window of cardiac maturation, as validated by gene expression profiling, RT-PCR, and immunostaining analyses. This deletion was associated with a measurable reduction in proliferating cardiomyocytes.

4.4 Investigating the Role of Zeb1 in Adult Cardiomyocytes after Complete Maturation

To delineate whether the cardiac phenotypes observed in Zeb1 cKO mice stem from developmental loss of Zeb1 or from its absence in fully mature cardiomyocytes, I utilized a temporally controlled, inducible conditional knockout (icKO) model. Zeb1 flox/flox mice were crossed with α-MHC-MerCreMer transgenic mice, which express tamoxifen-inducible Cre recombinase under the cardiomyocyte-specific α-myosin heavy chain promoter (Fig. 25a). This approach allowed for precise temporal deletion of Zeb1 exclusively in adult cardiomyocytes following tamoxifen administration.

Tamoxifen was administered to 6-week-old mice, representing a stage when cardiac development is complete and cardiomyocytes are fully matured (Fig. 25a). Subsequent western blot analysis confirmed efficient and cardiomyocyte-specific ablation of Zeb1 protein in adult cardiac tissue post-tamoxifen treatment (Fig. 25a), validating the inducible knockout model.

I started with investigating the cardiac physiology of mice 7 weeks post tamoxifen injection. Echocardiography data of the male mice did not show any cardiac dysfunction in the absence of Zeb1 after complete cardiomyocyte maturation (Fig. 26a). In comparison to the male mice, female Zeb1 icKO displayed a significant and rapid decline in left ventricular ejection fraction, with reductions indicative of early systolic dysfunction within just seven weeks after tamoxifen administration (Fig.26c). There was no overt ventricular chamber dilation, fibrosis, or increases in heart weight-to-body weight ratio detectable (Fig. 26b, d).

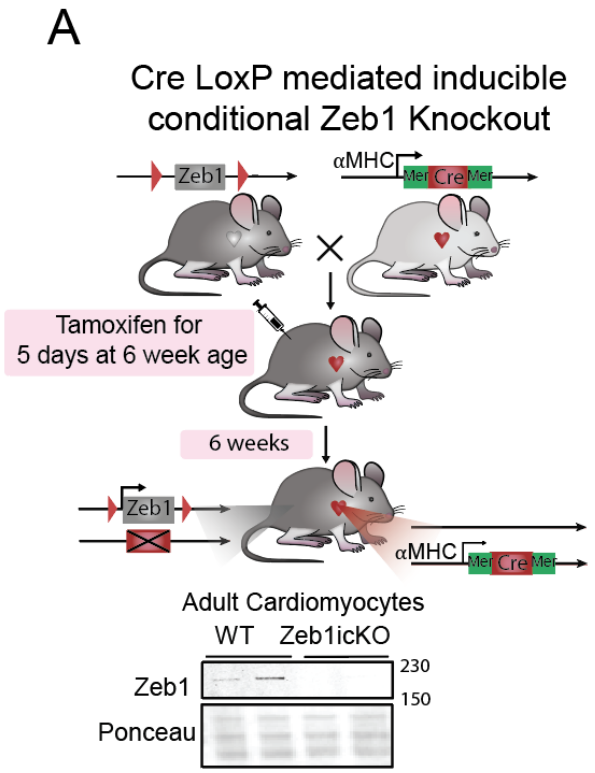

Figure 25. Mouse model to investigate cardiomyocyte homeostasis after complete maturation.

(a) Schematic of tamoxifen-induced, cardiomyocyte-specific Zeb1 inducible conditional knockout (icKO) model and validation of Zeb1 deletion by Western blot in adult mouse hearts.

In contrast, adult male Zeb1 icKO mice displayed resistance to Zeb1 ablation, preserving normal cardiac function and structural integrity (Fig. 26a, b). This clear sex difference underscores a fundamental biological divergence in the reliance on Zeb1-mediated transcriptional regulation between males and females.

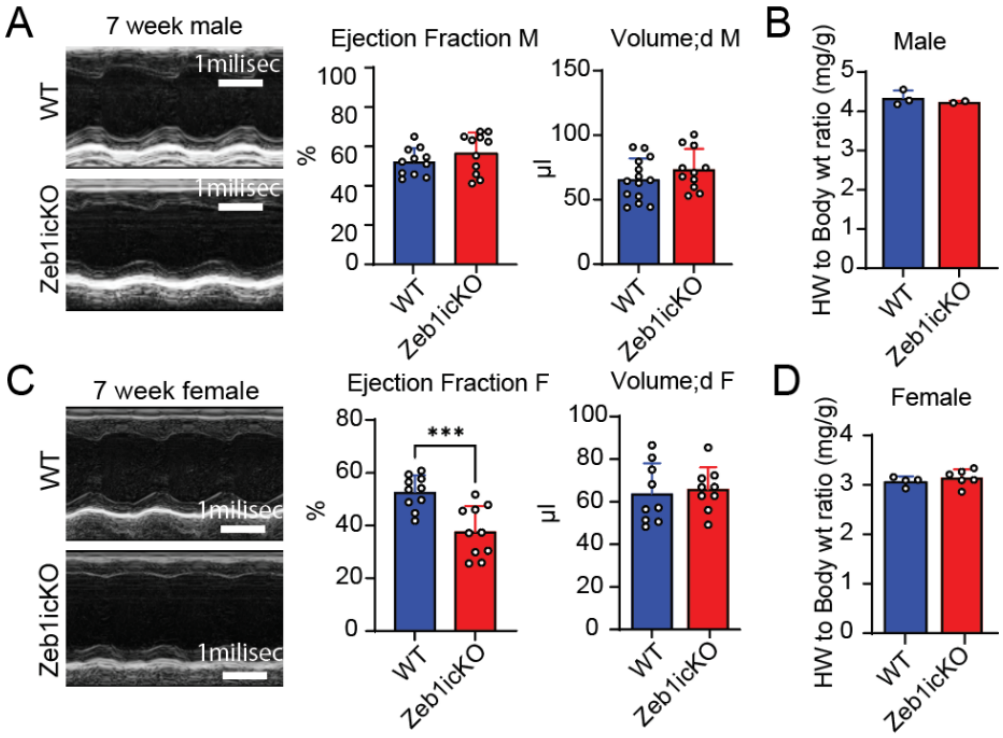

Figure 26. Investigating the role of Zeb1 in adult cardiomyocytes after complete maturation.

(a) EF% is unchanged in male Zeb1 icKO mice 7 weeks after induction. (b) No significant changes were observed in HW/BW ratio or LV volume in Zeb1 icKO mice. (c) EF% is significantly decreased in female Zeb1 icKO mice 7 weeks after induction. (d) No significant changes were observed in HW/BW ratio or LV volume in Zeb1 icKO mice. (Data are shown as mean ± SEM. Statistical analysis was performed using unpaired Student's t-test or one-way ANOVA, *=p<0.05, **=p<0.01, ***=p<0.001, ****=p<0.0001.)

4.5 Zeb1 Deletion Leads to Activation of Epithelial Gene Programs in Cardiomyocytes

Building on my functional observations of severe cardiac impairment in female Zeb1-deficient mice, I sought to elucidate the underlying molecular mechanisms driving this phenotype. To achieve this, I performed bulk RNA sequencing (RNA-seq) on left ventricular tissue harvested from male and female WT and Zeb1 cKO mice aged over 25 weeks, a timepoint representing established disease progression (Fig. 27a).

Specifically, I aimed to characterize how the loss of Zeb1 reshapes the transcriptional landscape in the adult female heart. Sequencing was performed at EMBL core facility and analysis of raw data was done by Prof. Tobias Jakobi at the University of Arizona. Analysis of the transcriptomic data revealed extensive alterations in gene expression following Zeb1 deletion. Gene Ontology (GO) enrichment analysis of the differentially expressed genes (DEGs) highlighted a

significant overrepresentation of pathways related to extracellular matrix (ECM) organization and epithelial cell-related processes (Fig. 27b).

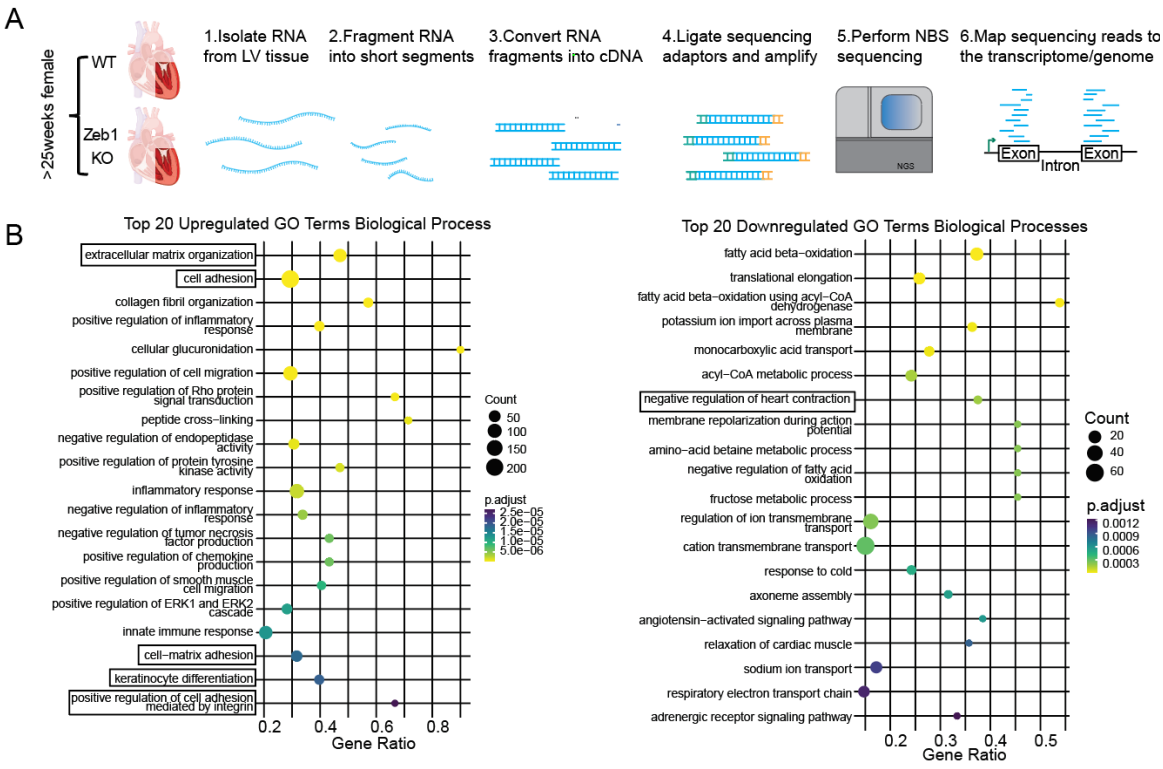

Figure 27. Loss of Zeb1 in female mice leads to upregulation of epithelial and extracellular matrix genes in the left ventricle.

(a) Schematic of the bulk RNA-sequencing workflow performed on left ventricular tissue from >25-week-old female wild-type (WT) and Zeb1 conditional knockout (cKO) mice (n = 3-5 per group). (b) Top20 upregulated and downregulated Gene Ontology (GO) term enrichment analysis highlights DEGs.

To further investigate whether these transcriptional changes were directly orchestrated by Zeb1, an unbiased de novo motif enrichment analysis was conducted by our collaborator Daniel Finke using the HOMER algorithm on the promoters of DEGs. Remarkably, the canonical Zeb1 DNA-binding motif emerged as the top-ranked enriched motif in the female Zeb1 cKO vs WT (Fig. 28a). Overlaying the DEGs and the Zeb1 motif containing genes providing strong evidence that many of the altered genes are direct transcriptional targets of Zeb1 in cardiomyocytes (Fig. 28b).

Closer examination of the DEG subsets revealed a notable asymmetry: out of 1,396 upregulated genes in female Zeb1 cKO hearts, 295 (approximately 3.67%) contained one or more Zeb1 binding motifs in their promoter regions. In contrast, only 96 (1.34%) of the 702 downregulated genes harbored Zeb1 motifs (Fig. 28c).

This disparity underscores the predominantly repressive function of Zeb1 in the cardiac context. Absence of Zeb1, leads to widespread activation of target genes, particularly those involved in maintaining epithelial characteristics and ECM remodeling.

A

HOMER analysis >25 weeks Zeb1 cKO vs WT Female

Rank	Motif	P-value	% of Targets	Best Match/Details
1		1e-20	21.95%	ZEB1
2		1e-14	10.32%	MafF
3		1e-13	1.13%	Gm397
4		1e-12	1.02%	PKNOX2
5		1e-12	1.42%	Gata1
6		1e-12	12.71%	Sp1
7		1e-12	2.72%	Meis1

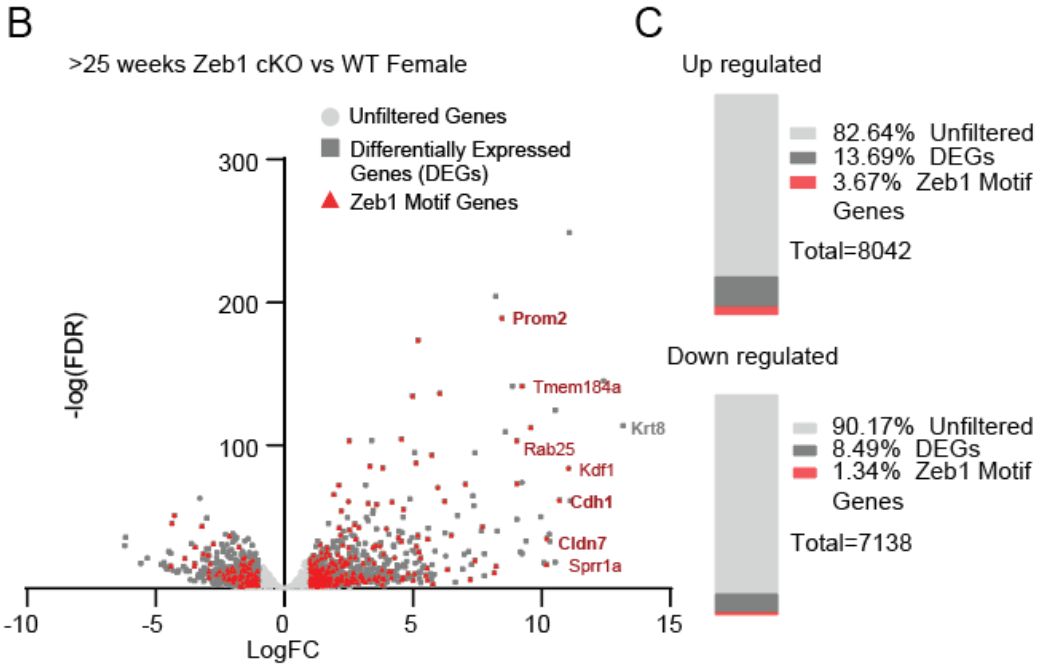

Figure 28. Zeb1 loss alters transcriptional landscape and induces epithelial gene expression in cardiomyocyte.

(a) HOMER de novo motif enrichment analysis of DEG promoter regions identifies Zeb1 as the top-enriched transcription factor binding motif in Zeb1 cKO transcriptomes. (b) Volcano plot showing distribution of genes with Zeb1 binding motifs among upregulated and downregulated DEGs in Zeb1 cKO mice compared to WT. (c) Proportion of genes containing Zeb1 motifs among upregulated and downregulated DEGs, indicating Zeb1's role as a transcriptional repressor.

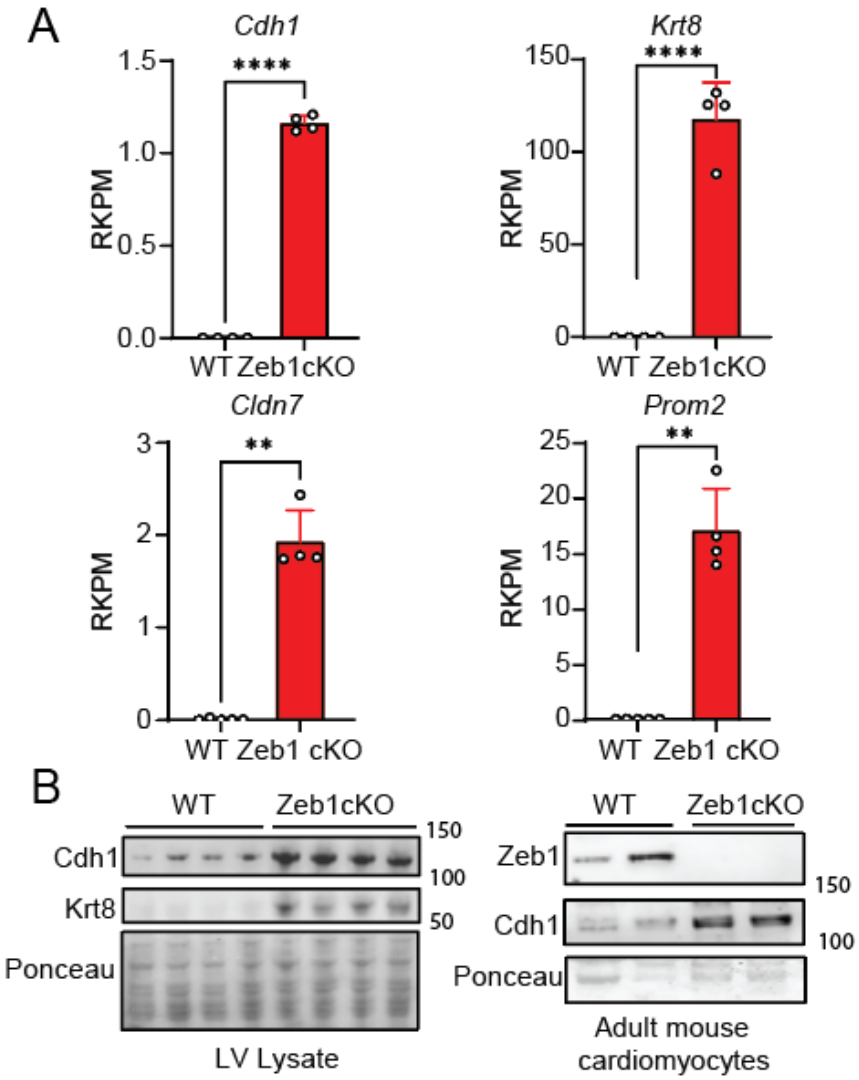

Figure 29. Prominent epithelial genes that are overexpressed in Zeb1 cKO females as compared to WT, identified from the RNA seq data.

(a) Identification of epithelial markers *Cdh1* (E-Cadherin), *Krt8* (Cytokeratin 8), *Cldn7* (Claudin 7), and *Prom2* (Prominin 2) among upregulated DEGs in female Zeb1 KO mice. (b) Elevated protein levels of CDH1and KRT8 in Zeb1 KO left ventricle tissue lysates and adult mouse cardiomyocytes confirm transcriptional effects. (Data are shown as mean ± SEM. Statistical analysis was performed using unpaired Student's t-test or one-way ANOVA, *=p<0.05, **=p<0.01, ***=p<0.001, ****=p<0.0001.)

Among the significantly upregulated genes, I identified several canonical epithelial markers such as *Cdh1*, encoding E-cadherin, *Krt8*, encoding cytokeratin 8, *Cldn7*, encoding claudin 7, *Prom2*, encoding Prominin 2 are all hallmark genes typically silenced during EMT to maintain a mesenchymal phenotype (Fig. 29a). From the motif analysis I found that except for *Krt8* all these mentioned genes have a Zeb1 motif, further cementing the role of Zeb1 in maintaining the mesenchymal phenotype by silencing their expression. The activation of these genes in Zeb1-

deficient cardiomyocytes suggests a partial reversion towards an epithelial-like transcriptional program, indicative of a loss of cellular identity essential for mature cardiomyocyte function. Supporting this transcriptional evidence, western blot analyses confirmed elevated protein expression of *Cdh1* and *Krt8* in Zeb1-null left ventricular tissue lysates as well as in isolated adult cardiomyocytes lacking Zeb1 (Fig. 29b).

In summary, bulk RNA sequencing of left ventricular tissue from male and female Zeb1 cKO and WT mice revealed widespread transcriptional changes in the adult female heart. Motif enrichment analysis identified the canonical Zeb1 binding motif among many differentially expressed genes, indicating that a subset of these genes is a direct Zeb1 targets. Upregulated genes included canonical epithelial markers, and increased protein expression of CDH1 and KRT8 was confirmed in Zeb1-deficient hearts and isolated cardiomyocytes, demonstrating coordinated transcriptional and protein-level alterations following Zeb1 loss.

4.6 Zeb1 is Required for Sarcomere Integrity and Mitochondrial Structure

Previous experiments strongly indicate that cardiomyocytes undergo significant molecular changes in the absence of Zeb1. To delve deeper into this phenomenon, I conducted detailed structural analyses of cardiomyocytes. Hematoxylin and Eosin (H&E) staining of male Zeb1 cKO hearts did not reveal major structural differences. However, in female Zeb1 cKO hearts, I observed misalignment of cardiomyocytes within the left ventricle wall (Fig. 30a). This finding prompted further investigation into cellular dimensions using Wheat Germ Agglutinin (WGA) staining, which highlights cardiomyocyte borders. Here, I observed a notable increase in cardiomyocyte cross-sectional area (Fig. 30b), indicative of cellular hypertrophy.

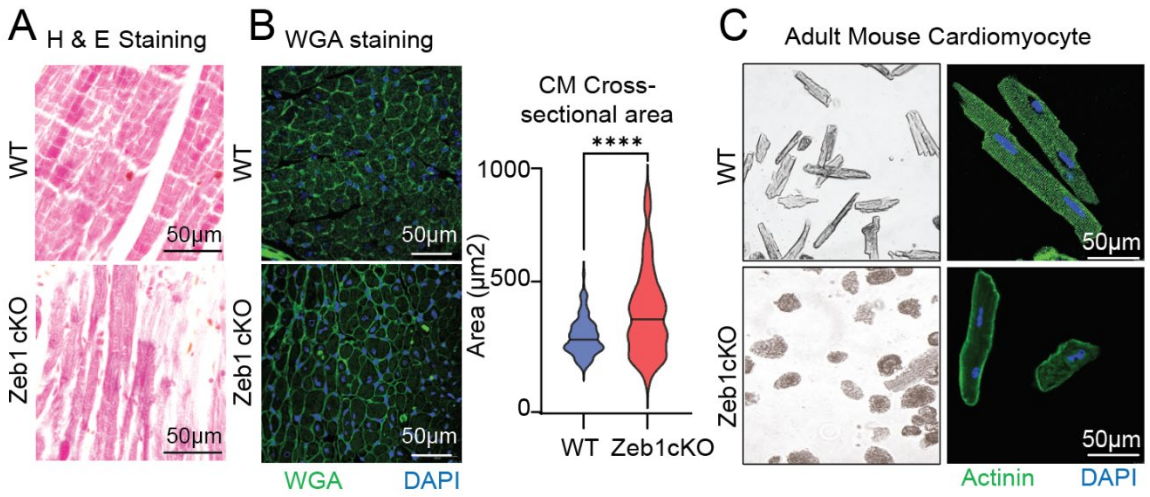

Figure 30. Structural and morphological alterations in female Zeb1 cKO hearts.

(a) H and E staining of left ventricle tissue section from >25 weeks female mice. (b) WGA staining of left ventricle tissue section from >25 weeks female mice and cardiomyocyte cross sectional area quantification showing a significant increase in the Zeb1 cKO. (c) Brightfield image and sarcomeric actinin immunostained Isolated Adult cardiomyocytes from WT and Zeb1 cKO hearts. (Data are shown as mean ± SEM. Statistical analysis was performed using unpaired Student's t-test or one-way ANOVA, *=p<0.05, **=p<0.01, ***=p<0.001, ****=p<0.0001.)

During the isolation of adult cardiomyocytes, a striking decrease in yield was observed from female Zeb1 cKO hearts. Moreover, these cells exhibited reduced size and viability compared to WT counterparts. While WT cardiomyocytes maintained their elongated rod-like shape and survived for 24 hours in culture media, Zeb1 cKO cardiomyocytes were notably smaller and had a significantly shorter lifespan, dying within an hour (Fig. 30c).

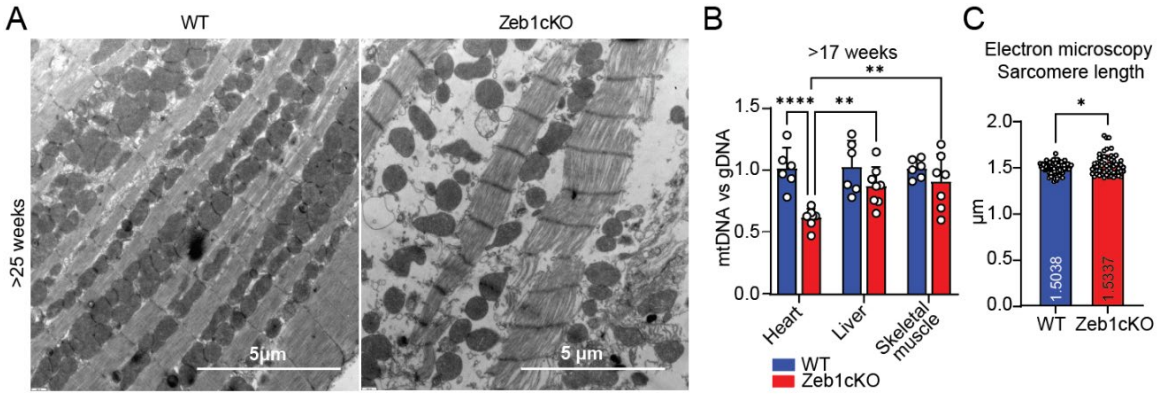

Figure 31. Zeb1 deletion disrupts sarcomeric architecture and mitochondrial integrity in cardiomyocytes, leading to structural remodeling and cardiac dysfunction.

(a) Transmission electron microscopy (TEM) images of left ventricular tissue from 25-week-old WT and Zeb1 cKO female mice show profound sarcomeric disorganization, with disrupted actin and myosin filament

structure, along with mitochondrial abnormalities such as reduced number and disorganized morphology. Scale bars: 500 nm. Performed with the assistance of EMCF Heidelberg. (b) Mitochondrial DNA (16s and ND1) vs genomic DNA (HK2) quantification by RT-PCR from heart, liver, and skeletal muscle from 17 weeks and older female mice. (c) Sarcomere length measurement from the TEM images. (Data are shown as mean ± SEM. Statistical analysis was performed using unpaired Student's t-test or one-way ANOVA, *=p<0.05, **=p<0.01, ***=p<0.001, ****=p<0.0001.)

To gain deeper insights into the structural alterations underlying cardiac dysfunction in Zeb1 cKO mice, I employed Transmission Electron Microscopy (TEM) to examine the ultrastructural integrity of cardiomyocytes from 25-week-old female mice. TEM analysis revealed extensive sarcomeric disarray in Zeb1 cKO hearts. Specifically, there was a near-complete loss of the organized actin and myosin filament arrays that are crucial for forming the contractile units within cardiomyocytes (Fig. 31a).

In addition to sarcomeric abnormalities, I observed significant mitochondrial defects, including marked ultrastructural disruption of mitochondrial cristae and a conspicuous reduction in mitochondrial density. The mitochondria in Zeb1-deficient hearts appeared swollen and fragmented, indicative of impaired mitochondrial integrity and potential bioenergetic failure (Fig. 31a). Quantitative RT-PCR analysis confirmed a substantial decrease in mitochondrial DNA content relative to genomic DNA in Zeb1 cKO hearts, further validating the compromised mitochondrial biogenesis or maintenance (Fig. 31b). Additionally, sarcomere length and Z-disc thickness were increased in the cardiac tissue of Zeb1 cKO mice compared to WT controls. Quantification of these structural alterations was performed by measuring sarcomere length using ImageJ software showing statistically significant increase in the Zeb1 cKO hearts (Fig. 31c).

Building on these ultrastructural observations, I hypothesized that the loss of Zeb1 leads to specific alterations in sarcomere morphology. To test this, I performed objective sarcomere dimension measurements. Unfortunately, the isolation of viable adult cardiomyocytes (ACMs) from female Zeb1 cKO mice proved largely unsuccessful, likely due to the severely compromised cellular integrity and overall poor constitution of these cells. However, ACMs isolated from younger, 8-week-old male Zeb1 cKO mice were successfully analyzed using the IonOptix system to measure sarcomere length dynamics (Fig. 32a). These male Zeb1 cKO ACMs

exhibited a significant and consistent increase in resting sarcomere length compared to WT controls (Fig. 32b).

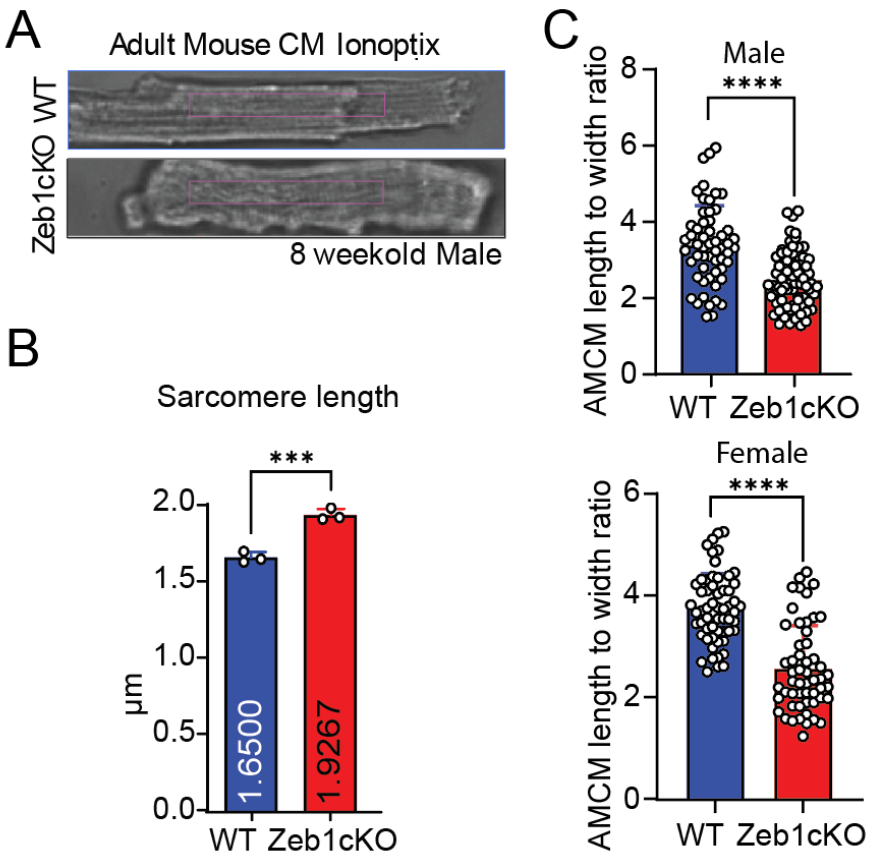

Figure 32. Functional assessment of contractility in Zeb1 cKO cardiomyocytes.

(a) IonOptix in adult cardiomyocytes isolated from 8-week-old male WT and Zeb1 cKO mice (b) Sarcomere length quantification reveals a significant increase in sarcomere length in Zeb1 cKO cells (n = 30-35 cells per mouse, 3 mice in total). (c) Cardiomyocytes isolated from formaldehyde-fixed hearts of mice ≥25 weeks showed reduced yield in Zeb1 cKO compared to WT. Zeb1-deficient cells displayed a significantly lower length-to-width ratio, indicating altered morphology in both male and female. (Data are shown as mean ± SEM. Statistical analysis was performed using unpaired Student's t-test or one-way ANOVA, *=p<0.05, **=p<0.01, ***=p<0.001, ****=p<0.0001.)

To validate these findings in older animals where viable cardiomyocyte isolation was not feasible, I employed a technique for isolating cardiomyocytes from formaldehyde-fixed frozen cardiac tissue from both male and female mice aged 25 weeks and older (143). Consistent with previous observations, the yield of isolated cardiomyocytes from Zeb1 cKO hearts was significantly lower than from WT hearts, reflecting compromised cellular viability or increased fragility. Morphometric analysis of these isolated cells revealed a pronounced decrease in the length-to-width ratio in Zeb1-deficient cardiomyocytes (Fig. 32 c).

Furthermore, immunohistochemical staining for Muscle LIM Protein 2 (MLP2), a Z-disc-associated protein critical for sarcomere stability and function, was performed on cardiac sections (Fig. 33a, d, g). This analysis revealed a significant increase in both sarcomere length and Z-disc thickness in female Zeb1 cKO hearts compared to male cKO mice (Fig. 33b, c). The thickening of the Z-disc, which serves as the anchoring site for actin filaments and transmits contractile force, likely reflects compensatory structural remodeling in response to sarcomeric destabilization.

Similarly, analysis of Zeb1 icKO hearts through MLP2 immunostaining showed no appreciable sarcomeric alterations in male mice (Fig. 33g, h, i). In striking contrast, female Zeb1 icKO hearts exhibited a significant increase in both sarcomere length and Z-disc thickness (Fig. 33d, e, f), reinforcing the critical role of Zeb1 in preserving adult cardiomyocyte sarcomeric architecture and function.

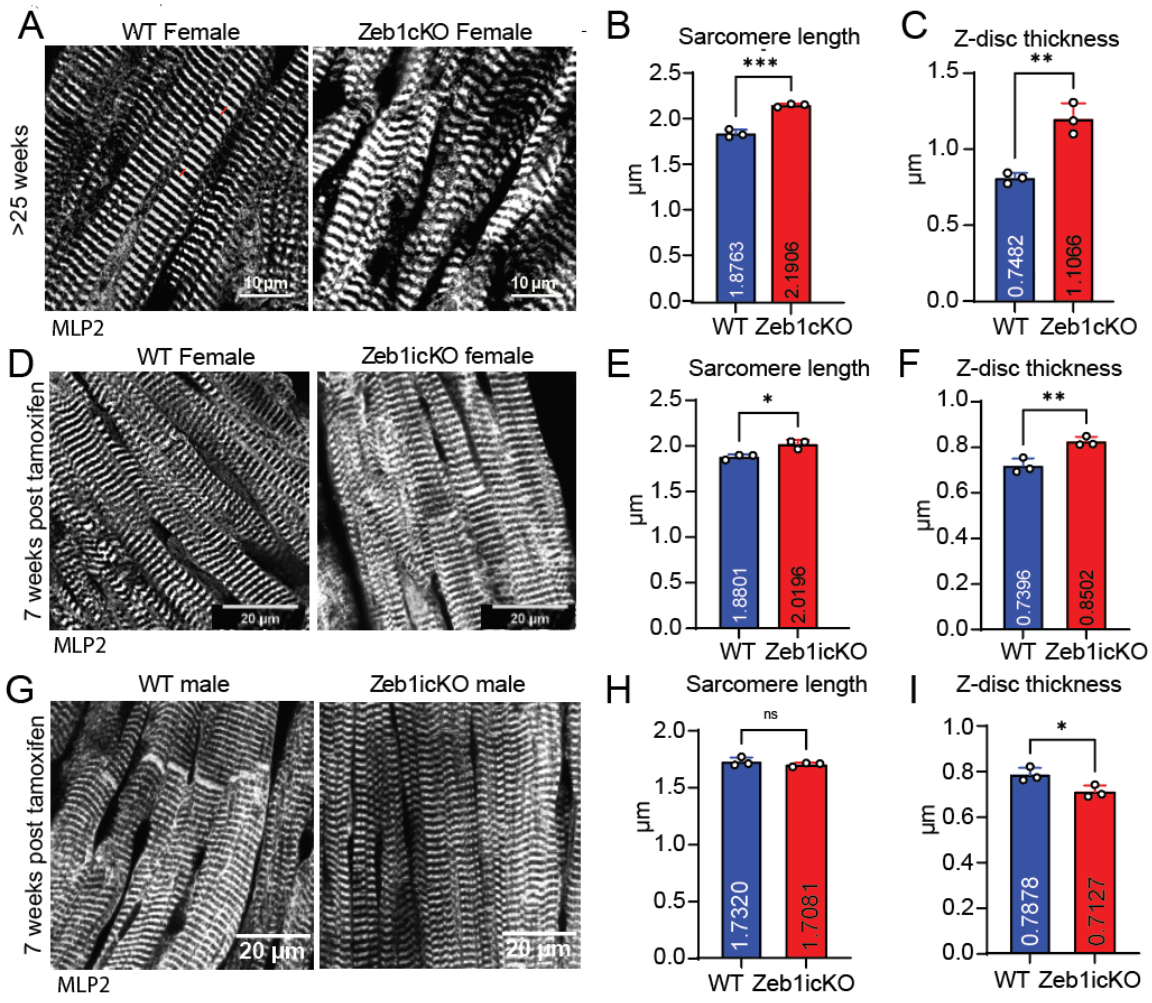

Figure 33. Zeb1 Loss Induces Sex-Specific Structural Alterations in Sarcomere Organization.

(a) Immunostaining for CSRP3 (Z-disc marker) on LV sections from 25-week-old female WT and Zeb1 cKO mice. Scale bar: 10 µm. (b,c) Increased sarcomere length and Z-disc thickness in Zeb1 cKO hearts (n = 3).

(d) CSRP3-based analysis of LV sections from female Zeb1 inducible conditional knockout (icKO) mice. Scale bar: 20 µm. (e,f) A significant increase in sarcomere length and Z-disc thickness (n = 3). (g) CSRP3-based analysis of LV sections from male Zeb1 inducible conditional knockout (icKO) mice. Scale bar: 20 µm. (h,i) No significant change in sarcomere length and Z-disc thickness (n = 3). (Data are shown as mean ± SEM. Statistical analysis was performed using unpaired Student's t-test or one-way ANOVA, *=p<0.05, **=p<0.01, ***=p<0.001, ****=p<0.0001.)

Structural analyses of Zeb1-deficient cardiomyocytes revealed sex-specific alterations, including increased cell cross-sectional area, reduced cardiomyocyte yield and viability, disrupted sarcomeric organization, altered sarcomere length, Z-disc thickening, and compromised mitochondrial integrity. These changes were consistently observed across multiple methods, including histology, immunostaining, TEM, sarcomere dynamics measurements, and morphometric analyses of both isolated and fixed cardiomyocytes.

5. Discussion

The heart is an exquisitely regulated organ where cellular structure and transcriptional control must remain in tight equilibrium to support life-long function (14,18,20). My findings point to Zeb1 as a comparatively less studied transcription factor with a potentially critical role in maintaining cardiomyocyte integrity. While Zeb1 has been extensively studied in cancer biology and EMT (87,96,101,117,144), these findings place it at the center of cardiomyocyte structural stability and functional maintenance. Using both gain- and loss-of-function mouse models, I demonstrate that Zeb1 is a dosage-sensitive regulator of cardiac homeostasis: its deficiency results in contractile failure and cellular disorganization, while its overexpression triggers maladaptive remodeling. Notably, these effects are sex-specific, female hearts exhibiting greater vulnerability to Zeb1 loss, whereas overexpression drives male heart towards pathological remodeling. These observations both enrich our understanding of sex differences in cardiac disease and open new lines of inquiry into sex-specific regulatory mechanisms in the heart.

5.1 Post-Transcriptional Regulation of Zeb1 as a Context-Dependent Modulator of Cardiac Remodeling

Pressure overload induces a rise in ZEB1 protein levels, with no similar increase in mRNA levels indicating post-transcriptional regulation. Also, ZEB1 protein is increased in hearts of the hypertrophic Mybpc3 KO mouse model. In contrast, ZEB1 protein is reduced in human patient samples from ICM and DCM, as well as in the Rbm20 KO induced dilated cardiomyopathy mouse model. These findings highlight an dynamic regulation of ZEB1 in the heart during pathological stress, adding a new layer of complexity to the role of this transcription factor outside of its well-known function in EMT.

The dissociation between Zeb1 protein and mRNA levels suggests that Zeb1 is regulated predominantly through post-transcriptional mechanisms. This has been reported for other proteins important during development like Poly(A)-Binding Protein Cytoplasmic 1 (PABPC1). While its mRNA levels are constant throughout embryogenesis till adulthood, the protein levels are downregulated shortly after birth and in healthy adult hearts. Its increased translation resulting in a rise in

PABPC1 protein levels is induced by pressure overload as well as exercise, with the transcript levels staying constant (145).

Importantly, the reciprocal expression patterns observed across different disease contexts suggest that Zeb1 regulation may represent a context-dependent, actively modulated response rather than a secondary consequence of cardiac pathology. Zeb1 upregulation appears to be associated with hypertrophic growth, whereas its downregulation aligns with dilated and thinning myocardium. The absence of parallel changes in mRNA expression further underscores the importance of post-transcriptional control in fine-tuning Zeb1 abundance. Together, these findings suggest that Zeb1 may play an active role in orchestrating cardiomyocyte responses to pathological stimuli in a manner that depends on the specific remodeling phenotype.

5.1.1 ZEB1 as a Direct Driver of Cardiomyocyte Hypertrophy and Maladaptive Remodeling

Adenovirus and AAV9-mediated Zeb1 overexpression in NRCMs and adult mice respectively, induce maladaptive hypertrophic remodeling, characterized by increased cardiomyocyte size, reactivation of fetal genes such as Nppa, sarcomeric disorganization, and progressive systolic dysfunction. This phenotype points to ZEB1 being more than a passive marker of stress in the heart, it acts as an active driver of hypertrophy and maladaptive remodeling. When ZEB1 levels are elevated, either experimentally or in response to physiological stimuli, cardiomyocytes are pushed into a growth program that resembles recapitulate features of pathological stress. This shift includes both the reactivation of fetal genes and the suppression of mature contractile machinery, classic hallmarks of a remodeling heart.

Overexpression of Zeb1 alone is enough to enlarge cardiomyocytes, reprogram the transcriptome, and, *in vivo*, recapitulate features of heart failure such as systolic dysfunction and concentric remodeling. In other words, ZEB1 can function as a molecular switch, directly imposing a hypertrophic phenotype rather than simply reflecting one.

Altogether, these insights underscore that ZEB1 is tightly integrated into the heart's stress-response machinery. Its natural induction by hypertrophic stimuli such as phenylephrine confirms its relevance to native signaling pathways, while its

overexpression shows just how powerfully it can redirect cardiomyocyte fate. Given its ability to orchestrate hypertrophic growth and transcriptional reprogramming, ZEB1 stands out as a central regulator of maladaptive remodeling. Potentially, as a promising therapeutic target to blunt or even reverse the progression toward heart failure.

5.1.2 Loss of Zeb1 Induces Cardiomyocyte Remodeling and Progressive Cardiac Dysfunction

Given Zeb1's established role in regulating cell fate transitions and cytoskeletal organization in other mesenchymal-derived tissues, I hypothesized that its absence in cardiomyocytes could compromise cellular architecture and homeostasis, ultimately leading to progressive cardiac dysfunction. The Zeb1 cKO model thus provides a powerful system to dissect the contribution of endogenous Zeb1 to maintaining myocardial structure, transcriptional programs, and overall cardiac performance.

Cardiomyocyte-specific Zeb1 knockout resulted in spontaneous, progressive cardiomyopathy even in the absence of overt stress. These mice develop early systolic dysfunction, ventricular dilation, disrupted sarcomere architecture, and mitochondrial abnormalities, highlighting Zeb1's critical role in maintaining homeostasis.

The cardiac remodeling observed in this model was characterized by eccentric remodeling, marked by ventricular dilation and myocardial thinning without proportional increase in myocardial mass. This phenotype reinforces the interpretation that loss of Zeb1 induces a pathological transcriptional shift reminiscent of maladaptive remodeling commonly observed in human and experimental models of heart failure.

To investigate the role of Zeb1 in cardiac gene regulation, I performed bulk RNA sequencing on left ventricular tissue from 12-week-old male WT and Zeb1 cKO mice, as well as a 33-week-old male and female WT and Zeb1 cKO mice. Comparative transcriptomic analysis revealed a consistent pattern of upregulated ECM and epithelial-associated genes, accompanied by a downregulation of mitochondrial genes. These transcriptional changes aligned with histological evidence, which demonstrated structural remodeling and mitochondrial damage in Zeb1 cKO hearts. The transcriptional profile observed in Zeb1 cKO mice suggests

that Zeb1 acts as a key regulator of myocardial integrity by balancing extracellular matrix remodeling and mitochondrial homeostasis. The upregulation of ECM genes reflects an early fibrotic or maladaptive remodeling, consistent with structural alterations detected histologically. Similarly, the induction of epithelial genes may indicate a shift toward an aberrant differentiation program. The downregulation of mitochondrial genes points to impaired energy metabolism, a hallmark of cardiac dysfunction. Given the high energetic demands of the heart, disruption of mitochondrial gene expression may underlie the mitochondrial structural abnormalities observed and contribute directly to impaired contractile performance. Together, these findings highlight Zeb1 as a potential guardian of structural and functional stability in the myocardium.

Notably, I found no evidence of compensatory upregulation of Zeb2, the closest homolog of Zeb1, in either young or aged Zeb1 cKO hearts. Despite sharing similar zinc finger and homeodomain structures and overlapping roles in other systems, such as during EMT and neural development, Zeb2 does not appear to compensate for the loss of Zeb1 in cardiomyocytes (90,91).

Finally, the phenotype may also indicate impaired cardiomyocyte proliferative capacity in the absence of Zeb1. A decline in proliferation during the critical perinatal period, when cardiomyocytes transition from an embryonic proliferative state to terminal differentiation, likely contributes to the abnormal cardiac development and dysfunction observed in Zeb1-deficient hearts. These findings collectively suggest that Zeb1 is important for proper cardiomyocyte maturation, proliferative expansion, and the establishment of a stable differentiated state. The observed perinatal effects in the αMHC-driven cKO model are consistent with a potential role for Zeb1 in coordinating the transition to mature, functional cardiomyocytes.

5.1.3 Zeb1: A Context- and Dose-Sensitive Regulator of Cardiac Homeostasis

So far it has been established that Zeb1 is essential for the overall maintenance of cardiomyocyte structural and functional ability to preserve a healthy cardiac function. At a mechanistic level, Zeb1 appears to act less like a simple on/off switch and more like a molecular gatekeeper. Consistent with this role, loss of Zeb1 activates epithelial and extracellular matrix gene programs that destabilize

contractile networks. This perturbation skews cardiac gene expression and culminates in severe structural damage. HOMER analysis indicated Zeb1's occupancy at promoters of structural and metabolic genes, supporting a direct regulatory contribution. Complementary gain-of-function experiments show that overactivation can transiently increase stress tolerance and mitochondrial output, but with sustained activity the myocardium becomes stiffer and exhibits maladaptive remodeling. *In vivo*, both insufficient and excessive Zeb1 activity are associated with cardiomyopathy, with Zeb1 deficiency favouring dilated features and Zeb1 overactivity aligning with diastolic impairment.

Taken together, the data supports a context-dependent model in which a narrow range of Zeb1 activity sustains myocardial homeostasis. Reduced ZEB1 level compromises cardiomyocyte identity and energetic support; increased ZEB1 level biases the heart toward fibrosis-like stiffness and impaired relaxation. These findings suggest that rather than binary therapeutic strategies, a more calibrated modulation of Zeb1 activity may be required to preserve structural integrity and metabolic adequacy while minimizing maladaptive remodeling.

5.2 Age-Dependent Consequences of Zeb1 Deficiency

My study underscores Zeb1 as a central regulator of cardiomyocyte biology, with functions that extend from early development through adulthood. In the absence of Zeb1, cardiomyocytes fail to undergo proper developmental maturation: their proliferative capacity is compromised at the neonatal stage. While this early exit from the proliferative state may initially produce cardiomyocytes with a mature phenotype, it comes at the cost of reduced adaptability and long-term stability. This developmental imbalance appears to lay the foundation for the progressive cardiac dysfunction I observed.

At eight weeks of age, Zeb1-deficient cardiomyocytes displayed poor survivability when isolated and underwent spontaneous death under electrical pacing. This suggests that Zeb1 is important for maintaining contractile stability and cellular viability under stress. These defects were consistently more severe in females, revealing a sex-dependent sensitivity to Zeb1 loss. By 12 weeks, the consequences translated into measurable physiological decline, with a significant reduction in LVEF compared to wild-type controls. This establishes Zeb1 not simply

as a developmental regulator but as a continuing requirement for the formation and function of a healthy, contractile myocardium.

As the mice aged further, the severity of dysfunction escalated. Female Zeb1 cKO mice began dying spontaneously around 20 weeks, and longitudinal analyses revealed a pattern of progressive cardiac failure in both sexes. Physiological, molecular, and histological studies demonstrated left ventricular dilation, pronounced wall thinning, and robust activation of pathological gene programs—hallmarks of maladaptive remodeling. By late adulthood, cardiac output had deteriorated to life-threatening levels, with LVEF falling below 20% in males and below 10% in females. These functional declines were mirrored by profound ultrastructural changes: transmission electron microscopy revealed sarcomeric disarray, Z-disc thickening, and loss of cardiomyocyte identity. Such structural collapse not only explains the contractile failure but also points to a possible identity shift in Zeb1-deficient cells, in which the genetic programs necessary for mesenchymal integrity and stress resistance are eroded.

These observations are consistent with Zeb1's well-established role as a master regulator of EMT, where it governs cellular identity, adhesion, and tissue architecture (146). A growing body of work places ZEB1 at a strategic crossroad between epithelial–mesenchymal plasticity (97,98,101,117), genome maintenance (147–150), and senescence programs (105,151,152)—three axes that collectively shape tissue ageing. Early genetic evidence established that Zeb1 is not just an EMT driver but also a brake on senescence: Zeb1-null or Zeb1-haploinsufficient Mouse Embryonic Fibroblasts (MEFs) undergo premature senescence associated with activation of the cyclin-dependent kinase inhibitors p15 Ink4b and p21 Cip1, which ZEB1 normally represses directly at their promoters (105). These cells also show impaired proliferative capacity and early cell-cycle exit, linking ZEB1 loss to a classic senescence phenotype (105).

At the same time, ZEB1 is embedded in feedback loops that are themselves age-sensitive. The reciprocal repression between ZEB1 and the miR-200 family—which intensifies under oxidative stress and in aged endothelium—links redox state to cell-identity and senescence decisions (152). Reviews of endothelial ageing highlight that miR-200 upregulation in older or stressed vasculature targets ZEB1/ZEB2 and SIRT1 (Sirtuin 1), promoting Reactive Oxygen Species (ROS)

accumulation, p53 activation, and pro-senescent signaling (152–155). This provides a plausible route for age-related microRNA drift to erode ZEB1 levels and favor senescence in vascular beds.

In cardiomyocytes, Zeb1 maintains the mesenchymal phenotype by repressing epithelial gene programs, and the activation of these genes in Zeb1-deficient cells suggests a partial reversion toward an epithelial-like transcriptional state (105). This shift reflects a loss of mesenchymal identity that is essential for mature cardiomyocyte function. Beyond development, Zeb1 also safeguards cytoskeletal organization, mitochondrial health, and metabolic networks that underpin structural integrity and stress adaptation (156). The persistence of dysfunction even when Zeb1 is deleted in adult mice demonstrates that cardiomyocytes require Zeb1 throughout life to preserve their contractile apparatus and maintain their cardiomyocyte identity and mesenchymal origin.

Collectively, my findings identify Zeb1 as a critical regulator that connects embryonic developmental pathways with the maintenance of myocardial function in the adult heart. Its absence triggers a cascade of defects—beginning with reduced proliferation, followed by contractile instability, and culminating in structural and functional collapse. Beyond illuminating a key mechanism of cardiomyopathy, these findings offer translational promise: therapies aimed at modulating Zeb1 or its downstream networks may hold potential to stabilize cardiomyocyte structure, restore mitochondrial integrity, and slow or reverse maladaptive remodeling. Crucially, such interventions will need to be carefully tuned to preserve Zeb1’s protective functions while avoiding maladaptive consequences, and tailored to account for sex-specific vulnerabilities.

5.3 Sexual Dimorphism in Zeb1 Function

One of the most striking and novel findings from this study is the pronounced sex-specific cardiac phenotype following Zeb1 deletion. Female mice, both in Zeb1 cKO and icKO models exhibited earlier and more severe systolic dysfunction, advanced chamber dilation, and lower ejection fractions compared to their male counterparts. Histological analyses revealed more prominent sarcomere disruption and mitochondrial damage in female hearts. The persistent vulnerability observed in female Zeb1 knockout models highlights the critical role of sex-dependent Zeb1

regulation in maintaining cardiomyocyte integrity and cardiac function. In contrast Zeb1 overexpression does not lead to maladaptive cardiac dysfunction in females.

Although ZEB1 is classically defined as a master regulator of EMT, an emerging body of literature demonstrates that its functions are modulated by sex and hormonal context. Much of what is known comes from reproductive tissues and hormone-responsive cancers, where ZEB1 operates at the intersection of EMT, steroid hormone signaling, and tissue remodeling.

In the female reproductive tract, ZEB1 expression is tightly linked to progesterone signaling. It rises during the secretory phase of the menstrual cycle and supports uterine receptivity, implantation, and myometrial quiescence. Conditional loss or downregulation of ZEB1 in endometrium or myometrium perturbs implantation efficiency and promotes premature uterine contractility, highlighting its role as a progesterone-dependent transcriptional safeguard. In pathological states such as endometriosis, aberrant upregulation of ZEB1 reinforces EMT-like transitions, contributing to invasive behavior of endometrial cells (157–159).

In breast cancer, ZEB1 plays a central role in reprogramming Estrogen Receptor (ERα) signaling. It represses Estrogen Receptor 1 (ESR1) transcription through recruitment of DNA Methyltransferase 3 beta (DNMT3B) and Histone Deacetylase 1 (HDAC1), thereby silencing ERα expression and driving endocrine resistance. During EMT, ZEB1 also rewires estrogen receptor programs to favor metastatic colonization. These findings establish ZEB1 as both an epigenetic silencer and a determinant of endocrine therapy outcomes, mechanisms that are inherently female-specific (117,160–162).

In male reproductive biology, ZEB1 is strongly integrated with the androgen Receptor (AR) axis. Prostate cancer studies show that AR directly regulates ZEB1 transcription, and androgen Deprivation Therapy (ADT) induces ZEB1-dependent EMT programs. This coupling contributes to castration resistance—occurs when prostate cancer continues to grow even though testosterone levels are reduced to very low (“castrate”) levels by surgery or medication. This underscores the importance of ZEB1 in male-specific hormone-driven pathophysiology (163–165).

Beyond reproduction, sex-biased effects of ZEB1 have also been identified in metabolism and cancer biology. In murine models, Zeb1 haploinsufficiency increases adiposity and glucose intolerance preferentially in females, an effect

linked to estrogen and progesterone regulation of Zeb1 expression. Transcriptomic analyses of liver cancer cell lines further reveal sex-biased ZEB1 networks: ZEB1 expression negatively correlates with DDR1 in female-derived, but not male-derived, cells, aligning with differences in invasion and survival outcomes (166).

The mechanistic underpinnings of the pronounced sexual dimorphism observed in our Zeb1 knockout models remain incompletely understood, but the described studies above point to a multifactorial basis with sex hormones, particularly estrogen, playing a central role. Estrogen receptor signaling intersects with key transcriptional regulators and chromatin remodelers, and several studies have shown that estrogen can modulate Zeb1 expression in cancer and immune cells (160,161,167,168). In the context of the heart, this regulatory axis may be especially relevant, as female Zeb1-deficient mice show disproportionately severe cardiac dysfunction, including earlier onset of systolic failure and pronounced chamber dilation. These structural and functional impairments suggest a critical role for Zeb1 in supporting female cardiomyocyte health.

One particularly compelling link involves mitochondrial biology. Mitochondrial damage is a hallmark of the Zeb1-deficient phenotype, and mitochondrial activity is known to be both sexually dimorphic and estrogen-sensitive (169). Additionally, estrogen's influence on cytoskeletal dynamics may also affect mitochondrial organization and sarcomere stability in the cardiomyocytes, further exacerbating the impact of Zeb1 loss in females.

Together, these studies highlight that ZEB1 does not operate in a sex-neutral fashion. Instead, its activity is deeply conditioned by the hormonal context and allosomes of males and females. While such mechanisms are well established in reproductive and metabolic systems, they remain largely unexplored in the heart. Given the finding that Zeb1-deficient cardiomyocytes upregulate epithelial markers in both sexes, yet exhibit progressively more severe dysfunction with age, it is plausible that sex hormones modulate ZEB1 activity in the myocardium as well. Future studies should therefore investigate whether estrogen- and androgen-responsive pathways converge on ZEB1 in cardiomyocytes, potentially explaining sex-biased vulnerability to structural and metabolic remodeling in the heart.

These insights raise important questions for future research:

- How does estrogen receptor signaling interact with Zeb1 transcriptional activity?
- Are there sex-specific cofactors or repressors that modulate Zeb1 function in female versus male cardiomyocytes?
- Do mitochondrial differences between sexes alter the downstream effects of Zeb1 on energy metabolism?

5.4 Zeb1's Role in Sarcomeric Homeostasis

Ultrastructural analysis of Zeb1-deficient hearts revealed classic hallmarks of myofibrillar cardiomyopathy, with sarcomeres showing striking and progressive disorganization. Transmission electron microscopy demonstrated elongated and uneven sarcomeres with highly variable lengths, reflecting a loss of the uniformity required for coordinated contraction. Z-discs appeared fragmented, thickened, and often irregularly spaced, in some cases completely detached from adjacent myofibrils, further confirming the myofibrillar disorganization. The normally crisp striation patterns of A- and I-bands were blurred or lost, and myofibrils frequently displayed waviness, misalignment, and regions of complete dissolution. In advanced stages, the contractile apparatus exhibited a mosaic of disassembled sarcomeric units interspersed with cytoplasmic voids, indicative of a progressive breakdown in structural integrity. Quantitative analyses further confirmed significant elongation and variability in sarcomere length, as well as increased Z-disc thickness—features that together point to a destabilization of the fundamental architecture of the contractile unit.

These ultrastructural abnormalities translate directly into functional impairment. Proper sarcomere organization is essential for synchronous force generation, and even the slightest misalignment can compromise contractility. In Zeb1-deficient hearts, widespread disruption of myofibril alignment and Z-disc integrity undermine the ability of cardiomyocytes to generate coordinated force, explaining the progressive systolic dysfunction and ventricular dilation observed *in vivo*. The phenotype intensified with age, consistent with a model in which loss of Zeb1 sets cardiomyocytes on a trajectory of gradual but relentless sarcomeric disassembly, ultimately leading to severe contractile failure.

Using a tamoxifen-inducible knockout model, I confirmed that these defects are not solely developmental in origin. Deletion of Zeb1 in mature cardiomyocytes reproduced the same pattern of elongated, fragmented sarcomeres and disorganized Z-discs, particularly in female mice, demonstrating that Zeb1 is continuously required in the adult heart to preserve contractile architecture. This ongoing requirement underscores Zeb1's role not only in establishing sarcomere organization during development but also in actively maintaining the integrity of the myofibrillar network throughout life.

Furthermore, ZEB1-deficient hearts exhibit changes in sarcomere length and Z-disc thickness, especially in female mice, consistent with the sex-dependent differences in how ZEB1 contributes to sarcomeric maturation and mechanical stability.

The perinatal loss of ZEB1 triggers a partial reversion of cell identity, reflected in the aberrant upregulation of epithelial markers in the adult cardiomyocytes such as *Cdh1*, *Krt8*, *Cldn7*, and *Prom2*. This transcriptional shift signals a breakdown in the mesenchymal program that ZEB1 normally enforces, and in doing so, compromises cardiomyocyte maturation. Notably, this reactivation of epithelial gene expression was observed consistently across sexes and age groups—12-week-old males, 33-week-old males, and 33-week-old females—underscoring that ZEB1's role in maintaining cardiomyocyte identity is both robust and broadly conserved. The fact that these epithelial markers are progressively upregulated with age suggests that ZEB1 loss initiates a destabilizing trajectory, where cumulative remodeling of cell fate exacerbates structural and functional decline over time. Together, these findings position ZEB1 not only as a developmental regulator but also as a lifelong safeguard of cardiomyocyte identity and homeostasis.

Motif enrichment confirmed Zeb1's direct role in silencing these genes. Their aberrant expression in Zeb1-deficient hearts implies a breakdown of lineage fidelity and a drift toward a more plastic, less differentiated state. Such transcriptional instability likely contributes to sarcomeric collapse, as dedifferentiation signatures are strongly linked to sarcomere disassembly in failing hearts. Thus, the structural phenotype I observe may be both a mechanical consequence of disrupted

contractile alignment and a molecular outcome of compromised cardiomyocyte identity.

Taken together, my findings position Zeb1 as a guardian of sarcomere architecture. Its loss unleashes a dual cascade of transcriptional reprogramming and ultrastructural collapse that erodes cardiomyocyte contractility, driving a dilated cardiomyopathy phenotype. In this light, Zeb1 emerges not only as a developmental regulator but as a lifelong custodian of the contractile apparatus, with its absence leaving the myocardium structurally fragile and functionally compromised.

I have performed Chromatin Immunoprecipitation Sequencing (ChIP-Seq) in the NRCMs to identify the direct transcriptional targets of Zeb1 and define the regulatory networks it controls under normal conditions. The analysis was not completed while writing the thesis hence I could not discuss the results here.

5.5 Broader Implications of Zeb1

Zeb1 appears to act as a molecular gatekeeper that suppresses non-cardiac gene programs while promoting sarcomeric stability and metabolic competence. It integrates stress signals to recalibrate gene expression profiles, preserving contractile function and metabolic balance under physiological conditions. However, dysregulation in either direction, excessive activation, or complete loss, leads to maladaptive outcomes. The precise tuning of Zeb1 activity appears to be essential, making it a potentially attractive, albeit challenging, therapeutic target.

My findings highlight several critical directions for future research. **First**, the upstream signals that regulate Zeb1 in cardiomyocytes remain unknown. Given its known responsiveness to TGF-β, Wnt, and inflammatory pathways in other systems (170), it is possible that Zeb1 integrates extracellular stress signals into nuclear transcriptional responses in the heart.

Second, dissecting the mechanisms underlying sex-specific differences in Zeb1 function will be essential. Future studies should include hormone manipulation models, sex-specific transcriptomics, and single-cell approaches to identify interacting partners and divergent regulatory circuits in male and female hearts.

Third, the potential for Zeb1 as a therapeutic target is intriguing but must be approached with caution. As both loss and overexpression of Zeb1 are detrimental,

therapeutic strategies would need to modulate its activity with high precision. Small molecules or epigenetic modulators that influence Zeb1 expression or its interaction with co-factors could represent one avenue.

Finally, these results underscore the value of exploring “non-traditional” transcription factors such as those best known in cancer biology in the context of cardiac disease. The heart undergoes profound remodeling and transcriptional rewiring under stress. Understanding how such regulators contribute to this plasticity may unlock new therapeutic paradigms.

Cardiac remodeling is a complex and multifactorial process involving changes in structure, function, and gene expression in response to physiological or pathological stress. While classical signaling pathways driving hypertrophy and heart failure, such as those involving calcineurin-NFAT, MAPKs, or β-adrenergic signaling, have been extensively characterized, the role of transcription factors in fine-tuning cardiomyocyte identity and plasticity remains incompletely understood (171,172).

Mechanistically, Zeb1 acts as a molecular hub, repressing epithelial gene programs while regulating cytoskeletal and metabolic networks that drive maladaptive remodeling. This positions it at the crossroads of developmental plasticity and adult cardiac disease, offering fresh insight into the pathogenesis of cardiomyopathy, particularly subtypes marked by impaired contractility and mitochondrial dysfunction.

5.6 Current Cardiovascular Therapeutics and Clinical Relevance of Zeb1 as a Potential Therapeutic Target

Gene therapy and molecular targeting approaches are emerging as potential strategies (27,29,58,63). For example, modulation of key transcription factors or signaling pathways involved in hypertrophy, fibrosis, and metabolism may enable more precise intervention (173). In this context, ZEB1 represents a promising candidate. Its dual role in promoting maladaptive remodeling when overexpressed but maintaining cardiac homeostasis when at physiological levels suggests that fine-tuning its activity could have therapeutic benefits.

The clinical relevance of ZEB1 extends to risk stratification and personalized medicine. Elevated myocardial ZEB1 expression in hypertrophic cardiomyopathy

models aligns with human data showing increased ZEB1 in patient biopsies with advanced disease (18). Conversely, reduced ZEB1 in dilated cardiomyopathy suggests differential roles that may guide treatment selection. Furthermore, sex-specific dependencies on ZEB1 function highlight the importance of tailoring therapies based on patient sex to optimize efficacy and reduce adverse outcomes (174).

Potential outcomes of targeting ZEB1 include stabilization of cardiomyocyte identity, preservation of mitochondrial function, and prevention of fibrosis and systolic dysfunction. However, therapeutic modulation must consider the context-dependent nature of ZEB1 and its complex gene regulatory networks to avoid unintended consequences such as excessive repression or activation of EMT-like programs.

Preclinical development of small molecules, antisense oligonucleotides, or gene-editing tools targeting ZEB1 or its downstream effectors could revolutionize heart failure treatment. Yet, challenges remain, including delivery specificity, off-target effects, and the need for a comprehensive understanding of ZEB1's interactions with other cardiac transcription factors.

Future strategies spanning small molecules, gene therapies, and RNA-based modalities, hold significant potential to restore healthy gene expression, preserve cardiac structure and energy metabolism, and ultimately improve outcomes in heart failure.

In summary, the study of ZEB1 in cardiomyocyte biology bridges fundamental molecular mechanisms and clinical cardiology. It reveals novel pathways contributing to heart failure pathogenesis and points toward innovative, sex-informed therapeutic strategies that could complement existing treatments and improve patient outcomes.

5.7 Future Directions and Unanswered Questions

To fully understand the multifaceted role of Zeb1 in cardiac health and disease, several critical questions must be addressed:

1. What upstream pathways regulate Zeb1 protein stability during cardiac stress?

   a. Investigate roles of ubiquitin-proteasome systems, autophagy, and phosphorylation.

2. How do hormonal and sex-specific signals modulate Zeb1 activity in cardiomyocytes?
   a. Assess estrogen and androgen receptor interactions with Zeb1 promoter/enhancer regions.
   b. Perform sex-specific epigenomic and transcriptomic analyses.
3. How does Zeb1 influence sarcomeric assembly and cytoskeletal architecture?
   a. Study regulation of actin, myosin, titin, and Z-disc-associated proteins.
   b. Assess post-translational modifications and protein-protein interactions.
4. What role does Zeb1 play in mitochondrial homeostasis and metabolic adaptation?
   a. Evaluate oxidative phosphorylation efficiency and reactive oxygen species handling.
5. Is it possible to therapeutically modulate Zeb1 safely and effectively?
   a. Develop antisense oligonucleotides, CRISPRa/i systems, or small molecules targeting Zeb1.
   b. Conduct preclinical trials in sex-stratified heart failure models.
6. Does Zeb1 function in a cell-autonomous manner, or does it influence cardiac fibroblasts and immune cells?
   a. Utilize lineage tracing and cell-type-specific knockouts.

   Perform single-cell RNA-seq to identify cross-talk and paracrine signaling.

6. Conclusion

This comprehensive study identifies Zeb1 as a pivotal transcriptional regulator essential for maintaining cardiomyocyte identity, structure, and function under both physiological and pathological conditions. ZEB1 is dynamically regulated post-transcriptionally in response to cardiac stress, and its precise modulation is critical for adaptive and maladaptive remodeling. Overexpression of Zeb1 induces maladaptive hypertrophy and cardiac dysfunction, whereas cardiomyocyte-specific deletion causes progressive cardiac dilation, contractile failure, and profound ultrastructural abnormalities in sarcomeres and mitochondria, highlighting its fundamental role in cardiac homeostasis.

A key and striking finding of this work is the pronounced sexual dimorphism in response to Zeb1 loss. Female mice exhibit significantly more severe cardiac dysfunction, earlier onset of dilated cardiomyopathy, and higher mortality compared to males. Whereas in case of Zeb1 overexpression male mice exhibited significant cardiac dysfunction as compared to females. This sex-specific sensitivity suggests that Zeb1's role in preserving cardiomyocyte structure and function is particularly critical in females. Female hearts display greater ventricular dilation, more severe decreases in ejection fraction, and exacerbated pathological remodeling markers, indicating that Zeb1 interacts with sex-dependent molecular pathways, potentially including hormonal regulation, metabolic differences, or mitochondrial dynamics, to maintain myocardial function. The absence of compensatory upregulation of Zeb2 further emphasizes Zeb1's unique function, especially in females.

Mechanistically, Zeb1 acts as a transcriptional repressor that maintains the mesenchymal-like identity of cardiomyocytes by repressing epithelial gene programs such as Cdh1 and Krt8, with this repression being more crucial in the female heart. Zeb1 also preserves sarcomeric integrity and mitochondrial structure, and its loss leads to marked ultrastructural disarray and impaired mitochondrial content, further compromising contractile function.

In particular, the sarcomeric defects in female cardiomyocytes are profound and multifaceted. Transmission Electron Microscopy revealed extensive sarcomeric disorganization, characterized by a near-complete loss of the orderly arrangement

of actin and myosin filaments, which are essential for efficient contraction. Immunostaining for the Z-disc-associated protein MLP2 demonstrated significant increases in both sarcomere length and Z-disc thickness specifically in female Zeb1-deficient hearts, changes that were notably less pronounced or absent in males. These alterations suggest not only a loss of sarcomere structural integrity but also a potential maladaptive remodeling of the contractile apparatus in females. Moreover, the failure to isolate viable adult cardiomyocytes from older female Zeb1 knockout hearts underscores the severe structural compromise of the cardiomyocytes. Functionally, sarcomere lengthening and abnormal Z-disc thickening likely disrupt the mechanical properties and force generation capacity of cardiomyocytes, contributing to the observed progressive systolic dysfunction and ventricular dilation in females. These sex-specific sarcomeric abnormalities reinforce the conclusion that Zeb1 is essential for maintaining the precise architecture of the contractile machinery in female hearts, linking transcriptional regulation directly to biomechanical integrity.

Together, these findings position Zeb1 as a molecular gatekeeper coordinating transcriptional, structural, and metabolic programs critical for cardiomyocyte homeostasis, with an importance in female cardiac physiology. This sexual dimorphism in Zeb1 function calls for increased attention to sex as a biological variable in cardiac research and therapeutic development. Understanding the mechanisms underlying this dimorphism may reveal sex-specific targets for treating heart failure. Future work should explore the upstream signals regulating Zeb1 stability, its direct genomic targets, interactions with classical cardiac transcription factors, and how sex hormones or metabolic pathways modulate Zeb1’s cardiac functions.

Conclusion figure

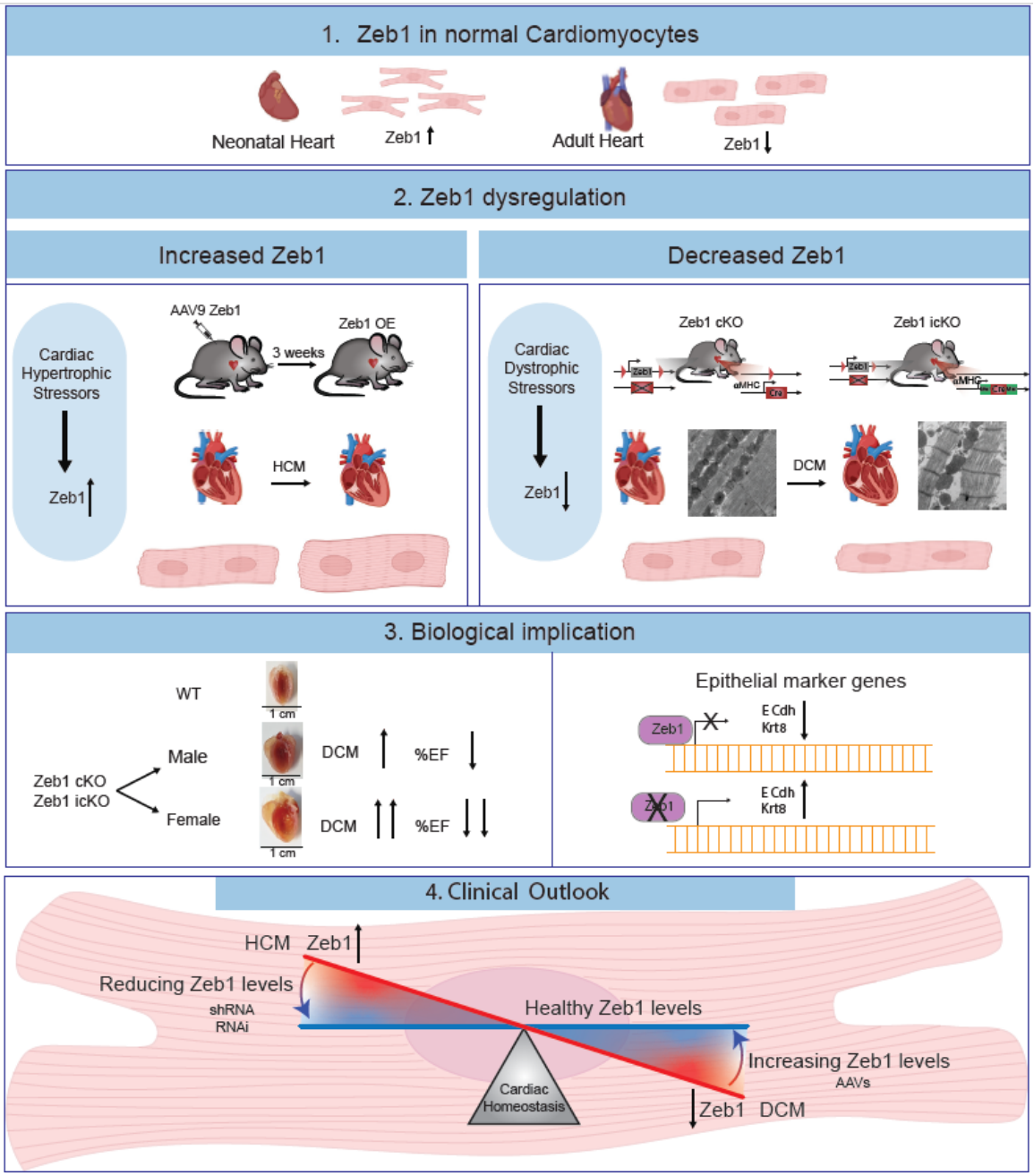

7. Reference

1. Hersch N, Wolters B, Dreissen G, Springer R, Kirchgeßner N, Merkel R, et al. The constant beat: cardiomyocytes adapt their forces by equal contraction upon environmental stiffening. Biol Open. 2013 Mar 15;2(3):351–61.
2. Karbassi E, Fenix A, Marchiano S, Muraoka N, Nakamura K, Yang X, et al. Cardiomyocyte maturation: advances in knowledge and implications for regenerative medicine. Vol. 17, Nature Reviews Cardiology. Nature Research; 2020. p. 341–59.
3. Hoshijima M. Mechanical stress-strain sensors embedded in cardiac cytoskeleton: Z disk, titin, and associated structures. Vol. 290, American Journal of Physiology - Heart and Circulatory Physiology. 2006.
4. Dorn GW. Mitochondrial pruning by nix and BNip3: An essential function for cardiac-expressed death factors. Vol. 3, Journal of Cardiovascular Translational Research. 2010. p. 374–83.
5. Severs NJ. The cardiac gap junction and intercalated disc. Vol. 26, International Journal of Cardiology. 1990.
6. Christoffels VM, Smits GJ, Kispert A, Moorman AFM. Development of the pacemaker tissues of the heart. Vol. 106, Circulation Research. 2010. p. 240–54.
7. Srivastava D. Making or Breaking the Heart: From Lineage Determination to Morphogenesis. Vol. 126, Cell. Elsevier B.V.; 2006. p. 1037–48.
8. Yigit G, Kaulfuß S, Wollnik B. Understanding inherited cardiomyopathies: Clinical aspects and genetic determinants. Medizinische Genetik. 2025 Jun 30;37(2):103–11.
9. Koelemen J, Gotthardt M, Steinmetz LM, Meder B. Rbm20-related cardiomyopathy: Current understanding and future options. Vol. 10, Journal of Clinical Medicine. MDPI; 2021.
10. Parikh VN, Day SM, Lakdawala NK, Adler ED, Olivotto I, Seidman CE, et al. Advances in the study and treatment of genetic cardiomyopathies. Vol. 188, Cell. Elsevier B.V.; 2025. p. 901–18.
11. Kan J yan, Wang D chen, Jiang Z hao, Wu L da, Xu K, Gu Y. Progression from cardiomyopathy to heart failure with reduced ejection fraction: A CORIN deficient course. Heliyon. 2024 Sep 30;10(18).
12. Savarese G, Lund LH. Global Public Health Burden of Heart Failure. Card Fail Rev [Internet]. 2017;03(01):7. Available from:

https://www.cfrjournal.com/articles/global-public-health-burden-heart-failure

13. Mensah GA, Roth GA, Fuster V. The Global Burden of Cardiovascular Diseases and Risk Factors: 2020 and Beyond. Vol. 74, Journal of the American College of Cardiology. Elsevier USA; 2019. p. 2529–32.

14. Di Cesare M, McGhie DV, Perel P, Mwangi J, Taylor S, Pervan B, et al. The Heart of the World. Glob Heart. 2024;19(1).

15. Borlaug BA, Sharma K, Shah SJ, Ho JE. Heart Failure With Preserved Ejection Fraction: JACC Scientific Statement. Vol. 81, Journal of the American College of Cardiology. Elsevier Inc.; 2023. p. 1810–34.

16. Roh J, Hill JA, Singh A, Valero-Muñoz M, Sam F. Heart Failure With Preserved Ejection Fraction: Heterogeneous Syndrome, Diverse Preclinical Models. Vol. 130, Circulation Research. Lippincott Williams and Wilkins; 2022. p. 1906–25.

17. Yeates K, Lohfeld L, Sleeth J, Morales F, Rajkotia Y, Ogedegbe O. A Global Perspective on Cardiovascular Disease in Vulnerable Populations. Vol. 31, Canadian Journal of Cardiology. Pulsus Group Inc.; 2015. p. 1081–93.

18. Mcmurray JJ V, Pfeffer MA. Heart failure [Internet]. Vol. 365, www.thelancet.com. 2005. Available from: www.thelancet.com

19. Simmonds SJ, Cuijpers I, Heymans S, Jones EAV. Cellular and Molecular Differences between HFpEF and HFrEF: A Step Ahead in an Improved Pathological Understanding. Vol. 9, Cells. NLM (Medline); 2020.

20. Ciarambino T, Menna G, Sansone G, Giordano M. Cardiomyopathies: An overview. Vol. 22, International Journal of Molecular Sciences. MDPI; 2021.

21. Murphy SP, Ibrahim NE, Januzzi JL. Heart Failure with Reduced Ejection Fraction: A Review. Vol. 324, JAMA - Journal of the American Medical Association. American Medical Association; 2020. p. 488–504.

22. Marian AJ, Braunwald E. Hypertrophic cardiomyopathy: Genetics, pathogenesis, clinical manifestations, diagnosis, and therapy. Circ Res. 2017 Sep 1;121(7):749–70.

23. Field E, Norrish G, Acquaah V, Dady K, Cicerchia MN, Ochoa JP, et al. Cardiac myosin binding protein-C variants in paediatric-onset hypertrophic cardiomyopathy: natural history and clinical outcomes. J Med Genet. 2022 Aug 1;59(8):768–75.

24. Parvari R, Levitas A. The mutations associated with dilated cardiomyopathy. Biochemistry Research International. 2012.

25. Tabish AM, Azzimato V, Alexiadis A, Buyandelger B, Knöll R. Genetic epidemiology of titin-truncating variants in the etiology of dilated cardiomyopathy. Vol. 9, Biophysical Reviews. Springer Verlag; 2017. p. 207–23.

26. Gregorich ZR, Zhang Y, Kamp TJ, Granzier HL, Guo W. Mechanisms of RBM20 Cardiomyopathy: Insights from Model Systems. Vol. 17, Circulation: Genomic and Precision Medicine. Lippincott Williams and Wilkins; 2024. p. E004355.

27. Fu Q, Hu L, Shen T, Yang R, Jiang L. Recent Advances in Gene Therapy for Familial Hypercholesterolemia: An Update Review. Vol. 11, Journal of Clinical Medicine. MDPI; 2022.

28. Birgaoanu M, Sachse M, Gatsiou A. RNA Editing Therapeutics: Advances, Challenges and Perspectives on Combating Heart Disease. Vol. 37, Cardiovascular Drugs and Therapy. Springer; 2023. p. 401–11.

29. Boada C, Sukhovershin R, Pettigrew R, Cooke JP. RNA therapeutics for cardiovascular disease. Vol. 36, Current Opinion in Cardiology. Lippincott Williams and Wilkins; 2021. p. 256–63.

30. Choi JY, Na JO. Pharmacological Strategies beyond Statins: Ezetimibe and PCSK9 Inhibitors. Vol. 8, Journal of Lipid and Atherosclerosis. Korean Society of Lipid and Atherosclerosis; 2019. p. 183–91.

31. Beltran RA, Zemeir KJ, Kimberling CR, Kneer MS, Mifflin MD, Broderick TL. Is a PCSK9 Inhibitor Right for Your Patient? A Review of Treatment Data for Individualized Therapy. Vol. 19, International Journal of Environmental Research and Public Health. MDPI; 2022.

32. Frąk W, Hajdys J, Radzioch E, Szlagor M, Młynarska E, Rysz J, et al. Cardiovascular Diseases: Therapeutic Potential of SGLT-2 Inhibitors. Vol. 11, Biomedicines. Multidisciplinary Digital Publishing Institute (MDPI); 2023.

33. Talha KM, Anker SD, Butler J. SGLT-2 Inhibitors in Heart Failure: A Review of Current Evidence. Vol. 5, International Journal of Heart Failure. Korean Society of Heart Failure; 2023. p. 82–90.

34. Tamargo J, Agewall S, Ambrosio G, Borghi C, Cerbai E, Dan GA, et al. New pharmacological agents and novel cardiovascular pharmacotherapy strategies in 2024. Vol. 11, European Heart Journal - Cardiovascular Pharmacotherapy. Oxford University Press; 2025. p. 292–317.

35. Pfeiffer ER, Tangney JR, Omens JH, McCulloch AD. Biomechanics of cardiac electromechanical coupling and mechanoelectric feedback. J Biomech Eng. 2014 Feb;136(2).

36. Bolaños P, Calderón JC. Excitation-contraction coupling in mammalian skeletal muscle: Blending old and last-decade research. Vol. 13, Frontiers in Physiology. Frontiers Media S.A.; 2022.

37. Gilbert G, Demydenko K, Dries E, Puertas RD, Jin X, Sipido K, et al. Calcium signaling in cardiomyocyte function. Cold Spring Harb Perspect Biol. 2020;12(3).

38. Benitah JP, Alvarez JL, Gómez AM. L-type Ca2+ current in ventricular cardiomyocytes. Vol. 48, Journal of Molecular and Cellular Cardiology. 2010. p. 26–36.

39. The Textbooks [Internet]. Available from: https://cvphysiology.com/cardiac-function/cf022

40. Barrick SK, Greenberg MJ. Cardiac myosin contraction and mechanotransduction in health and disease. Journal of Biological Chemistry. 2021 Nov 1;297(5).

41. Garg A, Lavine KJ, Greenberg MJ. Assessing Cardiac Contractility From Single Molecules to Whole Hearts. Vol. 9, JACC: Basic to Translational Science. Elsevier Inc.; 2024. p. 414–39.

42. Granzier H, Labeit S. Cardiac titin: An adjustable multi-functional spring. Journal of Physiology. 2002 Jun 1;541(2):335–42.

43. Krüger M, Kötter S. Titin, a central mediator for hypertrophic signaling, exercise-induced mechanosignaling and skeletal muscle remodeling. Vol. 7, Frontiers in Physiology. Frontiers Media S.A.; 2016.

44. Hwang H, Robinson DA, Stevenson TK, Wu HC, Kampert SE, Pagani FD, et al. PKCβ II modulation of myocyte contractile performance. J Mol Cell Cardiol. 2012 Aug;53(2):176–86.

45. Hwang H, Robinson DA, Stevenson TK, Wu HC, Kampert SE, Pagani FD, et al. PKCβ II modulation of myocyte contractile performance. J Mol Cell Cardiol. 2012 Aug;53(2):176–86.

46. Ravichandran VS, Patel HJ, Pagani FD, Westfall M V. Cardiac contractile dysfunction and protein kinase C–mediated myofilament phosphorylation in disease and aging. Journal of General Physiology. 2018 Sep 3;151(9):1070–80.

47. Hassoun R, Budde H, Mügge A, Hamdani N. Cardiomyocyte dysfunction in inherited cardiomyopathies. Vol. 22, International Journal of Molecular Sciences. MDPI; 2021.

48. Lehman SJ, Crocini C, Leinwand LA. Targeting the sarcomere in inherited cardiomyopathies. Vol. 19, Nature Reviews Cardiology. Nature Research; 2022. p. 353–63.

49. Vikhorev PG, Vikhoreva NN. Cardiomyopathies and related changes in contractility of human heart muscle. Vol. 19, International Journal of Molecular Sciences. MDPI AG; 2018.

50. Liu H, Wang S, Wang J, Guo X, Song Y, Fu K, et al. Energy metabolism in health and diseases. Vol. 10, Signal Transduction and Targeted Therapy. Springer Nature; 2025.

51. Reznick RM, Shulman GI. The role of AMP-activated protein kinase in mitochondrial biogenesis. Vol. 574, Journal of Physiology. 2006. p. 33–9.

52. Zhang H, Zhang Y, Zhang J, Jia D. Exercise Alleviates Cardiovascular Diseases by Improving Mitochondrial Homeostasis. Vol. 13, Journal of the American Heart Association. 2024. p. e036555.

53. Díaz-Villanueva JF, Díaz-Molina R, García-González V. Protein folding and mechanisms of proteostasis. Vol. 16, International Journal of Molecular Sciences. MDPI AG; 2015. p. 17193–230.

54. Noormohammadi A, Calculli G, Gutierrez-Garcia R, Khodakarami A, Koyuncu S, Vilchez D. Mechanisms of protein homeostasis (proteostasis) maintain stem cell identity in mammalian pluripotent stem cells. Vol. 75, Cellular and Molecular Life Sciences. Birkhauser Verlag AG; 2018. p. 275–90.

55. Vilchez D, Saez I, Dillin A. The role of protein clearance mechanisms in organismal ageing and age-related diseases. Vol. 5, Nature Communications. Nature Publishing Group; 2014.

56. Hofmann C, Katus HA, Doroudgar S. Protein Misfolding in Cardiac Disease. Vol. 139, Circulation. Lippincott Williams and Wilkins; 2019. p. 2085–8.

57. Mainali N, Ayyadevara S, Ganne A, Reis RJS, Mehta JL. Protein homeostasis in the aged and diseased heart. Vol. 3, Journal of Cardiovascular Aging. OAE Publishing Inc.; 2023.

58. Shi Y, Zhang H, Huang S, Yin L, Wang F, Luo P, et al. Epigenetic regulation in cardiovascular disease: mechanisms and advances in clinical trials. Vol. 7, Signal Transduction and Targeted Therapy. Springer Nature; 2022.

59. Schlesinger J, Schueler M, Grunert M, Fischer JJ, Zhang Q, Krueger T, et al. The cardiac transcription network modulated by gata4, mef2a, nkx2.5, srf, histone modifications, and microRNAs. PLoS Genet. 2011 Feb;7(2).

60. Durocher D, Dé F, Charron R, Warren R, Schwartz RJ, Nemer M. The cardiac transcription factors Nkx2-5 and GATA-4 are mutual cofactors have been shown to alter transcription of target genes via binding to the consensus WGATAR sequence through a DNA-binding domain consisting of two adjacent zinc. Vol. 16, The EMBO Journal. 1997.

61. Handy DE, Castro R, Loscalzo J. Epigenetic modifications: Basic mechanisms and role in cardiovascular disease. Circulation. 2011 May 17;123(19):2145–56.

62. Philippen LE, Dirkx E, da Costa-Martins PA, De Windt LJ. Non-coding RNA in control of gene regulatory programs in cardiac development and disease. Vol. 89, Journal of Molecular and Cellular Cardiology. Academic Press; 2015. p. 51–8.

63. Collins L, Binder P, Chen H, Wang X. Regulation of Long Non-coding RNAs and MicroRNAs in Heart Disease: Insight Into Mechanisms and Therapeutic Approaches. Vol. 11, Frontiers in Physiology. Frontiers Media S.A.; 2020.

64. Acharya P, Parkins S, Tranter M. RNA binding proteins as mediators of pathological cardiac remodeling. Vol. 12, Frontiers in Cell and Developmental Biology. Frontiers Media SA; 2024.

65. Gao C, Wang Y. mRNA metabolism in cardiac development and disease: Life after transcription. Physiol Rev. 2020 Apr 1;100(2):673–94.

66. De Bruin RG, Rabelink TJ, Van Zonneveld AJ, Van Der Veer EP. Emerging roles for RNA-binding proteins as effectors and regulators of cardiovascular disease. Vol. 38, European Heart Journal. Oxford University Press; 2017. p. 1380–8.

67. Guo Y, Pu WT. Cardiomyocyte Maturation: New Phase in Development. Vol. 126, Circulation Research. Lippincott Williams and Wilkins; 2020. p. 1086–106.

68. Zhao MT, Ye S, Su J, Garg V. Cardiomyocyte Proliferation and Maturation: Two Sides of the Same Coin for Heart Regeneration. Vol. 8, Frontiers in Cell and Developmental Biology. Frontiers Media S.A.; 2020.

69. Brade T, Pane LS, Moretti A, Chien KR, Laugwitz KL. Embryonic heart progenitors and cardiogenesis. Vol. 3, Cold Spring Harbor Perspectives in Medicine. Cold Spring Harbor Laboratory Press; 2013.

70. Bersell K, Arab S, Haring B, Kühn B. Neuregulin1/ErbB4 Signaling Induces Cardiomyocyte Proliferation and Repair of Heart Injury. Cell. 2009 Jul 23;138(2):257–70.

71. Pasumarthi KBS, Field LJ. Cardiomyocyte cell cycle regulation. Vol. 90, Circulation Research. 2002. p. 1044–54.

72. Øvrebø JI, Edgar BA. Polyploidy in tissue homeostasis and regeneration. Vol. 145, Development (Cambridge). Company of Biologists Ltd; 2018.

73. Bergmann O, Bhardwaj RD, Bernard S, Zdunek S, Barnabé-Heide F, Walsh S, et al. Evidence for cardiomyocyte renewal in humans. Science (1979). 2009 Apr 3;324(5923):98–102.

74. Lundy SD, Zhu WZ, Regnier M, Laflamme MA. Structural and functional maturation of cardiomyocytes derived from human pluripotent stem cells. Stem Cells Dev. 2013 Jul 15;22(14):1991–2002.

75. Goversen B, van der Heyden MAG, van Veen TAB, de Boer TP. The immature electrophysiological phenotype of iPSC-CMs still hampers in vitro drug screening: Special focus on IK1. Vol. 183, Pharmacology and Therapeutics. Elsevier Inc.; 2018. p. 127–36.

76. Veerman CC, Kosmidis G, Mummery CL, Casini S, Verkerk AO, Bellin M. Immaturity of Human Stem-Cell-Derived Cardiomyocytes in Culture: Fatal Flaw or Soluble Problem? Stem Cells Dev [Internet]. 2015 Jan 12;24(9):1035–52. Available from: https://doi.org/10.1089/scd.2014.0533

77. Papait R, Greco C, Kunderfranco P, Latronico MVG, Condorelli G. Epigenetics: A new mechanism of regulation of heart failure? Vol. 108, Basic Research in Cardiology. Dr. Dietrich Steinkopff Verlag GmbH and Co. KG; 2013.

78. Mohamed TMA, Stone NR, Berry EC, Radzinsky E, Huang Y, Pratt K, et al. Chemical enhancement of in vitro and in vivo direct cardiac reprogramming. Circulation. 2017 Jan 27;135(10):978–95.

79. Eulalio A, Mano M, Ferro MD, Zentilin L, Sinagra G, Zacchigna S, et al. Functional screening identifies miRNAs inducing cardiac regeneration. Nature. 2012 Dec 20;492(7429):376–81.

80. Porrello ER, Mahmoud AI, Simpson E, Hill JA, Richardson JA, Olson EN, et al. Transient regenerative potential of the neonatal mouse heart. Science (1979). 2011 Feb 25;331(6020):1078–80.

81. Karbassi E, Fenix A, Marchiano S, Muraoka N, Nakamura K, Yang X, et al. Cardiomyocyte maturation: advances in knowledge and implications for

regenerative medicine. Vol. 17, Nature Reviews Cardiology. Nature Research; 2020. p. 341–59.

82. Völkers M, Preiss T, Hentze MW. RNA-binding proteins in cardiovascular biology and disease: the beat goes on. Vol. 21, Nature Reviews Cardiology. Nature Research; 2024. p. 361–78.

83. Verma SK, Kuyumcu-Martinez MN. RNA binding proteins in cardiovascular development and disease. In: Current Topics in Developmental Biology. Academic Press Inc.; 2024. p. 51–119.

84. Riechert E, Kmietczyk V, Stein F, Schwarzl T, Sekaran T, Jürgensen L, et al. Identification of dynamic RNA-binding proteins uncovers a Cpeb4-controlled regulatory cascade during pathological cell growth of cardiomyocytes. Cell Rep. 2021 May 11;35(6).

85. Yao L, Conforti F, Hill C, Bell J, Drawater L, Li J, et al. Paracrine signalling during ZEB1-mediated epithelial–mesenchymal transition augments local myofibroblast differentiation in lung fibrosis. Cell Death Differ. 2019 May 1;26(5):943–57.

86. Poonaki E, Kahlert UD, Meuth SG, Gorji A. The role of the ZEB1–neuroinflammation axis in CNS disorders. Vol. 19, Journal of Neuroinflammation. BioMed Central Ltd; 2022.

87. Plaschka M, Benboubker V, Grimont M, Berthet J, Tonon L, Lopez J, et al. ZEB1 transcription factor promotes immune escape in melanoma. J Immunother Cancer. 2022 Mar 14;10(3).

88. Chen T, Pan P, Wei W, Zhang Y, Cui G, Yu Z, et al. Expression of Zeb1 in the differentiation of mouse embryonic stem cell. Open Life Sci. 2022 Jan 1;17(1):455–62.

89. Siles L, Ninfali C, Cortés M, Darling DS, Postigo A. ZEB1 protects skeletal muscle from damage and is required for its regeneration. Nat Commun. 2019 Dec 1;10(1).

90. Wang J, Farkas C, Benyoucef A, Carmichael C, Haigh K, Wong N, et al. Interplay between the EMT transcription factors ZEB1 and ZEB2 regulates hematopoietic stem and progenitor cell differentiation and hematopoietic lineage fidelity. PLoS Biol. 2021 Sep 1;19(9).

91. Gladka MM, Kohela A, Molenaar B, Versteeg D, Kooijman L, Monshouwer-Kloots J, et al. Cardiomyocytes stimulate angiogenesis after ischemic injury in a ZEB2-dependent manner. Nat Commun. 2021 Dec 1;12(1).

92. Vandewalle C, Van Roy F, Berx G. The role of the ZEB family of transcription factors in development and disease. Vol. 66, Cellular and Molecular Life Sciences. 2009. p. 773–87.

93. Brabletz S, Brabletz T. The ZEB/miR-200 feedback loop-a motor of cellular plasticity in development and cancer? Vol. 11, EMBO Reports. 2010. p. 670–7.

94. Vannier C, Mock K, Brabletz T, Driever W. Zeb1 regulates E-cadherin and Epcam (epithelial cell adhesion molecule) expression to control cell behavior in early zebrafish development. Journal of Biological Chemistry. 2013 Jun 28;288(26):18643–59.

95. Zhao Q, Shao T, Zhu Y, Zong G, Zhang J, Tang S, et al. An MRTF-A–ZEB1–IRF9 axis contributes to fibroblast–myofibroblast transition and renal fibrosis. Exp Mol Med. 2023 May 1;55(5):987–98.

96. Lindner P, Paul S, Eckstein M, Hampel C, Muenzner JK, Erlenbach-Wuensch K, et al. EMT transcription factor ZEB1 alters the epigenetic landscape of colorectal cancer cells. Cell Death Dis. 2020 Feb 1;11(2).

97. Krebs AM, Mitschke J, Losada ML, Schmalhofer O, Boerries M, Busch H, et al. The EMT-activator Zeb1 is a key factor for cell plasticity and promotes metastasis in pancreatic cancer. Nat Cell Biol. 2017 May 1;19(5):518–29.

98. Caramel J, Papadogeorgakis E, Hill L, Browne GJ, Richard G, Wierinckx A, et al. A Switch in the Expression of Embryonic EMT-Inducers Drives the Development of Malignant Melanoma. Cancer Cell. 2013 Oct 14;24(4):466–80.

99. Chen L, Gibbons DL, Goswami S, Cortez MA, Ahn YH, Byers LA, et al. Metastasis is regulated via microRNA-200/ZEB1 axis control of tumour cell PD-L1 expression and intratumoral immunosuppression. Nat Commun. 2014 Oct 28;5.

100. Gibbons DL, Lin W, Creighton CJ, Rizvi ZH, Gregory PA, Goodall GJ, et al. Contextual extracellular cues promote tumor cell EMT and metastasis by regulating miR-200 family expression. Genes Dev. 2009 Sep 15;23(18):2140–51.

101. Wellner U, Schubert J, Burk UC, Schmalhofer O, Zhu F, Sonntag A, et al. The EMT-activator ZEB1 promotes tumorigenicity by repressing stemness-inhibiting microRNAs. Nat Cell Biol. 2009 Dec;11(12):1487–95.

102. Sánchez-Tilló E, Lázaro A, Torrent R, Cuatrecasas M, Vaquero EC, Castells A, et al. ZEB1 represses E-cadherin and induces an EMT by recruiting the

SWI/SNF chromatin-remodeling protein BRG1. Oncogene. 2010 Jun 17;29(24):3490–500.

103. Amack JD. Cellular dynamics of EMT: lessons from live in vivo imaging of embryonic development. Vol. 19, Cell Communication and Signaling. BioMed Central Ltd; 2021.

104. Gonzalez DM, Medici D. Signaling mechanisms of the epithelial-mesenchymal transition. Vol. 7, Science Signaling. American Association for the Advancement of Science; 2014. p. re8.

105. Liu Y, El-Naggar S, Darling DS, Higashi Y, Dean DC. ZEB1 Links Epithelial-Mesenchymal Transition and Cellular Senescence [Internet]. Available from: http://www.upstate.com/misc/protocol

106. Drápela S, Bouchal J, Jolly MK, Culig Z, Souček K. ZEB1: A Critical Regulator of Cell Plasticity, DNA Damage Response, and Therapy Resistance. Vol. 7, Frontiers in Molecular Biosciences. Frontiers Media S.A.; 2020.

107. Cencioni C, Spallotta F, Savoia M, Kuenne C, Guenther S, Re A, et al. Zeb1-Hdac2-eNOS circuitry identifies early cardiovascular precursors in naive mouse embryonic stem cells. Nat Commun. 2018 Dec 1;9(1).

108. Jahan F, Landry NM, Rattan SG, Dixon IMC, Wigle JT. The functional role of zinc finger e box-binding homeobox 2 (Zeb2) in promoting cardiac fibroblast activation. Int J Mol Sci. 2018 Oct 17;19(10).

109. Frey N, Olson EN. Cardiac Hypertrophy: The Good, the Bad, and the Ugly. Vol. 65, Annual Review of Physiology. 2003. p. 45–79.

110. Thiery JP, Acloque H, Huang RYJ, Nieto MA. Epithelial-Mesenchymal Transitions in Development and Disease. Vol. 139, Cell. 2009. p. 871–90.

111. Peinado H, Olmeda D, Cano A. Snail, ZEB and bHLH factors in tumour progression: An alliance against the epithelial phenotype? Vol. 7, Nature Reviews Cancer. 2007. p. 415–28.

112. Gheldof A, Berx G. Chapter Fourteen - Cadherins and Epithelial-to-Mesenchymal Transition. In: van Roy F, editor. Progress in Molecular Biology and Translational Science [Internet]. Academic Press; 2013. p. 317–36. Available from: https://www.sciencedirect.com/science/article/pii/B9780123943118000145

113. Stemmler MP, Eccles RL, Brabletz S, Brabletz T. Non-redundant functions of EMT transcription factors. Vol. 21, Nature Cell Biology. Nature Publishing Group; 2019. p. 102–12.

114. Aigner K, Dampier B, Descovich L, Mikula M, Sultan A, Schreiber M, et al. The transcription factor ZEB1 (δEF1) promotes tumour cell dedifferentiation by repressing master regulators of epithelial polarity. Oncogene. 2007 Oct 25;26(49):6979–88.

115. McCulley DJ, Black BL. Transcription Factor Pathways and Congenital Heart Disease. In: Current Topics in Developmental Biology. Academic Press Inc.; 2012. p. 253–77.

116. Zhang GJ, Zhou T, Tian HP, Liu ZL, Xia S Sen. High expression of ZEB1 correlates with liver metastasis and poor prognosis in colorectal cancer. Oncol Lett. 2013 Feb;5(2):564–8.

117. Wu HT, Zhong HT, Li GW, Shen JX, Ye QQ, Zhang ML, et al. Oncogenic functions of the EMT-related transcription factor ZEB1 in breast cancer. Vol. 18, Journal of Translational Medicine. BioMed Central Ltd.; 2020.

118. Kitz J, Lefebvre C, Carlos J, Lowes LE, Allan AL. Reduced zeb1 expression in prostate cancer cells leads to an aggressive partial-emt phenotype associated with altered global methylation patterns. Int J Mol Sci. 2021 Dec 1;22(23).

119. Wirbel C, Durand S, Boivin F, Plaschka M, Benboubker V, Grimont M, et al. ZEB1 transcription factor induces tumor cell PD-L1 expression in melanoma. Cancer Immunology, Immunotherapy. 2025 Mar 1;74(4).

120. Yamaki S, Yanagimoto H, Tsuta K, Ryota H, Kon M. PD-L1 expression in pancreatic ductal adenocarcinoma is a poor prognostic factor in patients with high CD8+ tumor-infiltrating lymphocytes: highly sensitive detection using phosphor-integrated dot staining. Int J Clin Oncol. 2017 Aug 1;22(4):726–33.

121. Abstract [Internet]. Available from: https://elifesciences.org/articles/12717#abstract

122. Chung DWD, Frausto RF, Ann LB, Jang MS, Aldave AJ. Functional impact of ZEB1 mutations associated with posterior polymorphous and fuchs' endothelial corneal dystrophies. Invest Ophthalmol Vis Sci. 2014;55(10):6159–66.

123. Ong Tone S, Kocaba V, Böhm M, Wylegala A, White TL, Jurkunas U V. Fuchs endothelial corneal dystrophy: The vicious cycle of Fuchs pathogenesis. Vol. 80, Progress in Retinal and Eye Research. Elsevier Ltd; 2021.

124. Cortés M, Brischetto A, Martinez-Campanario MC, Ninfali C, Domínguez V, Fernández S, et al. Inflammatory macrophages reprogram to

immunosuppression by reducing mitochondrial translation. Nat Commun. 2023 Dec 1;14(1).

125. Brabletz T, Kalluri R, Nieto MA, Weinberg RA. EMT in cancer. Vol. 18, Nature Reviews Cancer. Nature Publishing Group; 2018. p. 128–34.

126. Ballav S, Ranjan A, Basu S. Partial Activation of PPAR-γ by Synthesized Quercetin Derivatives Modulates TGF-β1-Induced EMT in Lung Cancer Cells. Adv Biol. 2023 Oct 1;7(10).

127. Gubelmann C, Schwalie PC, Raghav SK, Röder E, Delessa T, Kiehlmann E, et al. Identification of the transcription factor ZEB1 as a central component of the adipogenic gene regulatory network. Elife. 2014 Aug 27;3(August2014):1–30.

128. Kurima K, Hertzano R, Gavrilova O, Monahan K, Shpargel KB, Nadaraja G, et al. A noncoding point mutation of Zeb1 causes multiple developmental malformations and obesity in Twirler mice. PLoS Genet. 2011 Sep;7(9).

129. Larsen TS, Jansen KM. Impact of obesity-related inflammation on cardiac metabolism and function. J Lipid Atheroscler. 2021;10(1):8–23.

130. Wynn TA, Ramalingam TR. Mechanisms of fibrosis: Therapeutic translation for fibrotic disease. Vol. 18, Nature Medicine. 2012. p. 1028–40.

131. Kalluri R, Weinberg RA. The basics of epithelial-mesenchymal transition. Vol. 119, Journal of Clinical Investigation. 2009. p. 1420–8.

132. Foglio E, D'Avorio E, Nieri R, Russo MA, Limana F. Epicardial EMT and cardiac repair: an update. Vol. 15, Stem Cell Research and Therapy. BioMed Central Ltd; 2024.

133. Hong JH, Zhang HG. Transcription Factors Involved in the Development and Prognosis of Cardiac Remodeling. Vol. 13, Frontiers in Pharmacology. Frontiers Media S.A.; 2022.

134. Madany M, Thoma T, Edwards LA. The Curious Case of ZEB1. Discoveries [Internet]. 2018 Dec 31;6(4):e86. Available from: https://www.discoveriesjournals.org/discoveries/D.2018.04.PA-Edwards.DOI

135. Buijtendijk MFJ, Barnett P, van den Hoff MJB. Development of the human heart. Am J Med Genet C Semin Med Genet. 2020 Mar 1;184(1):7–22.

136. Sedmera D, Thompson RP. Myocyte proliferation in the developing heart. Vol. 240, Developmental Dynamics. 2011. p. 1322–34.

137. Judge DP, Neamatalla H, Norris RA, Levine RA, Butcher JT, Vignier N, et al. Targeted Mybpc3 Knock-Out Mice with Cardiac Hypertrophy Exhibit Structural Mitral Valve Abnormalities. J Cardiovasc Dev Dis [Internet]. 2015;2(2):48–65. Available from: https://www.mdpi.com/2308-3425/2/2/48

138. Hershberger RE, Hedges DJ, Morales A. Dilated cardiomyopathy: the complexity of a diverse genetic architecture. Nat Rev Cardiol [Internet]. 2013;10(9):531–47. Available from: https://doi.org/10.1038/nrcardio.2013.105

139. Brabletz S, Lasierra Losada M, Schmalhofer O, Mitschke J, Krebs A, Brabletz T, et al. Generation and characterization of mice for conditional inactivation of Zeb1. Genesis. 2017 Apr 1;55(4).

140. Ravi V, Jain A, Taneja A, Chatterjee K, Sundaresan NR. Isolation and Culture of Neonatal Murine Primary Cardiomyocytes. Curr Protoc. 2021 Jul 1;1(7).

141. Ackers-Johnson M, Li PY, Holmes AP, O'Brien SM, Pavlovic D, Foo RS. A Simplified, Langendorff-Free Method for Concomitant Isolation of Viable Cardiac Myocytes and Nonmyocytes from the Adult Mouse Heart. Circ Res. 2016 Sep 30;119(8):909–20.

142. Cardoso-Moreira M, Halbert J, Valloton D, Velten B, Chen C, Shao Y, et al. Gene expression across mammalian organ development. Nature. 2019 Jul 25;571(7766):505–9.

143. Liu H, Bersell K, Kühn B. Isolation and characterization of intact cardiomyocytes from frozen and fresh human myocardium and mouse hearts. In: Methods in Molecular Biology. Humana Press Inc.; 2021. p. 199–210.

144. Zhang P, Sun Y, Ma L. ZEB1: At the crossroads of epithelial-mesenchymal transition, metastasis and therapy resistance. Vol. 14, Cell Cycle. Landes Bioscience; 2015. p. 481–7.

145. Abstract [Internet]. Available from: https://elifesciences.org/articles/24139#abstract

146. Nieto MA, Huang RYYJ, Jackson RAA, Thiery JPP. EMT: 2016. Vol. 166, Cell. Cell Press; 2016. p. 21–45.

147. Balestrieri C, Alfarano G, Milan M, Tosi V, Prosperini E, Nicoli P, et al. Co-optation of Tandem DNA Repeats for the Maintenance of Mesenchymal Identity. Cell. 2018 May 17;173(5):1150-1164.e14.

148. Wu C, Shi W, Zhang S. ZEB1 promotes DNA homologous recombination repair and contributes to the 5-Fluorouracil resistance in colorectal cancer [Internet]. Vol. 13, Am J Cancer Res. 2023. Available from: www.ajcr.us/

149. Genetta TL, Hurwitz JC, Clark EA, Herold BT, Khalil S, Abbas T, et al. ZEB1 promotes non-homologous end joining double-strand break repair. Nucleic Acids Res. 2023 Oct 13;51(18):9863–79.

150. Drápela S, Bouchal J, Jolly MK, Culig Z, Souček K. ZEB1: A Critical Regulator of Cell Plasticity, DNA Damage Response, and Therapy Resistance. Vol. 7, Frontiers in Molecular Biosciences. Frontiers Media S.A.; 2020.

151. Swahn H, Li K, Duffy T, Olmer M, D'Lima DD, Mondala TS, et al. Senescent cell population with ZEB1 transcription factor as its main regulator promotes osteoarthritis in cartilage and meniscus. Ann Rheum Dis. 2023 Mar 1;82(3):403–15.

152. Liuq Y, Sánchez-Tilló E, Lu X, Huang L, Clem B, Telang S, et al. The ZEB1 transcription factor acts in a negative feedback loop with miR200 downstream of ras and Rb1 to regulate Bmi1 expression. Journal of Biological Chemistry. 2014 Feb 14;289(7):4116–25.

153. Campagna R, Mazzanti L, Pompei V, Alia S, Vignini A, Emanuelli M. The Multifaceted Role of Endothelial Sirt1 in Vascular Aging: An Update. Vol. 13, Cells. Multidisciplinary Digital Publishing Institute (MDPI); 2024.

154. Magenta A, Ciarapica R, Capogrossi MC. The Emerging Role of MIR-200 Family in Cardiovascular Diseases. Vol. 120, Circulation Research. Lippincott Williams and Wilkins; 2017. p. 1399–402.

155. Magenta A, Cencioni C, Fasanaro P, Zaccagnini G, Greco S, Sarra-Ferraris G, et al. MiR-200c is upregulated by oxidative stress and induces endothelial cell apoptosis and senescence via ZEB1 inhibition. Cell Death Differ. 2011 Oct;18(10):1628–39.

156. Zhang K, Zhao H, Sheng Y, Chen X, Xu P, Wang J, et al. Zeb1 sustains hematopoietic stem cell functions by suppressing mitofusin-2-mediated mitochondrial fusion. Cell Death Dis. 2022 Aug 1;13(8).

157. Xu Z, Yang HH, Chen HZ, Huang BZ, Yang M, Liao ZH, et al. ZEB1 Promotes Epithelial-Mesenchymal Transition of Endometrial Epithelial Cells and Plays a Critical Role in Embryo Implantation in Mice. Reproductive Sciences. 2025 Apr 1;32(4):1331–7.

158. Wu SP, Li R, DeMayo FJ. Progesterone Receptor Regulation of Uterine Adaptation for Pregnancy. Vol. 29, Trends in Endocrinology and Metabolism. Elsevier Inc.; 2018. p. 481–91.

159. Li SY, DeMayo FJ. Revolutionizing Implantation Studies: Uterine-Specific Models and Advanced Technologies. Vol. 15, Biomolecules. Multidisciplinary Digital Publishing Institute (MDPI); 2025.

160. Mohammadi Ghahhari N, Sznurkowska MK, Hulo N, Bernasconi L, Aceto N, Picard D. Cooperative interaction between ERα and the EMT-inducer ZEB1 reprograms breast cancer cells for bone metastasis. Nat Commun. 2022 Dec 1;13(1).

161. Zhang J, Zhou C, Jiang H, Liang L, Shi W, Zhang Q, et al. ZEB1 induces ER-α promoter hypermethylation and confers antiestrogen resistance in breast cancer. Cell Death Dis. 2017;8(4).

162. Sarkar S, Venkatesh D, Kandasamy T, Ghosh SS. Epigenetic Modulations in Breast Cancer: An Emerging Paradigm in Therapeutic Implications. Vol. 29, Frontiers in Bioscience - Landmark. IMR Press Limited; 2024.

163. Mooney SM, Parsana P, Hernandez JR, Liu X, Verdone JE, Torga G, et al. The presence of androgen receptor elements regulates ZEB1 expression in the absence of androgen receptor. J Cell Biochem. 2015 Jan 1;116(1):115–23.

164. Papanikolaou S, Vourda A, Syggelos S, Gyftopoulos K. Cell plasticity and prostate cancer: The role of epithelial–mesenchymal transition in tumor progression, invasion, metastasis and cancer therapy resistance. Vol. 13, Cancers. MDPI; 2021.

165. Anose BM, Sanders MM. Androgen receptor regulates transcription of the zeb1 transcription factor. Int J Endocrinol. 2011;2011.

166. Saykally JN, Dogan S, Cleary MP, Sanders MM. The ZEB1 transcription factor is a novel repressor of adiposity in female mice. PLoS One. 2009;4(12).

167. Mangani S, Piperigkou Z, Koletsis NE, Ioannou P, Karamanos NK. Estrogen receptors and extracellular matrix: the critical interplay in cancer development and progression. Vol. 292, FEBS Journal. John Wiley and Sons Inc; 2025. p. 1558–72.

168. Bagheri M, Mohamed GA, Mohamed Saleem MA, Ognjenovic NB, Lu H, Kolling FW, et al. Pharmacological induction of chromatin remodeling drives chemosensitization in triple-negative breast cancer. Cell Rep Med. 2024 Apr 16;5(4).

169. Shaw GA. Mitochondria as the target for disease related hormonal dysregulation. Brain Behav Immun Health. 2021 Dec 1;18.

170. Deng Z, Fan T, Xiao C, Tian H, Zheng Y, Li C, et al. TGF-β signaling in health, disease, and therapeutics. Vol. 9, Signal Transduction and Targeted Therapy. Springer Nature; 2024.

171. Azevedo PS, Polegato BF, Minicucci MF, Paiva SAR, Zornoff LAM. Cardiac Remodeling: Concepts, Clinical Impact, Pathophysiological Mechanisms and Pharmacologic Treatment. Vol. 106, Arquivos brasileiros de cardiologia. 2016. p. 62–9.

172. Schirone L, Forte M, Palmerio S, Yee D, Nocella C, Angelini F, et al. A Review of the Molecular Mechanisms Underlying the Development and Progression of Cardiac Remodeling. Oxid Med Cell Longev. 2017;2017.

173. Prabhu SD, Frangogiannis NG. The biological basis for cardiac repair after myocardial infarction. Vol. 119, Circulation Research. Lippincott Williams and Wilkins; 2016. p. 91–112.

174. Regitz-Zagrosek V. Therapeutic implications of the gender-specific aspects of cardiovascular disease. Vol. 5, Nature Reviews Drug Discovery. 2006. p. 425–39.

Supplementary Data

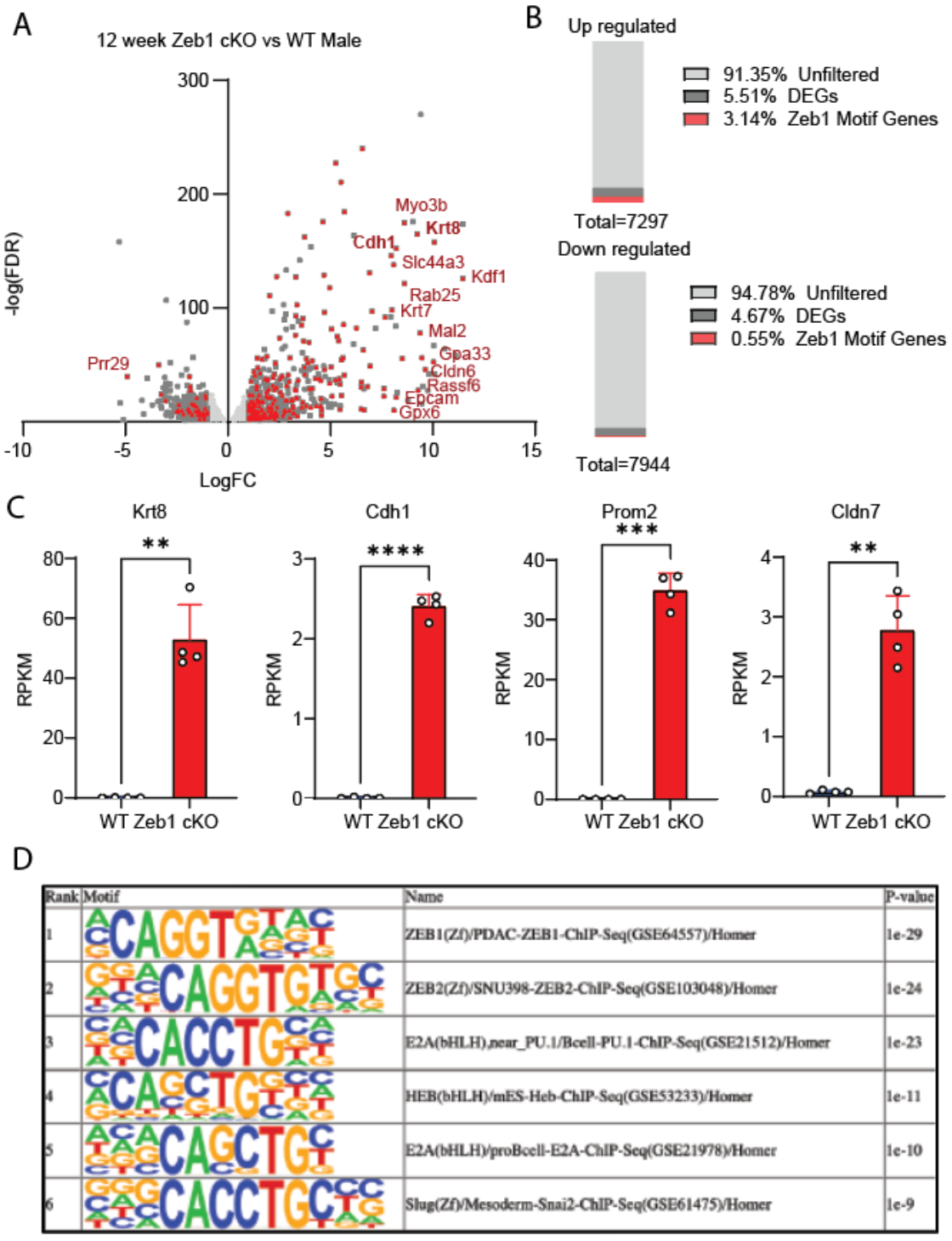

Suppl Figure 1 . Bulk RNA seq 12-week-old male data.

(a) Volcano plot showing distribution of genes with Zeb1 binding motifs among upregulated and downregulated DEGs in Zeb1 cKO mice compared to WT. (b) Proportion of genes containing Zeb1 motifs among upregulated and downregulated DEGs, indicating Zeb1's role as a transcriptional repressor. (c) Identification of epithelial markers *Cdh1* (E-Cadherin), *Krt8* (Cytokeratin 8), *Cldn7* (Claudin 7), and *Prom2* (Prominin 2) among upregulated DEGs in female Zeb1 KO mice. (d) HOMER de novo motif enrichment analysis of DEG promoter regions identifies Zeb1 as the top-enriched transcription factor binding motif in Zeb1 cKO transcriptomes. (Data are shown as mean ± SEM. Statistical analysis was performed using unpaired Student's t-test or one-way ANOVA, *=p<0.05, **=p<0.01, ***=p<0.001, ****=p<0.0001.)

Publications

1. *ZEB1 Is a Key Regulator of Cardiomyocyte Structure and Function.*
   Parul Gupta[1,2], Daniel Finke[1,2], Tobias Jakobi[3], Verena Kamuf-Schenk[1,2], Marc P. Stemmler[4], Simone Brabletz[4], Thomas Brabletz[4], Norbert Frey[1,2], Mirko Völkers[1,2] and Vivien Kmietczyk[1,2] - In preparation.
2. *Ythdf2 regulates cardiac remodeling through its mRNA target transcripts.* (2023) Kmietczyk V, Oelschläger J, Gupta P, Varma E, Hartl S, Furkel J, Konstandin M, Marx A, Loewenthal Z, Kamuf-Schenk V, Jürgensen L, Stroh C, Gorska A, Martin-Garrido A, Heineke J, Jakobi T, Frey N, Völkers M. Mol Cell Cardiol, doi: 10.1016/j.yjmcc.2023.06.001
3. *Translational control of Ybx1 expression regulates cardiac function in response to pressure overload in vivo* (2023) Varma E, Burghaus J, Schwarzl T, Sekaran T, Gupta P, Górska AA, Hofmann C, Stroh C, Jürgensen L, Kamuf-Schenk V, Li X, Medert R, Leuschner F, Kmietczyk V, Freichel M, Katus HA, Hentze MW, Frey N, Völkers M. Basic Res Cardiol, doi: 10.1007/s00395-023-00996-1

Acknowledgement

It is with profound gratitude that I acknowledge the many people who have supported me throughout my doctoral journey.

First and foremost, I extend my deepest thanks to my supervisors, Prof. Mirko Voelkers and Dr. Vivien Kmietczyk for their exceptional mentorship, intellectual guidance, and patience. Their unwavering support and constructive feedback have been invaluable in shaping both this work and my growth as a researcher.

I am equally grateful to my thesis committee members, Prof. Georg Stoecklin and Prof. Joerg Heineke, for their thoughtful feedback, constructive criticism, and constant encouragement. Thank you to Dr. Maarten van den Hoogenhof and Dr. Chi-Chung Wu for being part of the defense committee.

I owe heartfelt thanks to my colleagues, past and present members of the lab, whose collaboration, shared insights, and occasional moments of lighthearted distractions made the long days and nights far more enjoyable. Together, we navigated the highs and lows of research with persistence and some fun along the way.

To my close friends, Anushka, Eshita, Ram, Sumra, Tanu, Vikas, Vishwadeep, and Zakiya, to name a few, thank you for your unwavering encouragement, for checking in whenever I disappeared into my work and for providing much-needed escapes from the academic bubble.

To my family, I am endlessly grateful. To my parents, thank you for your love, sacrifices, and for teaching me the value of hard work, perseverance, and integrity. To my dear little sister Ojaswini, thanks for always being there whenever I needed to vent out. Your humor, perspective, and love for me have kept me grounded and motivated. This accomplishment is as much yours as it is mine.

To my life partner Shitij, you have been my rock, my safe place, and my unwavering source of encouragement. Thank you for listening to my endless academic monologues, helping me take the hard decisions, and celebrating even the smallest victories with me. Your belief in me carried me through moments when I doubted myself, and your love made the journey meaningful.

Finally, my deepest gratitude goes to Dr. Chandan Sahi, whose mentorship has been transformative. At a time when I could see only darkness, you showed me the light and guided me forward. This achievement would not have been possible without your support and belief in me.

To everyone who has contributed to this journey in ways both big and small, my sincerest thanks. This thesis stands as a testament not only to my work but to the generosity, kindness, and encouragement I have received along the way.

"कर्मण्येवाधिकारस्ते मा फलेषु कदाचन। मा कर्मफलहेतुर्भूर्मा ते सङ्गोऽस्त्वकर्मणि॥"